REVIEW AND CASE STUDY OF ELECTRIC SUBMERSIBLE PUMP PERFORMANCE WITH DISPERSIONS

By

Dexter Bryant Ellexson

A Project Submitted in Partial Fulfillment of the Requirements

for the Degree of

Master of Science

in

Petroleum Engineering

University of Alaska Fairbanks

December 2020

Dr. Obadare Awoleke, Committee Chair
Dr. Samson Ning, Co-Chair
Dr. Abhijit Dandekar, Committee Member
Department of Petroleum Engineering

ABSTRACT

Centrifugal pump performance is very sensitive to fluid viscosity, gas fraction, and flow pattern in impeller channels. Viscous oil reduces the head and rate capacity of the pump. High gas fraction reduces the head capacity of the pump at high rates and leads to unstable surging at low rates. If the flow pattern in the impeller transitions to an elongated bubble the pump can gas-lock causing loss of production and excessive heat buildup. The complex geometry and 3-dimensional flow in a pump stage make the analysis of flow in a pump difficult without simplifying assumptions. Empirical and mechanistic models have been developed for correcting pump performance for viscosity, gas fraction, and predicting flow pattern within the impeller with reasonable accuracy. Difficulties arise when produced fluids form stable dispersions. Foams, emulsions, and solid suspensions make the determination of viscosity, gas separation efficiency, and flow pattern more difficult. Interfacial properties between phases become important in determining the bulk fluid properties, and the presence of surfactants exacerbates the interfacial effects.

The objective of this project is to describe the fundamentals of electrical submersible centrifugal pumps, ESPs, and the effects that produced fluids have on their performance. These findings are then used to evaluate a case study of an ESP installed in a well with foamy and viscous crude. The ESP exhibits reduced head and rate compared to predicted viscous and gas corrections. Including interfacial effects on the fluid viscosity allow a satisfactory performance match of pump performance to be achieved. The effect of foam on pump performance can be attributed to the increased viscosity exhibited when gas behaves as a dispersed phase in a continuous oil phase rather than a separate phase in a mixture.

TABLE OF CONTENTS

LIST OF FIGURES

LIST OF SYMBOLS

β . . . . . Impeller Blade angle

ρ . . . . . Fluid Density, $\frac{m}{L^3}$

μ . . . . . Fluid Dynamic Viscosity, $\frac{m}{LT}$, cp

ω . . . . . Angular Velocity, $\frac{1}{T}$, $\frac{1}{sec}$

σ . . . . . Interfacial tension, $\frac{M}{T^2}$

η . . . . . Efficiency

γ . . . . . Fluid specific gravity

α . . . . . Local speed of sound, $\frac{L}{T}$, $\frac{ft}{sec}$

ν . . . . . Kinematic viscosity, $\frac{L^2}{T}$

Φ . . . . . Turpin coefficient

Γ . . . . . Foam quality

C_V . . . . . Heat capacity at constant volume

C_p . . . . . Heat capacity at constant pressure

D . . . . . Impeller Diameter, L, in

$F_{\omega r}$ . . . . . Froude number

H . . . . . Head, L, ft

I_s . . . . . Surging Parameter

$I_{s,Gaslock}$ . . . . . Onset of Gas Locking Parameter

$I_{s,Surge}$ . . . . . Onset of Gas Surging Parameter

L . . . . . Impeller channel length

L_G . . . . . Leakage gap length

N . . . . . Pump rotational speed, $\frac{1}{T}$, $\frac{1}{min}$

N_s . . . . . Pump specific speed, field units

P_{Brake} . . . . . Pump brake horsepower, hp

Q . . . . . Flow rate, $\frac{L^3}{T}$, $\frac{bbl}{day}$

R . . . . . Gas constant

R_e . . . . . Reynolds number

S_L . . . . . Leakage gap area

T . . . . . Temperature

T_{shaft} . . . . . Shaft torque, $\frac{mL^2}{T^2}$

U . . . . . Blade Velocity, $\frac{L}{T}$, $\frac{ft}{sec}$

V . . . . . Absolute Velocity, $\frac{L}{T}$, $\frac{ft}{sec}$

V_∞ . . . . . Terminal bubble velocity, $\frac{L}{T}$, $\frac{ft}{sec}$

V_{Gs} . . . . . Gas Superficial Velocity, $\frac{L}{T}$, $\frac{ft}{sec}$

V_{Ls} . . . . . Liquid Superficial Velocity, $\frac{L}{T}$, $\frac{ft}{sec}$

V_{bs} . . . . . Bubble Velocity, $\frac{L}{T}$, $\frac{ft}{sec}$

W . . . . . Flow Velocity, $\frac{L}{T}$, $\frac{ft}{sec}$

Z . . . . . Number of Impeller blades

$[\mu]$ . . . . . Intrinsic Viscosity

b . . . . . Impeller channel height, L, in

g . . . . . Gravitational constant, $\frac{L}{T^2}$

k . . . . . Ratio of heat capacities

$\dot{m}$ . . . . . Mass flow rate, $\frac{m}{T}$

n_s . . . . . Pump specific speed, metric units

r . . . . . Impeller radius, L, in

σ_s . . . . . Slip Factor

ω_s . . . . . Pump specific speed, dimensionless

z . . . . . Height, L, ft

LIST OF ABBREVIATIONS

BEP . . . . . Best Efficiency Point

ESP . . . . . Electric Submersible Pump

FPSO . . . . . Floating Production Storage and Offloading Unit

HPS . . . . . Horizonal Pumping System

IPR . . . . . Inflow Performance Relationship

OPR . . . . . Outflow Performance Relationship

PCP . . . . . Progressing Cavity Pump

PMM . . . . . Permanent Magnet Motor

ROR . . . . . Recommended Operating Range

RPM . . . . . Revloutions per Minute

STB . . . . . Stock Tank Barrels

VSD . . . . . Variable Speed Drive

CHAPTER 1

INTRODUCTION

Electric Submersible Pumps, or ESPs, are one of the most widely used forms of artificial lift around the world. They have been used for almost 100 years in the oil industry to increase the flowrate from oil wells and water wells. They are applied onshore and offshore and almost anywhere oil can be found. As the name suggests, ESPs require electricity to operate and in most cases this is not a problem, but even in remote locations where electricity may not be easily accessible by power line, ESPs can be run on genset power. ESPs are even applied in exploration and appraisal well testing and drill stem testing where they have been used to produce wells temporarily without installing extra facilities.

Artificial lift is required for wells that will not flow naturally, but can also increase the flow rate of naturally flowing wells. The drawdown that is capable depends on the method of lifting, where ESPs are most suitable in high liquid rate and deep set depths. ESPs are flexible when used with a variable speed drive that can change the rotational speed of the pump. The ESP gauge and surface data gathering equipment can be used with SCADA to monitor wells in real time and remotely, allowing frequency changes and operating modes to be adjusted from anywhere. Automation can be programmed to set system protections with automatic shutoffs to protect the ESP components.

There are several downsides to ESPs that need to be taken into account before selecting them for artificial lift. Reliability is a main concern, since pump failure means lost production. Because the system relies on a power cable that runs from surface to pump depth, usually strapped to the production tubing, the system is vulnerable to electrical failure. This is especially important during installation of the pump where tight clearances and deviations can smash the cable or in a worst case scenario just slightly damage the cable so that the failure is not caught until after the ESP is landed and the rig has moved

off the well. The damaged cable may allow the ESP to start up once or only a few times and lead to a very short runlife, what is called an infant mortality. Other failure modes are associate with the ESP motor which requires clean oil and fluid cooling to have an extended run life. Seals protect the motor from encroaching well fluids but these too sometimes fail. Finally, the pump itself can fail due to a shaft break or failure of the pump due to abrasive wear, corrosion, or scale. In some fluids, ESPs fail before even a 6 month run time, whereas in clean water applications they have been run for 20 years without trouble.

A significant amount of research and effort is put into increasing the reliability of ESPs for long run life in increasingly harsh well conditions. The other main concern with ESPs is their hydraulic performance and the ability to pump difficult fluids. With advancements in ESP reliability in harsh fluids, the ESP then needs to meet the hydraulic demand. High gas rates reduce the effectiveness of an ESP and can lead to gas locking, where the pump fails to surface fluid. Viscous fluids can greatly decrease the pumps efficiency. Sand production can quickly pack the pump or wear out the rotating components to reduce the efficiency. Historically if a well had high gas rate, high viscosity, or sand production then an alternative form of artificial lift would be required. More and more though, the ESP industry is tackling these difficult fluids and designing pumps that can meet drawdown targets. Predicting the performance in these fluids often requires trial and error in pilot wells or expensive flow loop testing is employed to determine pump performance before it is deployed field wide.

This project is concerned with the hydraulic performance of ESPs in difficult well fluids and the methods used to predict their performance. High free gas rates, viscous oil, sandy applications, and hard to pump emulsions and foams are being pumped more and more with ESPs as the technology of the systems allows effective production in these cases. Prediction of the performance in these fluids is still difficult due to the complex 3-dimensional flow through the ESP. Takacs (2018) recommends testing the ESP with well fluids to determine the pump operation and this has certainly been done, especially for

very expensive projects offshore. For most cases though, testing is impractical and another method of predicting the pump performance is necessary. There are several methods for de-rating pump performance based on fluid properties, this project aims to review the literature both in the oil industry as well as other industries where centrifugal pumps are used. The methods found in the literature are applied to a case study using data from an ESP well installed in Alaska on the North Slope. The case well is in a field known to have difficult to pump fluids, partially due to the low bottom hole temperature. Production often is accompanied by sand and asphaltene and the fluid itself is viscous and prone to emulsion and foaming.

CHAPTER 2

CENTRIFUGAL PUMPS

The first true centrifugal pump was developed by French inventor Denis Papin in 1698, though sketches of a fluid machine using centrifugal force is found earlier in the work of Leonardo da Vinci. Neither Papin nor da Vinci's designs were practical due to limitations of manufacturing methods at the time. The mathematics that define the ideal performance of a centrifugal pump were developed by Leonhard Euler more than 50 years later in 1751 and the first practical centrifugal pump was manufactured in 1818. The American Oil and Gas Historical Society (2020) details the early stages of advancing pump technology in the oil and gas industry in the late 1900's and early 20th century with the first electric pump patented for oil and gas designed by Harry Pickett in 1894. Pickett's design was a plunger pump driven by a screwdriver device with a downhole electric motor. In 1918, Robert Newcomb patented a reciprocating plunger pump driven from surface with sucker rods, but the design often failed in deep wells. Around the same time, in 1916, the first electric submersible pump system (ESP) was designed by Armais Arutunoff in Germany following experiments in the Baku oil fields near the Caspian Sea.

Arutunoff was born in the Russian Empire to Armenian parents and immigrated to the United States in 1923 looking for financial backing for his design. He obtained the patent for his design in the US in 1926 and Frank Phillips, head of Phillips Petroleum Company, provided the financial backing for Arutunoff to start Bart Manufacturing in Bartlesville Oklahoma in 1928. Arutunoff installed the first ESP in the El Dorado field in Kansas in 1926 and 4 years later Bart Manufacturing became Russian Electrical Dynamo of Arutunoff or REDA. By 1930 the Oklahoma City Field had converted from beam pumping to ESPs with 2 to 3 times greater lifting capacity (Korpela 2011). Early ESPs were run on switchboards at a single operating speed; usually based on 60 Hz at surface which

translates to around 3500 pump RPM due to the asynchronous nature of the induction motors powering the pump. Later innovations in ESP technology came in 1977 with the introduction of Variable Speed Drive technology that allowed pumps to rotate at variable RPM and more recently with the introduction of synchronous permanent magnet motor (PMM) technology. In 1992 the first coiled tubing deployed ESP system led the way to other alternative deployment methods. ESP operation has broadened with the needs of the industry, leading to more complicated completions involving innovative designs. Newer technology deploys a "wet connect" system that allows the motor to be deployed independent of the cable. The wet connect allows the pump, seals, and motor to be deployed via wireline or coiled tubing and replaced without a heavy rig intervention.

The components of an ESP may vary for unique designs, but the basic design is shown in Figure 2.1. The pump is the main area of study for this project since it is the fluid mover and main element of the system. The rotating element or rotor of the pump is termed the impeller while the stationary portion is termed the diffuser. An impeller and diffuser pair is called a stage. Because the diameter is restricted, multiple pump stages are stacked in series to meet the required head needed for the system. These stacks are cased in pump housings up to 20 ft in length. If a single housing cannot meet the system head requirements, multiple housings can be used in series by bolting the housings together and connecting the shafts via a coupling between pumps. Usually, a pump housing has only one type of stage enclosed. Stacking multiple housings of different pump stages allows flexibility in the system design.

There are other components in a pump housing such as radial support bearings, and the head and base of the pump as shown in Figure 2.2, but the impeller and diffuser are the components responsible for the work done by the pump. The intake of the pump is usually a small separate piece of equipment but can also be integral to the pump body. The intake can be a simple bolt on type, or what is called a gas separator which is designed to process the incoming well fluid and separate out free gas and expel it to the annulus to

allow a more liquids rich fluid flow into the pump stages. Other components of the system of an ESP are the motor, seals (or protectors), cable, and surface equipment. The motor converts electrical energy from the cable to torque that drives the pump through a series of shafts. Seals protect the motor from well fluids by way of a tortuous path or mechanical seals and provide a volume that acts as an accumulator allowing the motor oil to expand and contract with temperature variation without inflowing well fluids. The shaft of each component is connected in series with couplings between the equipment and heads and bases on the equipment allow bolting of the equipment in a modular way. The shaft diameter must be large enough to accommodate the high torque generated by the motor which further limits the pump geometry by limiting the inlet radius.

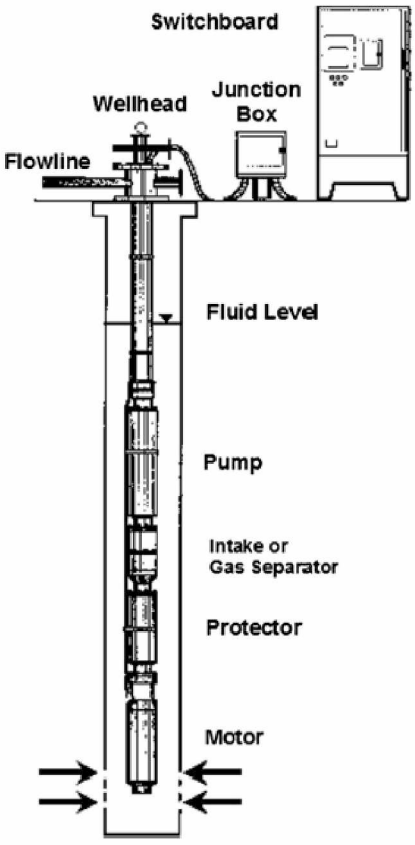

Figure 2.1 ESP System components (Takacs 2018).

Figure 2.2 Multistage Pump Housing Showing Head and Base, Shaft, and 7 stages. Radial Support Bearings at top and bottom in Blue and Thrust Bearings in Red. (from Halliburton.com A).

Impellers are the main feature of a pump as they impart the velocity to the fluid. An impeller cutaway is shown in Figure 2.3 for a radial pump stage on top of a diffuser. The shroud is cut away to show the internals of the impeller. The blades, or vanes, curve to form the flow path of the fluid between the upper and lower shroud. This stage is radial, sometimes called a pancake stage, because of the flat profile and nearly radial flowpath through the impeller. With the shaft removed, the keyway is visible where the impeller would key to the shaft allowing the impeller to rotate with the shaft. The diffuser is installed in the housing with compression to prevent it from rotating.

Figure 2.3 Radial Stage Impeller Cutaway (Takacs 2018).

A cross-section view of the flow path in an impeller stage is shown in Figure 2.4. The discharge of the impeller is directed radially outward into the diffuser and directed up through the diffuser axially and into the intake of the next stage. At the last stage in a pump housing the fluid is discharged into the tubing to flow to surface. The fluid gains pressure incrementally through each stage

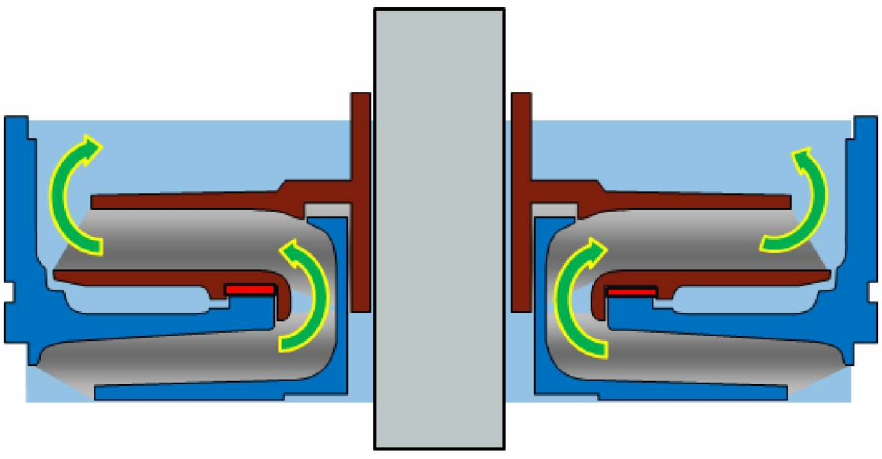

Figure 2.4 One Stage Impeller (red) and Diffuser (blue) Cross Section with Shaft.

Many stage geometries exist for ESP impellers with a range from radial flow to axial flow and each has its advantages and drawbacks. An axial flow impeller, such as in Figure 2.5, looks more like a screw and has no shrouds at all. The fluid flows axially through the stage and experiences less dramatic changes in direction. The main advantage of this type of design is the ability to handle a higher volume of gas, though they often require more horsepower.

Figure 2.5 Two Stage Axial Impeller and Diffuser (Halliburton.com B).

Impellers impart kinetic energy to the fluid by increasing the velocity. Diffusers convert kinetic energy into pressure energy by diffusion, or deceleration, of the fluid. The diffuser is similar to a nozzle, where no external work or energy is added, but simply converted from one form to another. Most turbomachinery pump applications use a volute, also called a scroll collector or vaneless diffuser, because of the simplicity and low cost. Volutes have one exit path for the fluid while vaned diffusers have several channels formed by the vanes similar to the channels in the impeller. Vaned diffusers are used where space is limited, which is the case in ESP applications. A volute casing is shown in Figure 2.6.

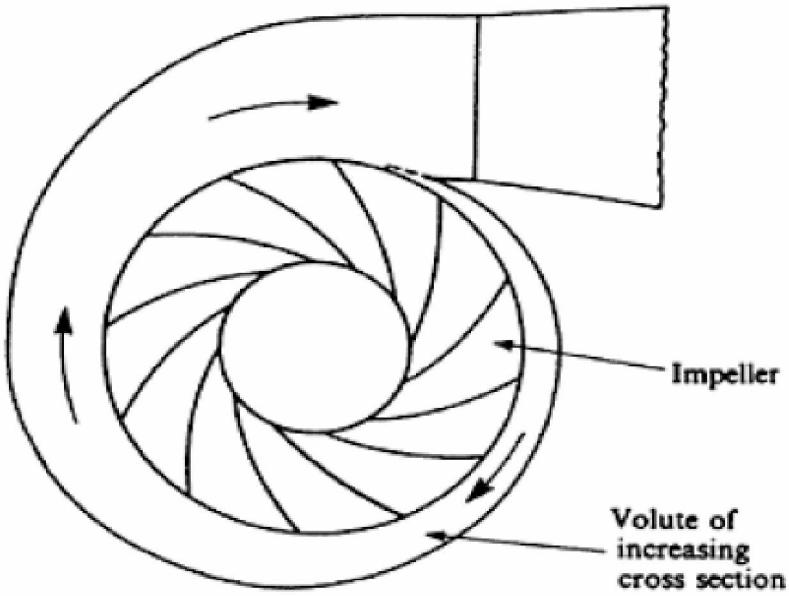

Figure 2.6 Volute Casing Pump Stage (Gorla and Khan 2003).

ESPs are mechanical systems with technology common to many other industries, however the application in oil and gas completions is unique and the technology has adjusted to suit the environment. Since pumps are used so frequently in many industries it is important to understand the different terminology and differences between pump systems. The initial design by Arutunoff for an ESP was used for dewatering ships and even today the pumps used in mine dewatering applications are sometimes manufactured by the same companies that supply the oil industry. Electric submersible pumps used as

sump pumps and sold at hardware stores follow the same principles on a much smaller scale. Other applications of submersible pumps include municipal water treatment and sewage pumping, industrial and slurry pumping, pond filters and fountains, and irrigation. In wellbore applications, ESPs are used in water wells and geothermal wells to move large amounts of water. In the oil industry, the term ESP is normally used to describe an artificial lift method of using a centrifugal pump and submersible motor (ESP system) to produce fluids to surface from deep in a wellbore to surface. Larger diameter high rate ESPs may be installed near the surface in a sump, or can, where they are called a Booster Pump or Canned Booster. Other methods of submersible pumping are used for artificial lift such as Electric Submersible Progressing Cavity Pumps (ESPCP) and hydraulic pumps, or jet pumps.

Centrifugal pumps are also used extensively in applications that are not submerged and the hydraulic performance is the same even though the motor construction and other components are different. Centrifugal pumps are used in fire protection for boosting water pressure, nuclear power plants, food processing, chemical plants, and for pumping cryogenics and refrigerants. Other applications in the oil industry include fluid boosting for transportation and boosting for injection. Centrifugal pumps are installed on surface where diameters are not restricted and the system is not submerged which allows the use of a conventional motor to operate the pump, this application, called a Horizontal Pumping System (HPS), is shown in Figure 2.7.

Due to the complexity of offshore operations, subsea pumping is a separate market from the traditional ESP market. Subsea pumps may be used in several applications, some of which are shown in Figure 2.8, and may include production fluid pumping from wellhead to an FPSO or other topside facility, water injection, and pipeline transportation. These pump systems are more complicated than onshore systems and can come in a modular form as shown in Figure 2.9. Subsea pumps can be centrifugal pumps or positive displacement. The most common positive displacement pump for subsea pumping is the

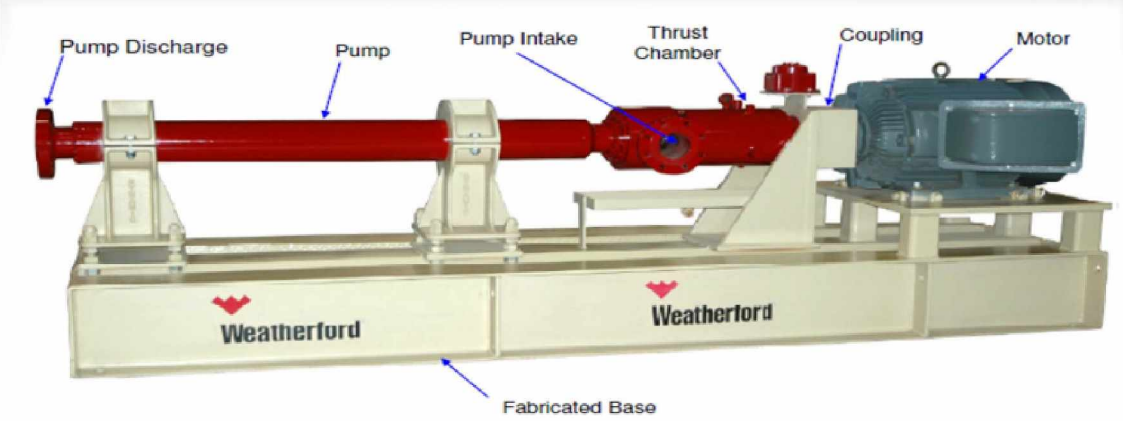

Figure 2.7 Horizontal Pumping System with Centrifugal Pump- HPS. (ifcpump.com)

twin screw type. In applications where the produced fluid contains a large amounts of gas, up to 100% in slugging conditions, a Multiphase centrifugal pump can be used. Subsea pumps can also be deployed via caisson or pod encapsulated.

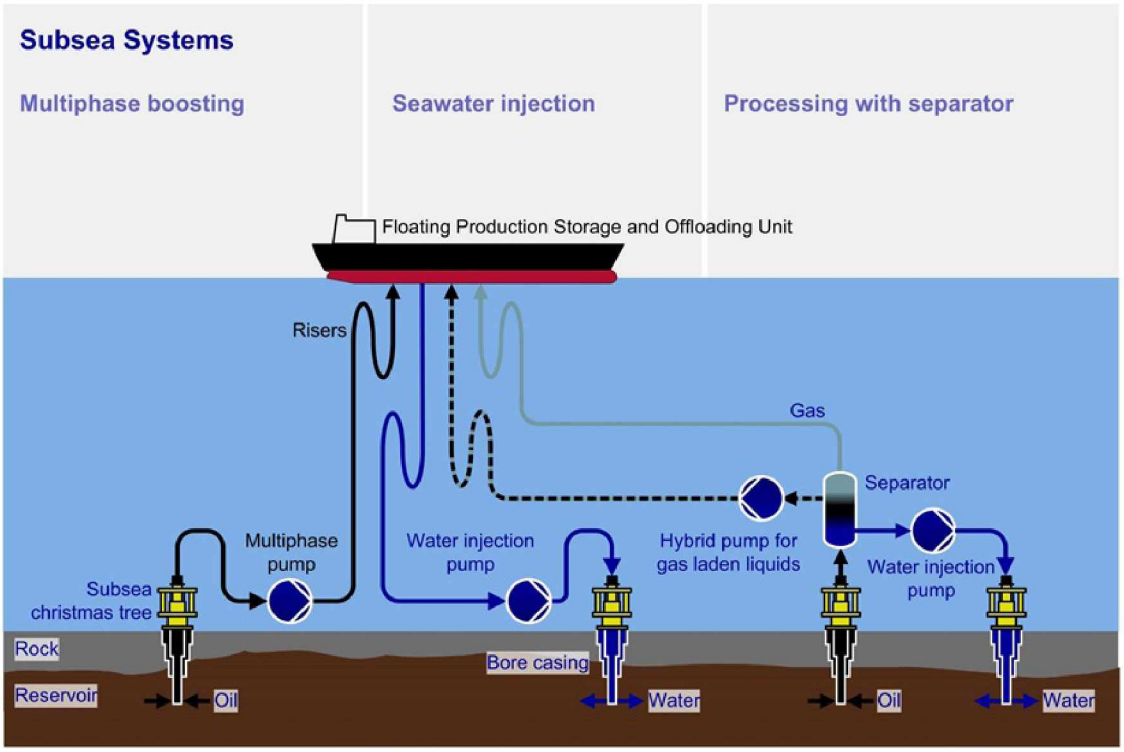

Figure 2.8 Subsea Pumping (Sulzer.com).

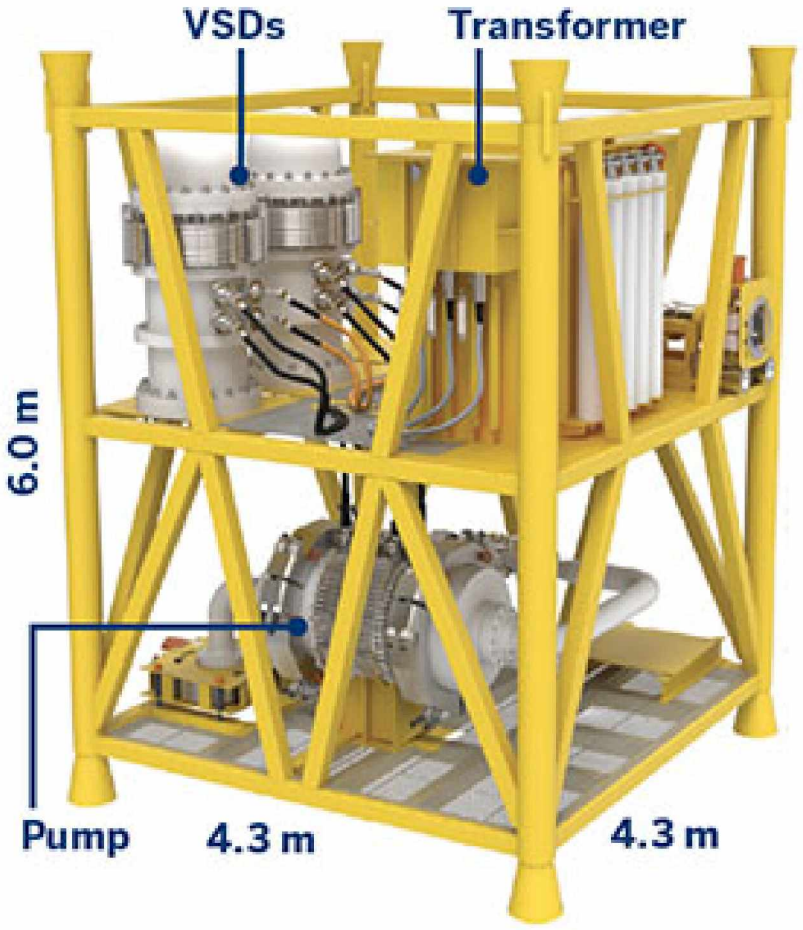

Figure 2.9 Modular Subsea Pump (OEDigital.com).

Pressure pumping is the application of pumps in cementing, or fracturing operations that require high pressure service. These applications typically use positive displacement reciprocating type pumps with a number of piston/plungers which are better suited than rotodynamic pumps. The number of piston/plungers can vary and includes duplex, triplex, quintuplex, and hex pumps. Triplex pumps are often used in drilling mud circulation where they are called mud pumps. Pressure pumping can also be applied to low pressure operations such as acid pumping and wireline pump down. Pressure pumping units can be quite large and trailer mounted as in Figure 2.10, and for a hydraulic fracturing operation several of these units may be required.

Figure 2.10 Pressure Pumping Unit (Pressurepumping.com).

The most obvious difficulty in applying ESPs to artificial lift vs surface pumping is the problem of a limited diameter. For ESPs to be most effective in achieving drawdown targets they need to be placed deep in a well and thus must be able to be deployed and operate within relatively small diameter pipes. This is why Arutunoff's invention was so important and formed the foundation for an entire industry. The electric motor and centrifugal pump were invented and in operation before Arutunoff but his application of a small diameter system deployed in a submerged environment and powered with a long electric cable was a very new solution. Many manufactures of pumps and motors never get into the ESP industry because the unique pump and motor requirements are quite different than for surface equipment. Typical ESP pump stages are between 3.38" and 6.75" OD, but the most common is 4.00" OD which translates to an impeller OD of 3". In comparison, a large dredge pump used in mining applications such as in Figure 2.11 commonly reach diameters of 55 inches but can be much larger (Wilson et al. 2006).

A significant amount of research has been directed at pump design to increase ESP component run life and decrease the cost of replacement, but the goal of this study is to

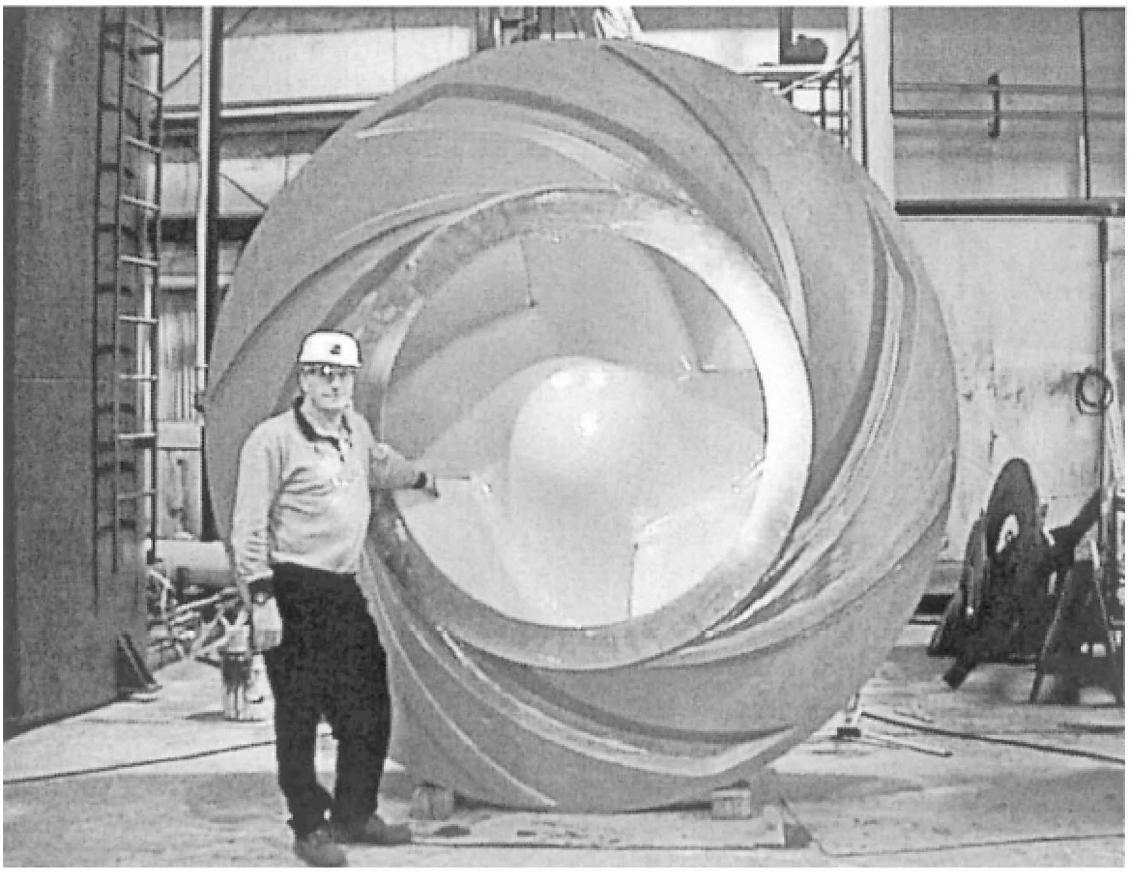

Figure 2.11 Large diameter dredge pump used in the mining industry (Wilson et al. 2006).

focus on the design as it relates to the hydraulic performance of the system. If the ESP cannot achieve the target flowing bottom hole pressure, then the run life may be a moot point. Operating conditions often change over time and external factors may preclude the use of other artificial lift methods for an ESP. ESPs run in many harsh conditions and the performance of the system is important for the successful implementation.

2.1 ESP's as an Artificial Lift Method

ESP's are a form of artificial lift that assist production with oil and natural gas wells by introducing energy into the fluid in the form of pressure. ESP's are the artificial lift option used most frequently to produce high rates and lift from wells of great depths. Historically ESP's were avoided for sandy, viscous, and high gas applications though technological advances have increased the range of applicability of ESPs to include a wider range of

operating conditions and fluids. Many of these advancements are in the reliability of the ESP and the ability of the system to operate without failure in harsh conditions. Some advancements in system design have also pushed the boundaries of what a centrifugal pump can effectively produce in terms of gas, viscosity, and solids. Several case studies have shown that ESPs can be used effectively in heavy oil and are beneficial for exploration and appraisal of heavy oil (Crossley 1986, Brennan et al 2011, De Leonardis et al 2017). ESP gauges can transmit data in real time via the ESP power cable to surface. The ability to vary the pump speed utilizing a surface variable speed drive (VSD) allows well testing procedures that generate important testing information such as the reservoir deliverability at very low bottom hole pressures.

The role of the ESP is to create a differential pressure to increase the rate of a naturally flowing well or to allow flow in a well that will not flow without artificial lift. The inflow and outflow curves of a flowing well are shown in Figure 2.12. In this case the well cannot produce naturally and a differential pressure is required by the pump. Including an ESP in this well could allow production.

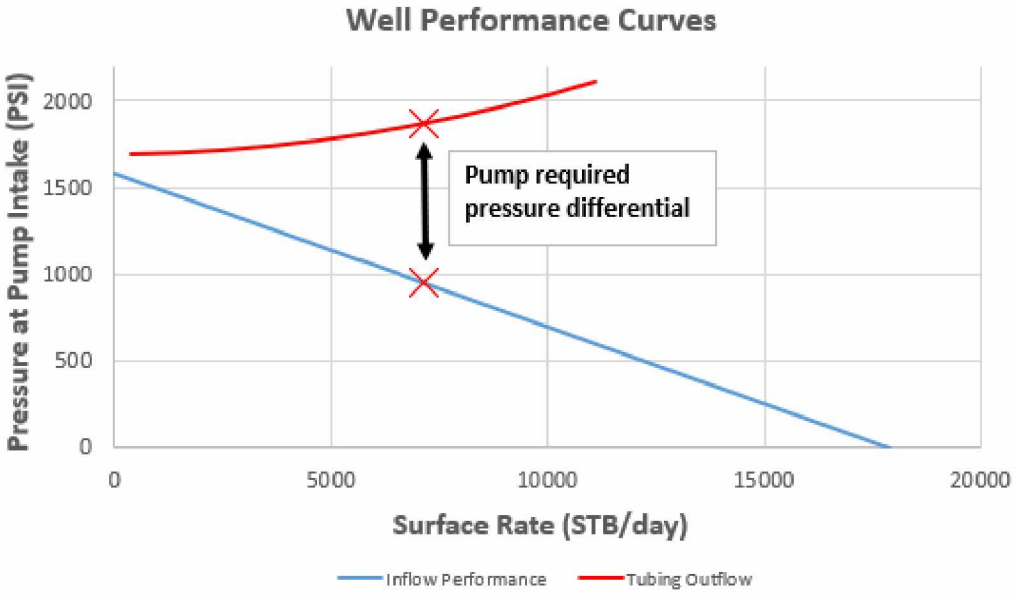

Figure 2.12 Well Inflow and Outflow well performance curves.

At the target rate, the difference between the Inflow and Outflow pressures is the required pressure differential the pump has to supply. This differential curve is shown in figure Figure 2.13, with the x axis adjusted to the total rate at pump intake conditions.

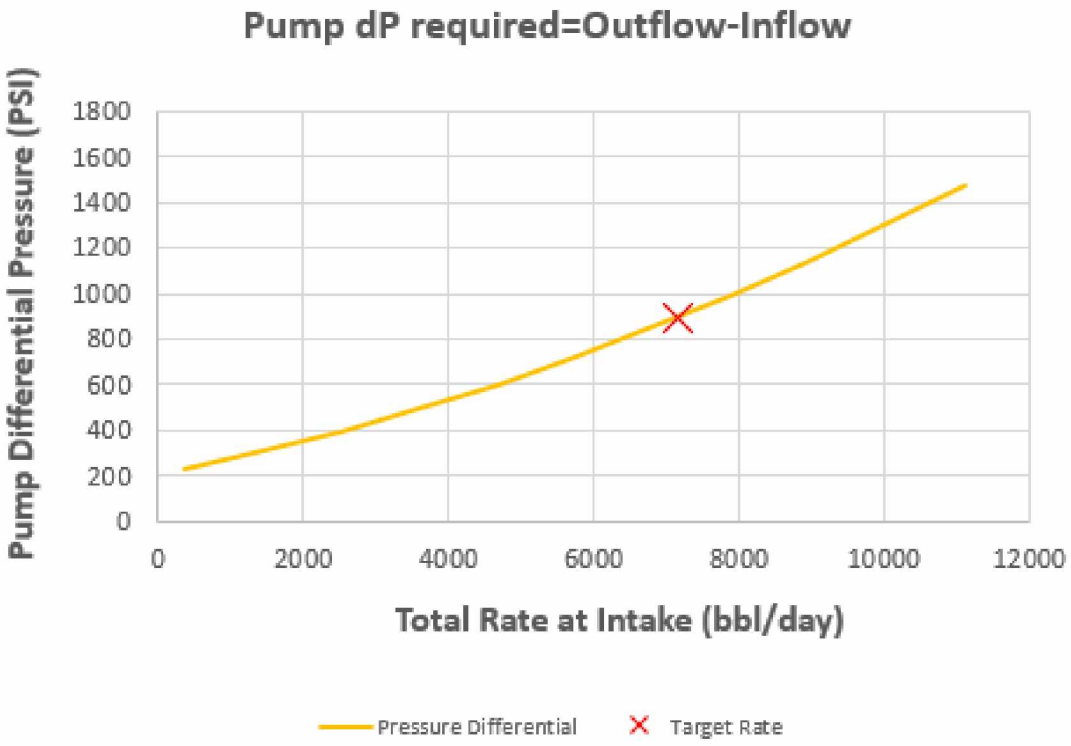

Figure 2.13 Pump Required Pressure Curve, converted to Rate at Pump Intake Conditions.

Pump performance curves are reported in feet of head with water. Converting the pressure differential curve to head by dividing the pressure by the fluid gradient allows direct comparison of the well performance and pump performance as shown in Figure 2.14. The intersection of the pump and well performance will depend on the quality of the data and calculations used to generate the curves. The well performance depends on well test quality and pressure traverse calculations, where different pressure drop correlations may need to be applied to find a good match for the well. The pump curve when reported with water needs to be adjusted for fluid properties, which is not always simple and is the reason for this research project.

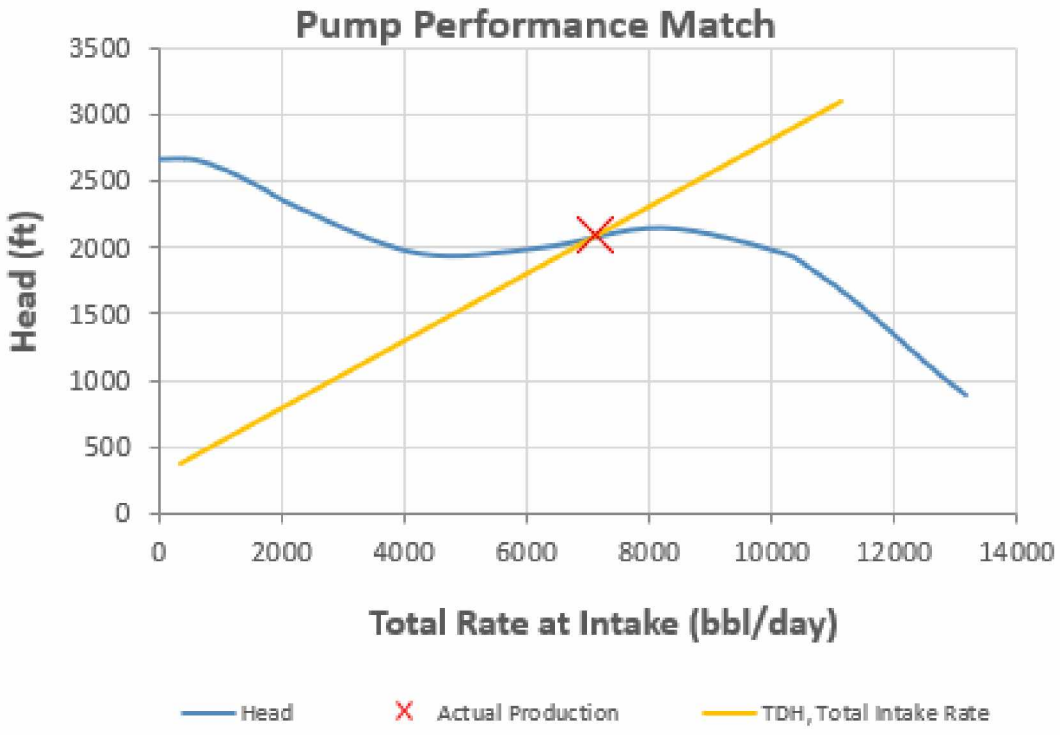

Figure 2.14 Pump Performance Match to Well Performance.

This basic principle of an ESP is adding pressure to the system to achieve a higher flow rate than could be achieved naturally. That is why ESPs are important in the completion of a well. There are many factors that complicate the system and make achieving this goal more difficult. On one hand, ESPs are mechanical and electrical systems that operate with rotating elements and amperage that tend to lead to failure over time. Since ESPs run on electrical power, they incur operating costs based on the electricity used and the initial installation can be quite expensive. If the costs outweigh the benefit then a different form of artificial lift may be necessary. The design of the components needs to last long enough to be economically viable and produce an incremental oil rate that offsets the cost of the system and the cost to replace it.

One method of increasing the interval between ESP replacements is to run multiple pump systems for full redundancy. When one system fails, the redundant system can

produce fluid while waiting on a rig intervention. Another common backup plan is to run gas lift design in conjunction with an ESP. If the ESP fails, gas lift backup can ensure some production from the well without costly rig work. ESPs can be run on Y-tools to allow the pump to sit offset to the tubing and allow wireline tools to run below the ESP. Normally the flow of fluid across the motor requires the pump to be set above the perforations, but shrouds can be installed that force the fluid to flow past the motor before entering the pump intake. This allows the pump to be installed below the perforations and can limit the free gas into the pump by letting the well naturally separate the liquid and gas.

Wet connect technology applied to ESPs allows the cable to be installed on the production tubing without the motor. The cable connects to a female wet connect system which requires a rig to install. The motor can then be run via wireline through the tubing with a male wet connect to make the connection downhole while submerged. This allows the motor, seals, and pumps to be deployed and replaced via much cheaper wireline operations rather than a heavy rig intervention. Another form of rigless ESP deployment uses coiled tubing with integral cable to deploy the system on a hydraulic unit without killing the well.

The hydraulic performance of an ESP determines how much pressure the pump can add to a system. Turbomachinery fundamentals are discussed in the next section to determine the theoretical boosting pressure of a pump.

2.2 Turbomachinery and Pump Fundamentals

Turbomachinery is a topic covered in most Fluid Mechanics textbooks and includes the fundamentals of centrifugal pumps. A turbomachine is a machine that exchanges energy between the continuous flow of a fluid and a continuously rotating blade system, with the energy exchange based on flow-generated forces. When energy from flow is used to drive rotating equipment, it is considered to be power delivering and includes different types of turbines. When power is received from a motor to be supplied to the fluid it is considered power receiving and includes pumps, compressors, blowers, and fans. If the fluid is

incompressible, or constant density, the term pump is generally used. If the fluid is compressible, the term used depends on the pressure ratio between discharge and intake pressure.

```
Compressor = high pressure ratio, P_2/P_1>2

Blower = intermediate pressure ratio 1.25<P_2/P_1<2

Fan = low pressure ratios P_2/P_1<1.25
```

The Hydraulic Institute has attempted to classify pumps based on mechanical design and distinguishes between two major classes of pumps: positive displacement pumps and dynamic displacement, sometimes called kinetic or rotodynamic pumps (ANSI/HI 2000). Centrifugal pumps are a subset of kinetic pumps and are also sometimes called velocity pumps due to their use of increased velocity to pump fluids. Centrifugal pumps can even further be classified as radial, axial, or mixed flow design based on the severity of the flow path through the pump. The rotating portion of the machine is called the rotor, or impeller in the case of ESPs. Turbomachines can be unducted with only a rotating element such as a windmill or ceiling fan, but in the case of ESP's the pump also includes a stationary casing that forms the flow passageway for the fluid called a diffuser. Vaneless diffusers are often called volutes and have one or more outlet paths, but ESP diffusers will have vanes similar to the vanes of an impeller.

The basis of turbomachine operation is the conversion of energy which follows the basic equations of conservation of energy, mass, and momentum. The equations can be derived from a simple depiction of an impeller with simple geometrical parameters, inlet radius, outer radius, channel height, and blade angle. The inlet and outlet conditions involve 3 velocity vectors each, one corresponding to the blade velocity, one corresponding to the fluid velocity, and the resultant velocity vector. From the conservation of angular momentum applied to the impeller in Figure 2.15, the shaft torque applied to a pump impeller is calculated using equation (2.1) where the subscripts are 1=inlet conditions, 2=impeller exit, r=radial, and θ=tangential or circumferential component.

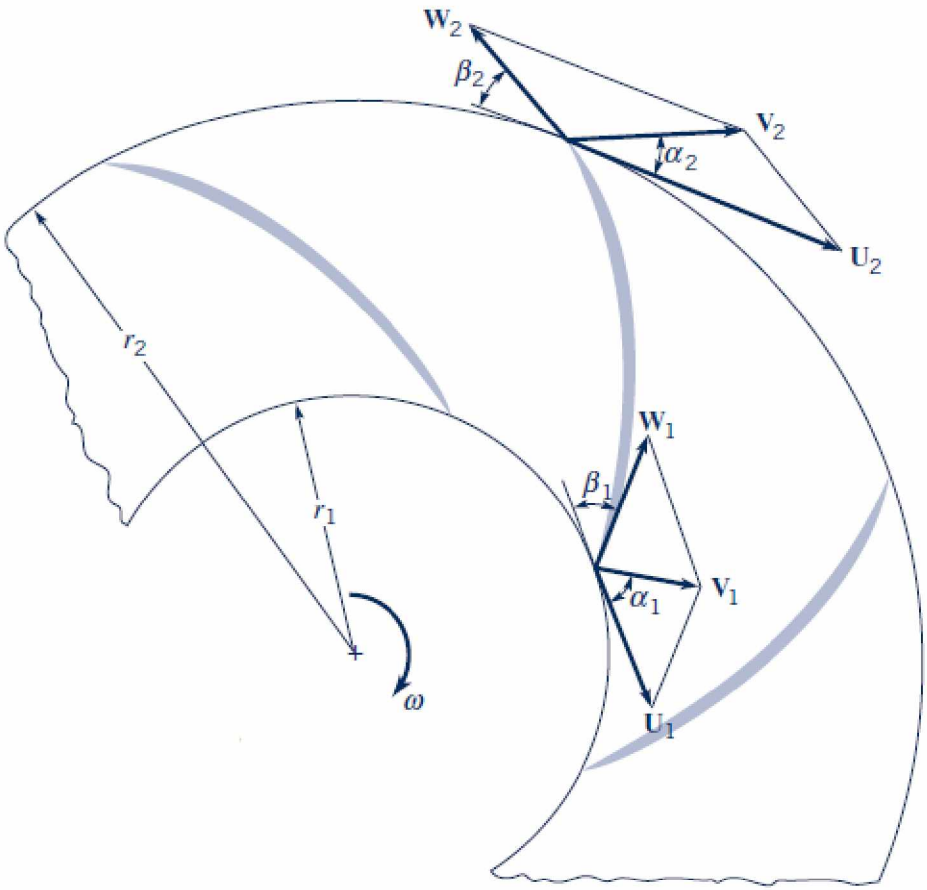

Figure 2.15 Velocity triangles.

$$T_{Shaft} = \dot{m}_2 r_2 V_{\theta 2} - \dot{m}_1 r_1 V_{\theta 1} \tag{2.1}$$

For $\dot{m}_1 = \dot{m}_2$ the shaft torque is 2.2.

$$T_{Shaft} = \dot{m}(r_2 V_{\theta 2} - r_1 V_{\theta 1}) \tag{2.2}$$

where T_{Shaft} = the shaft torque required to rotate the impeller, $\dot{m}$ = mass flow rate, r = radius of impeller, and V = absolute velocity. The inlet and outlet triangles with radial and tangential components are shown in Figure 2.16 and Figure 2.17.

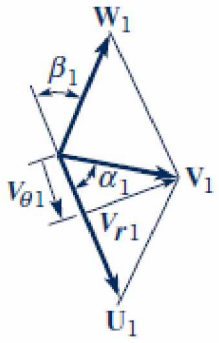

Figure 2.16 Inlet Velocity triangle.

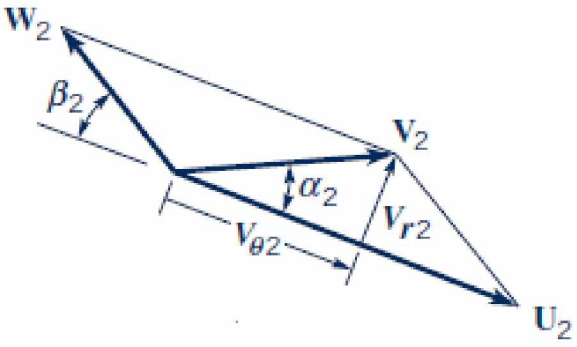

Figure 2.17 Outlet Velocity triangle.

Multiplying shaft torque by angular velocity results in the shaft power (2.3) and divided by mass flow rate equals specific work (2.4)

$$\dot{W} = T_{Shaft}\omega \tag{2.3}$$

$$\frac{\dot{W_{Shaft}}}{\dot{m}} = w_{Shaft} = \omega r_2 V_{\theta 2} - \omega r_1 V_{\theta 1} \tag{2.4}$$

where $\dot{W}$ = the shaft power required to rotate the impeller, ω = angular velocity, and w_{Shaft} = shaft specific work. Using the relation in (2.5) yields equation (2.6)

$$U = \omega r \tag{2.5}$$

where U=impeller blade velocity.

$$w_{Shaft} = U_2 C_{\theta 2} - U_1 V_{\theta 1} \tag{2.6}$$

This is the fundamental equation for the shaft work of a turbomachine where the work is positive for pumps and negative for turbines. This equation applies to compressible and incompressible flows and impellers of radial, mixed, or axial flow. For incompressible flow and the conservation of energy, specific work is defined in equation (2.7)

$$w_{Shaft} = (\frac{p_2}{\rho} + \frac{V_2^2}{2} + gz_2) - (\frac{p_1}{\rho} + \frac{V_1^2}{2} + gz_1) + losses \tag{2.7}$$

where p = pressure, ρ = density, V = aboslute velocity, g = gravitational constant, z = height. Combining equations (2.6) and (2.7) yields (2.8)

$$U_2 V_{\theta 2} - U_1 V_{\theta 1} = (\frac{p_2}{\rho} + \frac{V_2^2}{2} + gz_2) - (\frac{p_1}{\rho} + \frac{V_1^2}{2} + gz_1) + losses \tag{2.8}$$

and defining total head, H, with equation (2.9) and replacing each term on the right hand side of (2.8) yields equation (2.10).

$$H = (\frac{p}{\rho g} + \frac{V^2}{2g} + z) \tag{2.9}$$

$$\frac{U_2 V_{\theta 2} - U_1 V_{\theta 1}}{g} = H_{Out} - H_{In} - H_{losses} \tag{2.10}$$

The ideal head rise excluding losses is equation (2.12).

$$H_{Ideal} = \frac{U_2 V_{\theta 2} - U_1 V_{\theta 1}}{g} \tag{2.11}$$

To simplify even further, assuming no swirl as the fluid enters the impeller, at design point or best efficiency point (BEP) the inlet tangential component of absolute velocity, $V_{\theta 1}$, is negligible. The ideal head then simplifies to equation (2.12).

$$H_{Ideal} = \frac{U_2 V_{\theta 2}}{g} \tag{2.12}$$

From the velocity triangle at impeller exit Figure 2.17, equations (2.13) - (2.17) can be derived where the angle β_2 is measured opposite of the tip speed so that for backward curved vanes $\beta_2 < 90$ degrees, for forward curved vanes $\beta_2 > 90$ degrees, and for straight vanes $\beta_2 = 90$ degrees.

$$V_{\theta 2} = U_2 - V_{r2} \cot \beta_2 \tag{2.13}$$

$$H_{Ideal} = \frac{U_2^2}{g} - \frac{U_2 V_{r2} \cot \beta_2}{g} \tag{2.14}$$

$$V_{r2} = \frac{Q}{2\pi r_2 b_2} \tag{2.15}$$

$$H_{Ideal} = \frac{U_2^2}{g} - \frac{Q U_2 \cot \beta_2}{2\pi r_2 b_2 g} \tag{2.16}$$

$$H_{Ideal} = \frac{\omega^2 r_2^2}{g} - \frac{Q \omega \cot \beta_2}{2\pi b_2 g} \tag{2.17}$$

This is a usable form of the ideal head rise equation that depends only on parameters that we can obtain from a specific pump stage geometry and operating conditions. For straight vanes the second term on the right hand side of the equation goes to 0 so that head is independent of rate. For backward curved vanes the term is positive which means the head is decreasing with increasing rate, and for forward curving vanes the term is negative and is then additive and creates a head curve that increases with increasing rate. This effect of blade angle is shown in Figure 2.18. To calculate the total head for a housing of multiple pump stages, the individual stage head rise are added since the pumps are stacked in series. In surface applications it is common to run pumps in parallel, in this case

the pump rate of each pump is added instead of the head. So for the case of a multistage pump of only one stage type in the housing, the number of stages is multiplied by the head per stage to get the total pump head rise. This head is dependent on the speed of the pump and it is useful to compare the pump head at different speeds.

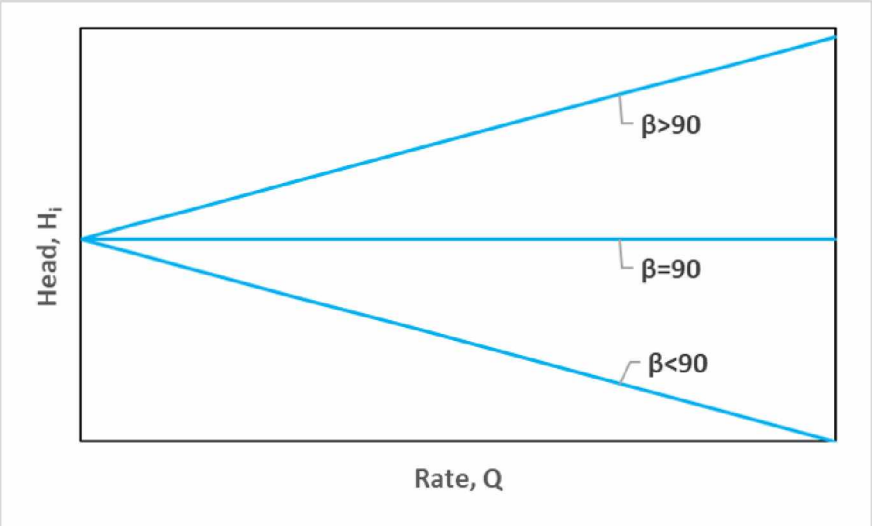

Figure 2.18 Effect of Impeller Blade Angle on Head Performance Curve.

Similarity of ESPs is used to generate pump performance curves and determine operating points for different operating speeds. Geometric similarity exists when the ratios of all corresponding linear dimensions are equal. Kinematic similarity exists when the ratios of the velocities are equal. Dynamic similarity exists when the ratio of forces are equal. If the similarity laws are satisfied, then the efficiency will also be equal. The representative values used to determine pump similarity are (N, Q, D, ρ, μ, gH). From these parameters and using the Buckingham Pi theorem, dimensionless groups can be obtained. The 4 most commonly cited terms in pump textbooks are the flow coefficient, head coefficient, power coefficient, and Reynolds number which are calculated in (2.18) - (2.21).

$$\Pi_1 = \frac{Q}{ND^3} \tag{2.18}$$

$$\Pi_2 = \frac{gH}{N^2D^2} \tag{2.19}$$

$$\Pi_3 = \frac{P_{Brake}}{\rho N^3 D^5} \tag{2.20}$$

$$\Pi_4 = \frac{\rho N D^2}{\mu} \tag{2.21}$$

where Q= Flow rate, N= Pump speed, RPM, D= Pump diameter, g= Gravitational constant, H= Head rise of the pump, P_{Brake}= Brake Horsepower, ρ= Density of the fluid, μ = Viscosity of the fluid.

From these dimensionless quantities and the assumptions of similarity we can see how changing values affects other parameters for similar pumps. The affinity laws are the relations that define the parameters. These can be used to compare pumps of different diameter or operating at different speeds. If the pump performance is known at one speed, usually tested on a flow loop, then the performance at another speed can be calculated. The pump curve is plotted for various speeds and is called the Tornado curve as shown in Figure 2.19. The affinity laws are fundamental to ESP performance and are calculated below.

$$Q_2 = Q_1 \frac{N_2}{N_1} (\frac{D_2}{D_1})^3 \tag{2.22}$$

$$H_2 = H_1 (\frac{N_2}{N_1})^2 (\frac{D_2}{D_1})^2 \tag{2.23}$$

$$P_{Brake2} = P_{Brake1} (\frac{N_2}{N_1})^3 (\frac{D_2}{D_1})^5 \tag{2.24}$$

The affinity laws are useful for generating performance of a pump at different speeds and diameter, but another useful value that is used to compare pumps og different

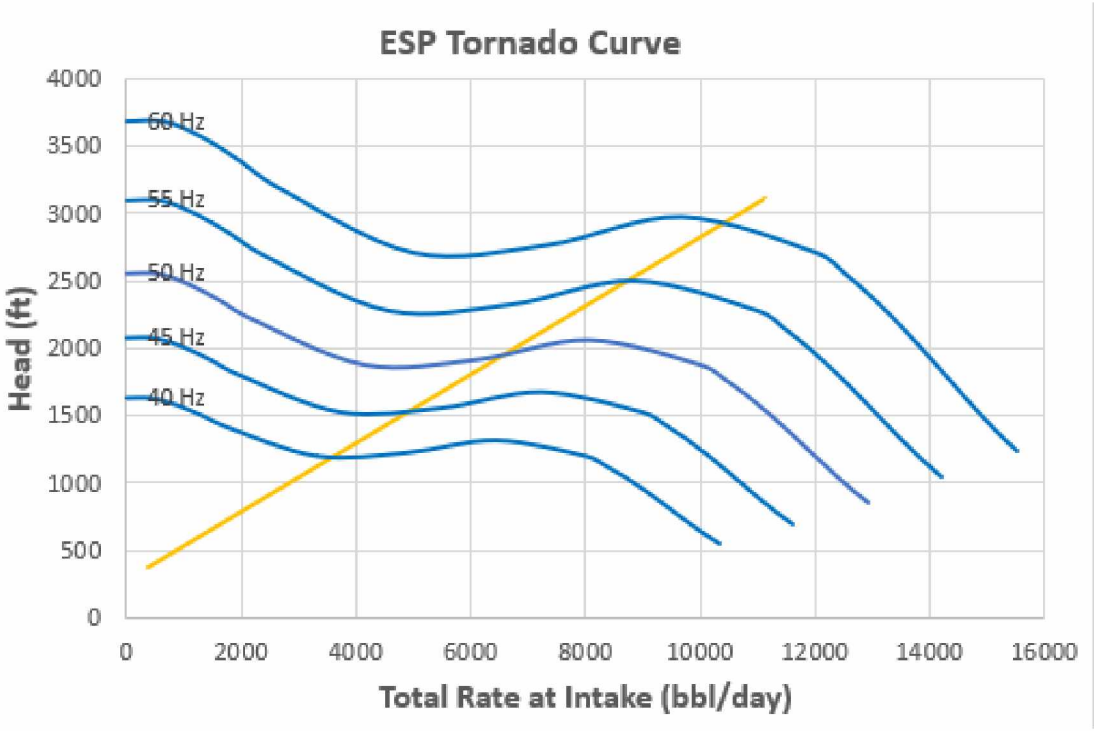

Figure 2.19 Tornado Curve Shows Pump Performance at Different Operating Frequencies.

geometries and designs is called specific speed. Specific speed is calculated by combining the rate and flow coefficients where the pump's BEP point head and rate are used for the calculation (2.25). For US oilfield units the equation is (2.26) where the gravitational constant is dropped and the rotational speed (N) is 3500.The specific speed can also be calculated for metric units by the following conversion (2.27) and sometimes a dimensionless value is also used (2.28).

$$N_s = \frac{\Pi_1^{0.5}}{\Pi_2^{0.75}} = \frac{N * \sqrt{Q_{BEP}}}{(gH_{BEP})^{0.75}} \tag{2.25}$$

$$N_s = \frac{3500 * \sqrt{\frac{Q_{BEP}}{34.296}}}{(H_{BEP})^{0.75}} \tag{2.26}$$

$$n_s = \frac{N_s}{51.6} \tag{2.27}$$

$$\omega_s = \frac{N_s}{2733.016} \tag{2.28}$$

Specific speed is commonly used to compare pumps performance to other pumps. Figure 2.20 shows the trend from radial to axial flow as specific speed is increased as well as some general pump curve characteristics.

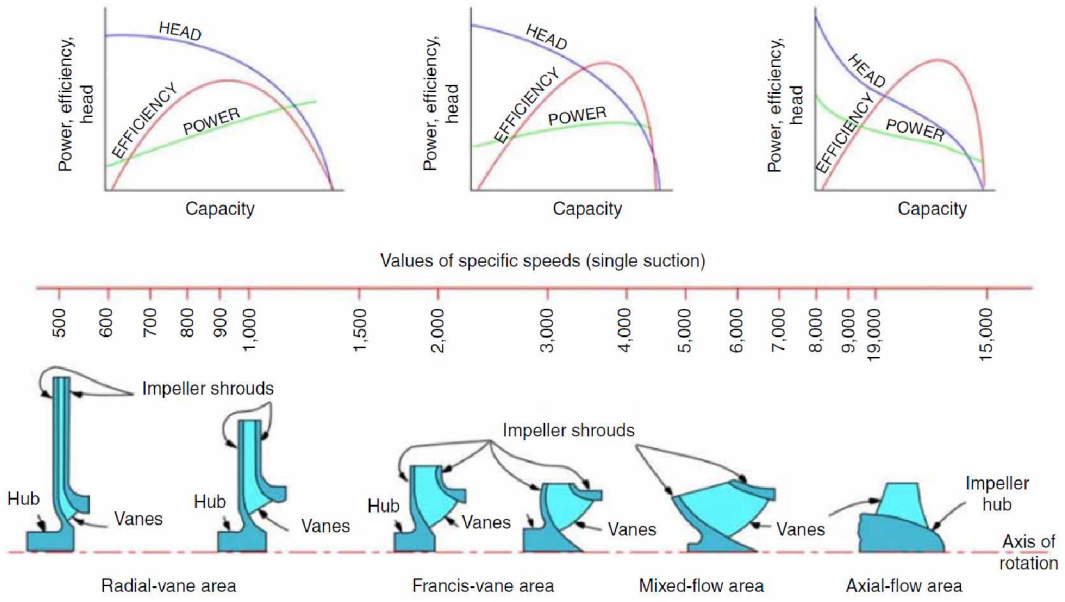

Fig. 1—Classification of centrifugal pumps on the basis of specific speed N_S.

Figure 2.20 Specific Speed for Different Pumps (Zhu et al. 2019 A).

Radial pumps tend to have an increasing power curve and the head curve slope decreases towards the shutoff head. In some cases these pumps head curve exhibits what is called Type F instability, or drooping curve instability, where the head capacity characteristic can have a maximum at $Q > 0$. This type of instability can occur with pumps of specific speed below around 1500. At higher specific speeds a different type of instability can occur called Type S instability, or saddle instability. These curves differ from the ideal Euler pump curve due to losses in real pumps. The next section discusses the operation of actual pump performance and the reasons and ways the performance differs from the ideal case.

2.3 Real Performance of Pumps

The actual pump performance listed in a pump providers catalog is determined using API RP 11S2 (1997). The practice uses water, SG=1, at 60 F as the testing fluid and requires testing head and brake horsepower of the pump over a range of flowrates including shutin (no flow), minimum recommended operating rate (Min ROR), best efficiency point rate (BEP), maximum recommended operating rate (Max ROR), and open flow. The curve is then polynomial fit to establish the catalog curves for head and brake horsepower vs rate. Efficiency (η) is calculated using (2.30) with the measured values of head in feet (H), flowrate in bbl/day (Q), and brake horsepower in hp (P_{Brake}). Efficiency is graphed as the third of the pump curves in a typical catalog such as in Figure 2.21. Each manufactured pump must fall within an allowable range of the published catalog curve for acceptance testing, +- 5% for head and rate, +-8% for BHP, and 90% of efficiency.

$$\eta = \frac{P_{Hydraulic}}{P_{Brake}} \tag{2.29}$$

$$\eta = \frac{HQ}{136,000 P_{Brake}} \tag{2.30}$$

This is the actual measured pump performance for a single stage in water, the efficiency is the hydraulic efficiency, and to apply to an application that only requires pumping clean water the curve only needs to be multiplied by the number of stages and corrected for operating speed using the affinity laws. To calculate the performance for an incomressible fluid with a different specific gravity, the head performance is unchanged and the hydraulic horsepower is multiplied by the specific gravity of the fluid, γ.

$$P_{Hydraulic} = \frac{HQ\gamma}{136,000} = \frac{Q(p_2 - p_1)}{58,773} \tag{2.31}$$

The polynomial for each pump is used as the basis for each pump's catalog operating performance. The conditions in the field are used to adjust the pump catalog curve for

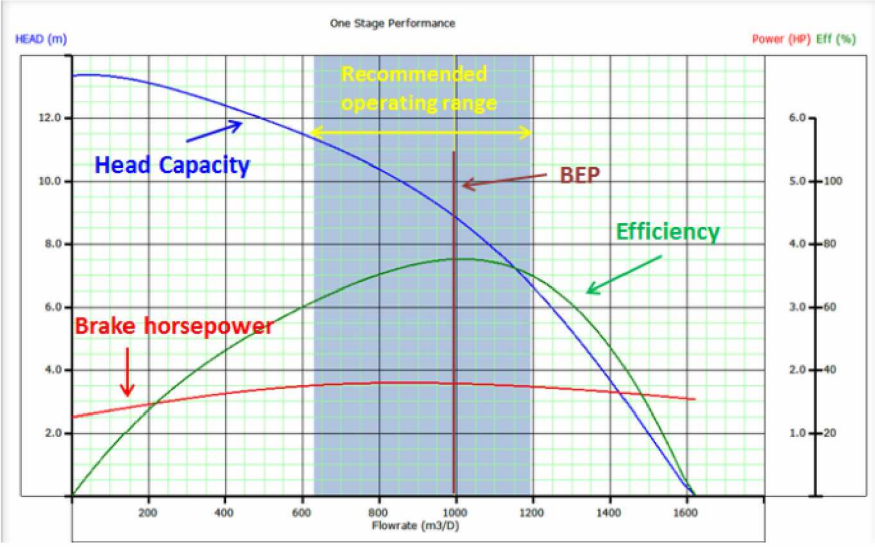

Figure 2.21 Typical Catalog Pump Curve with Head, Brake Horsepower, and Efficiency curves (Production-Technology.org).

fluid specific gravity, gas, viscosity, operating speed, and multiplied by the number of stages. Correlations used to correct for gas and viscosity have been developed with laboratory testing of many centrifugal pumps. These can be used to try to match field performance with actual performance, but using field experience for a particular field or reservoir can be used to design pumps more appropriately for the application once sufficient field data is available.

Studies have been carried out on pump performance to try to develop a mechanistic model of pump losses, but the number of different stage geometries and the complexity of the flow make generalizations difficult. Zhu et al. (2019) devised a mechanistic model that calculates losses of different types and sums up the losses to get to the actual head. The models were correlated with the pump stages available in the study and even among the studied stages the error was as much as 25%. Generalizing to other stages leads to a large margin of error.

It is worth looking at the loss models developed to understand what losses occur and why. Many of these studies are carried out in other industries and have developed loss models that accurately predict losses for very specific cases such as mixtures of only water

and sand or water and air. General loss types are shown in Figure 2.22 for pump head and Figure 2.23 for pump brake horsepower.

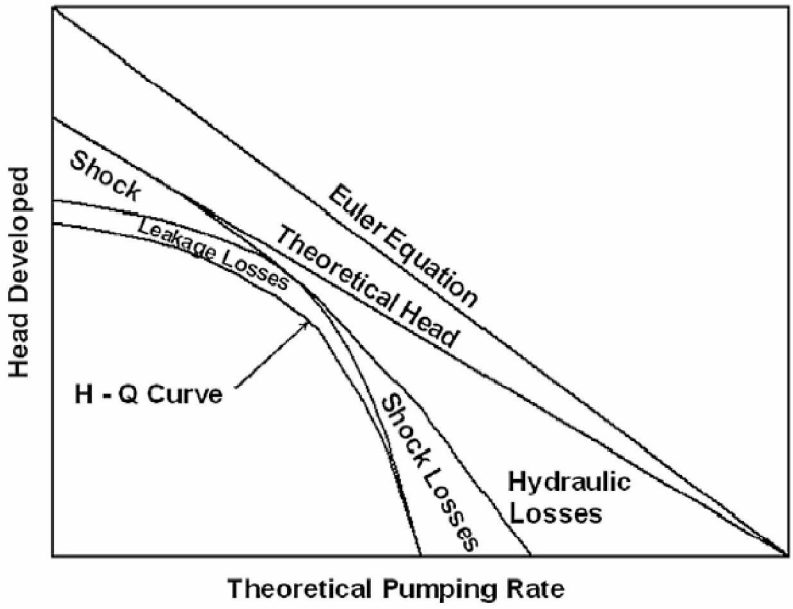

Figure 2.22 Losses Resulting in Decreased Pump Head and Rate (Takacs 2018).

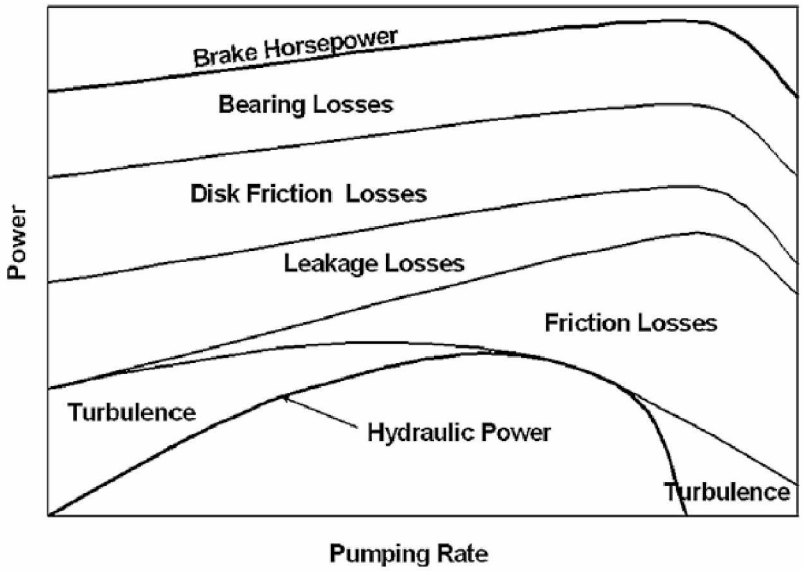

Figure 2.23 Losses Resulting in Increasing Brake Horsepower Required (Takacs 2018).

The head and rate losses start with the assumption of backwards curved blades, or $\beta_2 < 90$, in the ideal head equation. This is due to the significant losses in forward curving blades when pumping liquid. Forward curved blades are used in compressors where gas viscosity is much lower than water viscosity, but since pumps are designed to pump liquid the analysis assumes backwards curved blades and a downward sloping head curve.

Real flow departs from the ideal Euler head and must be taken into account for performance analysis of real pumps. The first deviation to consider is the slip factor. The impeller blade is very similar to the wing of a plane and the surface of the blade is not evenly loaded due to the distribution of velocity around the blades. This causes a higher pressure side and lower pressure side forming a pressure gradient in the blade channel. Due to the pressure gradient in the impeller passage, the fluid has a flow relative to the impeller that alters the relative exit velocity angle as shown in Figure 2.24 This phenomena is known as slip and is defined as the ratio of the tangential components of the absolute velocities for the actual blade angle and the relative flow angle. It is not an energy loss, only a factor that reduces the magnitude of the theoretical head an impeller can produce and is equivalent to an increased blade exit angle.

$$\sigma_s = \frac{C'_{\theta 2}}{C_{\theta 2}} \tag{2.32}$$

The most common correlation for calculating slip factor is from Wiesner (1967)

$$\sigma_s = 1 - \frac{\sqrt{\sin 90 - \beta_2}}{Z^{0.7}} \tag{2.33}$$

where σ_s=slip factor, Z= number of impeller blades. Another method of calculating slip factor comes from Zhu et al. (2019) and includes the specific speed and a reference specific speed determined experimentally

$$\sigma_s = 1 - \frac{\sqrt{\sin 90 - \beta_2}}{Z^{1.5\frac{N_{s,ref}}{N_s}^{0.4}}} \tag{2.34}$$

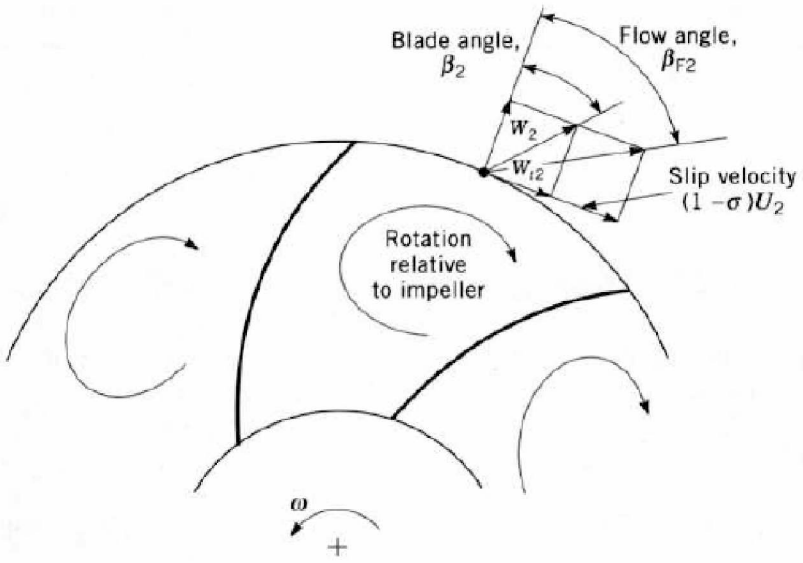

Figure 2.24 Slip Effect on Relative Flow Angle.

where N_s= specific speed, $N_{s,ref}$=reference specific speed. The ideal head equation including slip is

$$H_{Ideal} = \frac{\sigma_s \omega^2 r_2^2}{g} - \frac{Q\omega \cot \beta_2}{2\pi b_2 g} \tag{2.35}$$

The assumption that simplified equation (2.11) to (2.12) was that at BEP the inlet velocity does not have a tangential component. In reality the inlet velocity will deviate from the blade angle and a relative flow angle exists similar to the slip at the impeller exit. The difference between the inlet blade angle, β_1, and the flow angle, β_1', is called Incidence. Unlike the slip component, Incidence affects the pump curve as a hydraulic loss and reduces the pumps produced head at rates above and below BEP and is assumed negligible at BEP. The relative flow angle for rates above and below BEP are shown in Figure 2.25. Incidence at the impeller inlet is caused by pre-swirl and sudden change of flow direction that leads to flow separation often called shock losses.

Shock loss is calculated with empirical correlations, two examples are below from Stepanoff (1967) (2.36) and Zhu et al. (2019) (2.37).

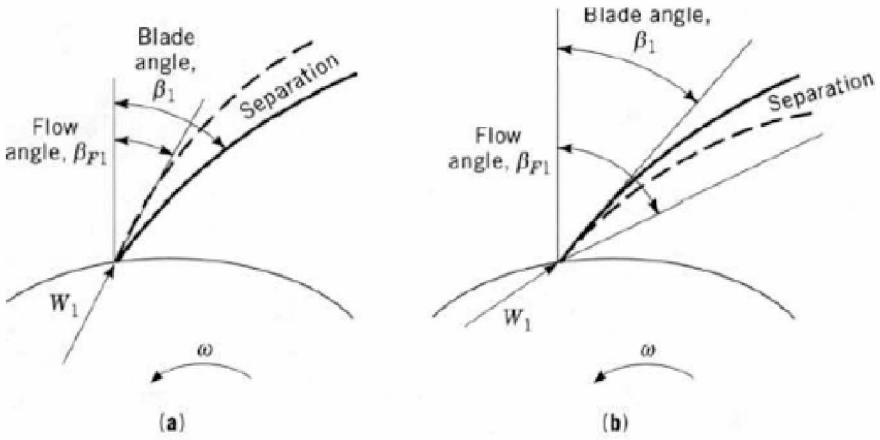

Figure 2.25 Incidence at pump inlet. (a) inlet flow rate $Q > Q_{BEP}$ (b) inlet flow rate $Q < Q_{BEP}$ (Tuzson 2000).

$$H_{Shock} = k_{Shock}(Q - Q_{BEP})^2 \tag{2.36}$$

$$H_{Shock} = f_{TI}\frac{V_I^2}{2g} \tag{2.37}$$

where k_{Shock} and f_{TI} are empirical constants, V_I is the flow velocity in the impeller.

Friction loss models also use empirical correlations to calculate a head loss coefficient. The friction loss in an impeller increases with increasing flow rate and is negligable at no-flow conditions. The Zhu et al (2019) mechanistic model calculates friciton losses with equation (2.38).

$$H_{Friction} = f_{FI}\frac{V_I^2 L_I}{2gD_I} \tag{2.38}$$

where f_{FI} is an empirical constant, L_I is the impeller length, D_I is the impeller diameter. Leakage losses and recirculation losses are not as well defined but there are correlations that attempt to calculate these losses. The impeller and diffuser have clearances that allow fluid leakage and recirculation that requires energy input but does not contribute to increased fluid head. These losses are greatest at low flow rates where pump head is the

greatest. Calculations for these losses from Zhu et al (2019) are below.

$$H_{Recirculation} = \frac{C_2^2 - C_{2E}^2}{2g} \tag{2.39}$$

$$H_{Leakage} = \frac{3V_L^2}{4g} + f_{LK}\frac{V_L^2 L_G}{2gS_L} \tag{2.40}$$

where C_2 is the absolute velocity at the blade exit, C_{2E} is the effective velocity at the blade outlet, f_{LK} is an empirical constant, L_G is the leakage gap length, S_L leakage gap area.

Zhu et al. (2019) define another loss that is not found in other literature called Shearing factor. For a fluid with viscosity equal to water the factor is 0, but for more viscous fluids an empirical correlation is calculated below. Section 3.1 discusses viscosity effects in more detail.

$$\delta = \frac{\frac{\mu_w}{\mu}^{0.1}}{1 + 0.02(R_{eC})^{0.2}} \tag{2.41}$$

$$R_{eC} = \frac{\rho V_S D_C}{\mu} \tag{2.42}$$

$$D_C = \frac{2\pi R_2}{Z}\sin\beta_2 - T_B \tag{2.43}$$

where R_{eC} is the Reynolds number due to shear velocity, V_s is shear velocity, D_C is the representative diameter at impeller outlet, T_B is blade thickness.

In turbomachinery, pumps are generally described for applications of incompressible flow, however ESPs produce oil and gas. It is worth looking at the design of Compressors and the changes necessary to take compressibility into account. The Euler equation remains the same for this case since it is a generalization of the exchange of energy, but the affinity laws need to be adjusted for additional parameters. The head (H) is replaced by the pressure ratio at inlet and outlet conditions (P2/P1). The flow rate (Q) is replaced by

the mass flow rate $\dot{m}$. Utilizing the ideal gas equation $\rho = PM/RT$, the functional parameters are $(p_1, RT_1, R_T 2, \dot{m}, N, D, \rho)$. A couple new Pi groups are obtained, mainly the Mach number, Temperature ratio, and rate parameter

$$\Pi_5 = \frac{ND}{\sqrt{kRT}} = \frac{V}{\alpha} \tag{2.44}$$

$$\Pi_6 = \frac{T_2}{T_1} \tag{2.45}$$

$$\Pi_7 = \frac{\sqrt{\frac{\dot{m}}{RT_1}}}{p_1 D^2} \tag{2.46}$$

where α is the speed of sound in the fluid, k is the ratio of heat capacities $\frac{C_P}{C_V}$, R is the universal gas constant or difference of heat capacities $(C_P - C_V)$. For a compressor pumping pure gas, the compressor horsepower required is

$$P_{Compressor} = \frac{k}{k-1} Q_{gas} * p_1 * \ln\left(\left(\frac{p_2}{p_1}\right)^{\frac{k}{k-1}} - 1\right) \tag{2.47}$$

For the case of multiphase flow which is common in oil and gas production, the ideal power required is somewhere between the extreme cases of an Isentropic process and an Isothermal process (k=1). The actual ideal power for multiphase flow can be modeled with a polytropic process (k=n)

$$P_{Isothermal} = \frac{Q_{liquid} H}{136,000} + \frac{Q_{gas} * p_1}{58,773} * \ln(\frac{p_2}{p_1} - 1) \tag{2.48}$$

$$P_{Isentropic} = \frac{Q_{liquid} H}{136,000} + \frac{k}{k-1} \frac{Q_{gas} * p_1}{58,773} * \ln((\frac{p_2}{p_1})^{\frac{k}{k-1}} - 1) \tag{2.49}$$

$$P_{Polytropic} = \frac{Q_{liquid} H}{136,000} + \frac{n}{n-1} \frac{Q_{gas} * p_1}{58,773} * \ln((\frac{p_2}{p_1})^{\frac{n}{n-1}} - 1) \tag{2.50}$$

where n is the polytropic index. Since a multiphase process is not hydraulic, the original definition of efficiency using hydraulic horsepower is no longer directly applicable, though it is still useful. Other useful definitions of efficiency are below. Effective efficiency

$$\eta_{Effective} = \frac{P_{Polytropic}}{P_{Hydraulic}} \tag{2.51}$$

Mechanical efficiency

$$\eta_{Mechanical} = \frac{P_{Polytropic}}{P_{Brake}} \tag{2.52}$$

Process efficiency

$$\eta_{Process} = \frac{P_{Polytropic}}{P_{Isentropic}} \tag{2.53}$$

and Pump efficiency

$$\eta_{Pump} = \frac{P_{Isothermal}}{P_{Brake}} \tag{2.54}$$

The efficiency of a pump can be described by several metrics depending on the chosen ideal case. Since the pump is not truly adiabatic there is some heat transfer in the process and can be calculated based on the heat produced by the pump due to inefficiencies and heat absorbed by the fluid.

$$Q_{Produced} = 42.41 * (P_{Brake} - P_{Polytropic}) \tag{2.55}$$

$$Q_{Absorbed} = \frac{350}{1440} * Cq\gamma\Delta T \tag{2.56}$$

$$\Delta T = \frac{H(1-\eta)}{778 * C * \eta} \tag{2.57}$$

where γ is specific gravity, q is flow rate in bbl/day, T is temperature in degrees F, C is specific heat in BTU/lb/F and equals 1 for water and 0.5 for methane.

Electric submersible pumps impart velocity to wellbore fluid through centrifugal action. The performance of an ESP is heavily determined by the fluid properties being pumped. This pumping mechanism is most effective at generating pressure at higher fluid densities and low viscosities. The next chapter deals with fluids encountered in oil production and the effects on ESP performance.

CHAPTER 3

FLUIDS AND DISPERSIONS

Understanding how fluids and solids effect ESP performance requires a deeper understanding of the fluids. This chapter defines what fluids, and sometimes solids, ESPs are likely to pump and some of the methods to correct the performance curves. Some definitions and concepts are introduced. Fluids are aggregations of molecules which are distributed in space not in a fixed lattice but freely moving. In general, liquid molecules are spaced closely compared to gas molecules. The spacing between molecules is also large compared to the diameter of the molecules but can be ignored if we are concerned with the properties of a large control volume of fluid. A large volume can be defined as greater than a limiting value of $10^{-}9\ mm^3$ for liquids and gases at atmospheric pressure as shown in Figure 3.1 (White, 2011). If the volume of fluid is too large though, the properties may not be represented by a single value. In most Engineering problems the dimensions are greater than the limiting value and the fluid properties can be modeled as varying smoothly and continuously so that differential calculus applies to analyze the fluid.

This modeling of the mechanical behavior of materials as a continuous mass rather than as discrete particles is called Continuum Mechanics and the governing equations are the conservation of mass, momentum, and energy. Continuum Mechanics includes the studies of Fluid Mechanics, Solid Mechanics, and Rheology (the study of materials with both solid and fluid characteristics).

Fluids in oil and gas production can involve a large number of components. The properties of these fluids and their interactions will determine how they affect the ESP system. Complex non-linear behavior and phase change complicate the calculations of fluid properties needed for flow equations. Fluids can be compressible or incompressible, viscous or inviscid, Newtonian or non-Newtonian, have elastic or plastic behavior, and can be

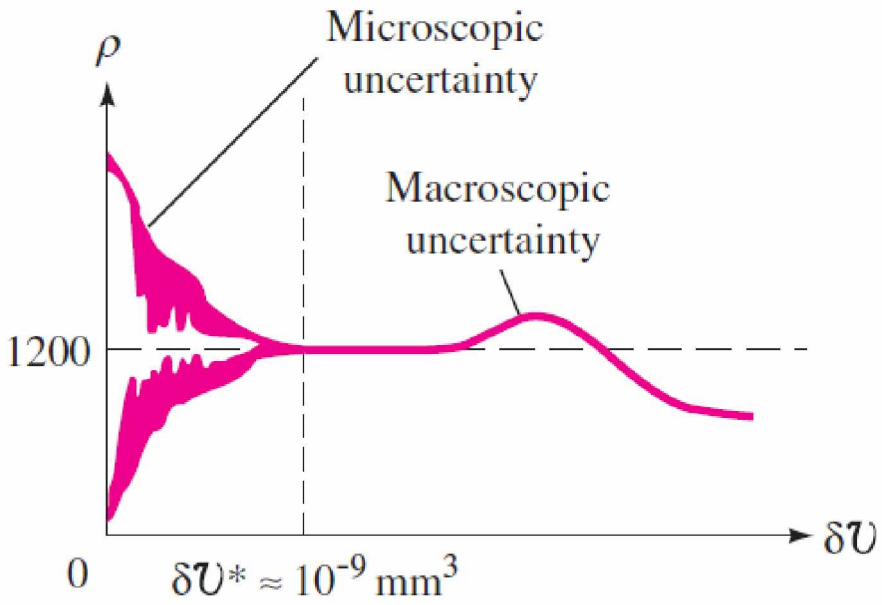

Figure 3.1 Fluid Properties for a Continuum where δv is the control volume (White, 2011).

affected by surface forces and body forces. Flow may be steady state or transient, turbulent or laminar, subsonic or supersonic. We can observe behavior of a fluid from an absolute reference frame with fixed coordinates, or a relative reference frame as a co-rotating observer. Common fluids in oil production include oil with its variety of components including asphaltene, paraffin, and scale, natural gas, H2S, fines or solids from the reservoir, produced water, frac sand flowback from completion operations, and completion fluid. If injection occurs adjacent to a producer an ESP may also encounter injection water with different properties than produced water, steam, polymer, and CO2 from flooding operations.

When the system is complex, you have to extend investigation from fluid properties to include the interactions between particles, whether fluid or solid. This modeling of interactions is a separate area of literature called Interfacial and Colloid Science. The main deviation in this area is that the assumption of a Continuum is not assumed on the scale of interfaces and for very small particles the microscopic uncertainty that could be ignored now has to be investigated. The science behind these interactions is beyond the scope of an

introductory Fluid Mechanics course but introduces important concepts that help solve Engineering problems, both quantitatively and qualitatively. The concepts are complicated and can get very application specific, but highlights can hopefully glean information about where to look for new information.

The next sections delve into how certain fluids effect ESP performance. Starting with the easiest fluid, water, and then how increasing viscosity, gas fraction, solids, and dispersions. Any fluids not specifically covered should have a basis for what properties are important for ESP lift.

3.1 Water, Oil, and Viscosity

Water is the standard fluid against which all ESPs are tested to API specifications. When pumping fluids other than water, the pump performance needs to be corrected. For the simplest case of a fluid with constant density, the correction is as simple as dividing the Brake Horsepower by the fluid specific gravity. The pump head curve is unchanged by a change in density, but the fluid specific gravity will determine the pressure rise across the pump. A more difficult case is a fluid with higher viscosity than water. Viscosity, or the resistance to deformation, has a detrimental effect on ESP performance by increasing Brake Horsepower required while simultaneously decreasing the head rise and rate through the pump. This has an overall effect of decreasing the pump efficiency, somtimes significantly. There are few instances where the opposite has been shown for small increases in viscosity. Guang (2000) describes this phenomena as Sudden Rising Head Effect which occurs in some low Specific Speed pumps when an increase in viscosity transitions the boundary layer flow in the ESP channels from hydraulically rough to hydraulically smooth. The increase in viscosity decreases the Reynolds number resulting in lower friction losses up to a limiting viscosity, which in Guang's study was 29 centiStokes (cSt). Above this viscosity the losses due to skin friction increase dramatically as is more typical of ESP performance, this effect is shown in Figure 3.2.

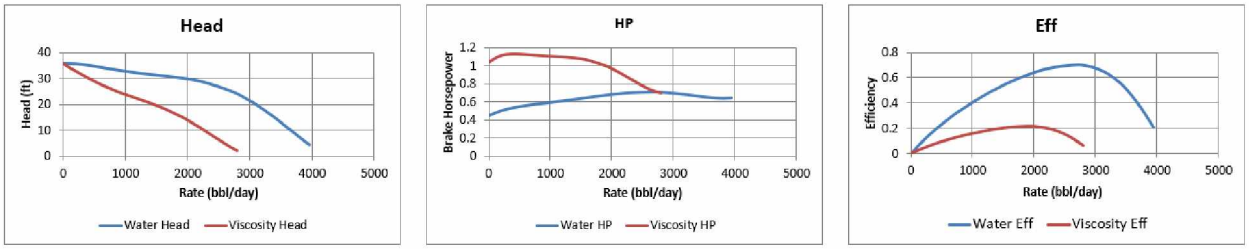

Figure 3.2 Viscosity Corrections to Pump curve Performance show reduced head, rate, and efficiency with increased Brake Horsepower required.

Centrifugal pump correction factors for viscosity have been around since at least 1926, the same year an ESP was first installed in the oilfield by Arutunoff (Daugherty 1926). Stepanoff (1940, 1949, 1967) provided diagrams for correcting pump performance based on experimental results with oils up to 2000 cSt. First, a parameter similar to the Reynolds number is calculated and used to locate the correction factor for pump head at BEP in oil, H_{oBEP}

$$R_{Stepanoff} = 248,387 \frac{Q_{wBEP}}{D\nu_o} \tag{3.1}$$

where Q_{wBEP}= the pump rate at BEP with water, D = pump diameter, ν_o= kinematic viscosity of the oil. The pump rate with oil is then calculated from the correct value of H_{oBEP}

$$\frac{Q_{wBEP}}{Q_{oBEP}} = \frac{H_{wBEP}}{H_{oBEP}}^{1.5} \tag{3.2}$$

where Q_{oBEP}= the pump rate at BEP with oil. Another common correction method was developed by the Hydraulic Institute (1969) with correction factor diagrams developed using single stage pumps at low rotational speeds. Turzo et al. (2000) later converted the Hydraulic Institute diagrams to equations to calculate correction factors for pump rate, head, and efficiency.

$$Q_{oil} = C_Q Q_w \tag{3.3}$$

$$H_{oil} = C_H H_w \tag{3.4}$$

$$\eta_{oil} = C_\eta \eta_w \tag{3.5}$$

Where C_Q, C_H, and C_η are correction factors to convert the pump performance curve with water to performance with viscous oil. The corrections are calculated using an adjusted rate, Q^*, which is dependent on $H_{w,BEP}$, $Q_{w,BEP}$, and kinematic viscosity of the oil, ν.

$$y = -7.5946 + 6.6504 * ln(H_{w,BEP}) + 12.8429 * ln(Q_{w,BEP}) \tag{3.6}$$

$$Q^* = exp(\frac{39.5276 + 26.5605 * ln(\nu) - y}{51.6565}) \tag{3.7}$$

$$C_Q = 1 - 4.0327 * 10^{-3}(Q^*) - 1.724 * 10^{-4}(Q^*)^2 \tag{3.8}$$

$$C_\eta = 1 - 3.3075 * 10^{-2}(Q^*) + 2.8875 * 10^{-}4(Q^*)^2 \tag{3.9}$$

The head correction factor is calculated at 4 points at fractions of BEP (0.6, 0.8, 1.0, and 1.2) and the pump curve is drawn through these 4 points and the shut-in head from the water curve.

$$C_{H,0.6} = 1 - 3.68 * 10^{-3}(Q^*) - 4.36 * 10^{-}5(Q^*)^2 \tag{3.10}$$

$$C_{H,0.8} = 1 - 4.4723 * 10^{-3}(Q^*) - 4.18 * 10^{-}5(Q^*)^2 \tag{3.11}$$

$$C_{H,1.0} = 1 - 7.00763 * 10^{-3}(Q^*) - 1.41 * 10^{-}5(Q^*)^2 \tag{3.12}$$

$$C_{H,1.2} = 1 - 9.01 * 10^{-3}(Q^*) + 1.31 * 10^{-}5(Q^*)^2 \tag{3.13}$$

Another method of accounting for viscous fluids comes from Riling (1975) and Sheth and Crossley (2009) where pump stages are tested directly with liquid of various viscosity instead of water. A table as in Figure 3.3 could then be used to calculate the performance at various viscosities using equations (3.3) - (3.5). Ideally these curves would be generated by the manufacturer for each stage to give accurate corrections that can be used with only a viscosity in Saybolt Universal Seconds (SSU). Unfortunately the testing is time consuming and has not been performed for a majority of pumps. This correction differs from the Hydraulic Institute in that it decreases the pump shut-in head which more accurately describes the performance of pumps from testing.

The mechanistic model from Zhu et al. (2019) has already been discussed in regards to loss models in Section 2.3. This model starts with the Euler pump head and uses loss models to calculate the actual pump performance. The pump water curve is used to tune the loss models to get a best fit for the water curve and then with tuned parameters the viscous curve is developed. The Shearing factor, (2.41), takes viscosity into account in the recirculation losses. The friction loss also takes viscosity into account implicitly with the empirical friction factor.

Correction factors for viscosity generally assume that the fluid behaves as a Newtonian purely viscous fluid. The dynamic viscosity, measured in centipoise, and kinematic viscosity, dynamic viscosity divided by density, do not change with a change in shear rate or shear stress. A graph of shear stress and shear rate would create a straight line where the slope is equal to the dynamic viscosity. This graph is called a Rheogram and is helpful for comparing the behavior of fluids that do not behave as a simple Newtonian fluid. Several non-Newtonian fluids are shown in the Rheogram in Figure 3.4. Non-Newtonian fluids and their effects are discussed in Section 3.4. The next section will first introduce gas

	Correction Factors			
Viscosity (SSU)	Capacity	Head	Efficiency	BHP
50	1.000	1.000	0.945	1.058
80	0.980	0.990	0.870	1.115
100	0.970	0.985	0.825	1.158
150	0.947	0.970	0.736	1.248
200	0.924	0.958	0.674	1.341
300	0.886	0.933	0.566	1.460
400	0.847	0.909	0.497	1.549
500	0.819	0.897	0.462	1.590
600	0.792	0.883	0.434	1.611
700	0.766	0.868	0.410	1.622
800	0.745	0.858	0.390	1.639
900	0.727	0.846	0.368	1.671
1,000	0.708	0.833	0.349	1.690
1,500	0.659	0.799	0.307	1.715
2,000	0.621	0.771	0.272	1.760
2,500	0.590	0.750	0.245	1.806
3,000	0.562	0.733	0.218	1.890
4,000	0.518	0.702	0.278	2.043
5,000	0.479	0.677	0.149	2.176

BHP, brake horsepower.

Figure 3.3 Viscosity Corrections for a pump given by pump manufacturer.

and its effect on pump performance.

3.2 Gas

Natural Gas production is an inevitable side effect of producing oil. Gas effects ESP systems in several ways and the effects are not necessarily negative. When the gas gets to the pump intake it has two possible routes to surface, up the casing/tubing annulus or into the pump intake through the pump and up the tubing. The preference of gas migration is dependent on the fluid viscosities and velocities which are in turn dependent on the inclination at the set depth of the pump. If a packer is installed above the pump and the annulus path is blocked, then the only flow path is through the pump and tubing. The tubing pressure traverse from surface to the pump discharge will be reduced with higher

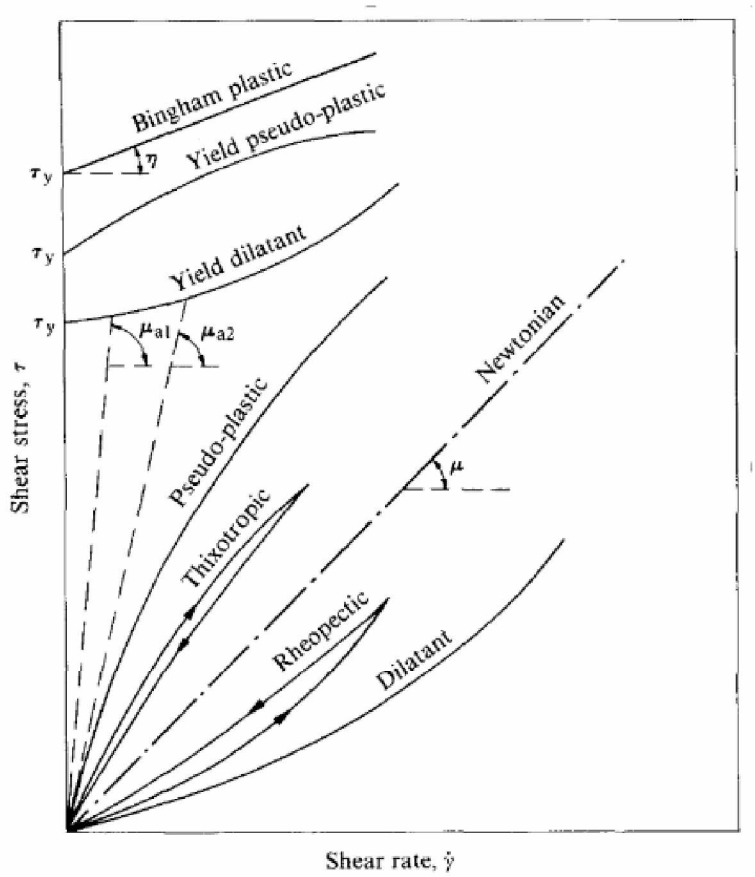

Figure 3.4 Rheogram for Several non-Newtonian Fluid Behaviors as well as the Linear Newtonian Line (Walker and Goulas 1984).

rates of gas up the tubing similar to the effect of gas lift. At reduced discharge pressure requirements, the pump should be able to attain a lower bottomhole pressure, or intake pressure, with the same boosting pressure. The downside of producing gas up the tubing is that it has to first go through the pump, and in general pumps do not handle gas well unless they are specifically designed to do so. Gas into the pump increases the total fluid rate through the pump, moving the operating point to the right on the pump head curve which decreases the pumps produced head at constant speed. The mixture specific gravity will be reduced with larger gas volumes which decreases the boosting pressure of the pump. The largest problem with gas interacting with the pump is gas surging and gas locking. If the gas fraction becomes too high the pump can cease to generate enough head to lift the

fluids to surface, this causes a stall, or gas lock. With a no flow condition the cooling effect of flowing fluid across the motor is stopped and the motor can overheat. In extreme gas locking wells the ESP operates in cycles of gas locking, the motor heats up and cools down with this cycle. If the system is designed properly the surface drive will shut down before the motor reaches a level that could cause permanent damage to the components. The system stays down for a period of time that allows the fluid to equalize and the density difference allows the gas in the pump to migrate out. The pump is started back up and runs for a period of time until the cycle begins again.

To calculate the effect of gas on a pump, you first have to determine how much gas is entering the pump intake vs flowing up the annulus. This separation can happen naturally, or a gas separator can aid in increasing the separation. The University of Tulsa started conducting research regarding natural separation in 1993 with the Tulsa University Artificial Lift Projects group (TUALP). Alhanati (1993) was the first researcher on this project with his dissertation on separation efficiency. Alhanati used a drift flux model to develop equations for two phase flow in the annular space and through a gas separator and performed experimental tests to verify the models accuracy. The model involves complex calculation of two-phase flow which is computationally expensive. A simplified model was also developed that sufficiently matched the experimental data and is much easier to compute. The natural separation efficiency is defined as the volume of gas that separates and flows up the annulus divided by the total gas volume just below the pump intake and is calculated in (3.14).

$$E = \frac{V_{Lsz}}{V_{Lsz} + V_{\infty,z}} \tag{3.14}$$

where E=separation efficiency, V_{Lsz} is the superficial liquid velocity in the vertical direction, and $V_{\infty,z}$ is the vertical terminal velocity of a gas bubble. The terminal velocity is dependent on the flow regime and physical properties of the fluids, where for the experimental results in Alhanati's study the churn-turbulent regime was observed, the

terminal velocity can be calculated with (3.15).

$$V_\infty = \sqrt{2}\left(\frac{\sigma(\rho_l - \rho_g)g}{(\rho_l^2)}\right)^{0.25} \tag{3.15}$$

where σ is the surface tension, ρ_l and ρ_g are the liquid and gas phase densities, and g is the gravitational constant.

Marquez (2004) developed a mechanistic model similar to Alhanati's but also included the terminal and slip velocity in the radial direction. Correlations for the terminal velocity in the radial direction are not as readily available as in the vertical case so Marquez used experimental data to correlate the values used empirically determined constants to calculate efficiency (3.16).

$$E = \left(\left(1 + \frac{ab + c\left(\frac{V_{Lsz}}{V_{\infty,z}}\right)^d}{b + \left(\frac{V_{Lsz}}{V_{\infty,z}}\right)^d}\right)^{272} + \left(\frac{V_{Lsz}}{V_{\infty,z}}\right)^{272}\right)^{1/272} - \frac{V_{Lsz}}{V_{\infty,z}} \tag{3.16}$$

Once the volume of gas into the pump is known, it is necessary to determine how the gas moves through the pump. Zhu and Sachdeva (2008) show how changing gas volume effects the total rate in the pump as pressure increases through the stages in Figure 3.5. For a total flow rate at pump intake of just over 1300 bbl/day, the average rate through the pump changes dramatically depending on the gas fraction and whether the free gas is compressed or dissolved into solution as pressure increases through the pump. For this figure, low GOR=4.7% and high GOR=49%. The small circles indicate the average rate between the pump intake and discharge and at what stage this average rate occurs. High fluid gas fraction makes designing pump section more difficult because the rate is variable. Zhu and Sachdeva noted that the actual behavior of gas is unknown but that the flow through the pump is likely too fast to actually go into solution and the decrease in rate is probably due to compression. Studies on the diffusion coefficient of gas-oil systems by Guo et al. (2009) and Reamer and Sage (1958) indicate that the time to reach equilibrium,

where gas has time to fully dissolve in solution, is on the order of days. For a methane-oil solution at 20 Mpa and 60 degrees C, the equilibrium time was measured at 91 hours (Guo et al 2009). These studies do not take into account the mixing that would occur in an ESP, but the mixing would have to increase the diffusion rate by several orders of magnitude for the gas to dissolve in the short retention time of the pump.

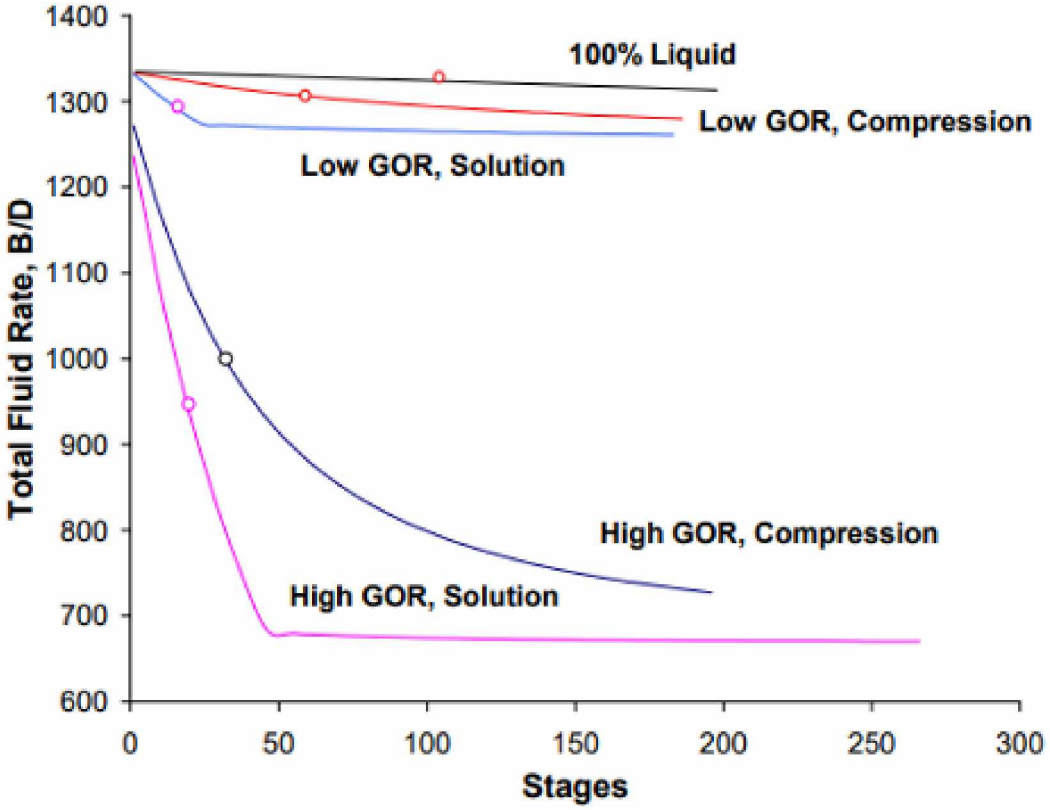

Figure 3.5 Gas Volume Effect on Total Fluid Rate as Pump Stages Increase Pressure (from Zhu and Sachdeva 2008).

Gas has other effects on ESP performance in addition to increasing the total rate. Free gas degrades the pump pressure at high rates, and at part load conditions surging instabilities can occur and ultimately lead to gas locking. Zhu and Zhang (2018) have provided an excellent reference for the review of gas-liquid flow in ESPs. I will highlight some of the important models and current state of the literature.

Murakami and Minemura (1974) appear to be the earliest referenced study of two-phase flow in centrifugal pumps. They authors used transparent apparatus for investigating the behavior of gas in an impeller. Lea and Bearden (1982) were the first experimental study of two-phase flow in ESP pumps. Turpin et al (1986) correlated experimental data to develop a relation for calculating the head degradation due to free gas, they also imposed a limit to which the correlation is applicable which is a function of the gas fraction and pump intake pressure. The head correlation (3.17) and coefficient (3.18) are below.

$$H_m = H * \exp\left(-\frac{q_g}{Q} * \left(\frac{346430}{0.021025 * p_{in}^2}\frac{q_g}{Q} - \frac{410}{0.145 * p_{in}}\right)\right) \tag{3.17}$$

$$\Phi = \frac{2000 * \frac{q_g}{Q}}{3 * p_{in}} \tag{3.18}$$

where Φ is the Turpin coefficient, Q is the total fluid rate, q_g is the gas rate, p_{in} is the pump intake pressure, H_m is the pump head with gas-liquid flow, and H is the pump head for water. The constants are used for field units. When the operating conditions are below a calculated Turpin coefficient of 1, gas interference is not predicted. Operating conditions that lead to a Turpin coefficient greater than 1 are not recommended.

Gamboa (2008) studied the effects of changing gas fraction and intake pressure to predict the onset of surging and gas lock. He used a transparent casing to view the flow pattern in the ESP impeller and developed correlations for the transition boundaries. As gas rate increases, the flow pattern in an ESP impeller changes which affects the performance of the pump curve by degrading the pressure produced. At lower flowrates, the curve becomes unsteady and the performance drops off rapidly, this corresponds to the limit that Turpin et al. had defined. Gamboa also found that at high gas rates, the pressure increment of the pump was negative. In this case the pump acts as a choke. The pump curves from Gamboa's experiments are shown in Figure 3.6. Goridko et al (2020) found similar results with field and lab testing of ESPs with high gas rates. With high

rates of free gas at the pump intake, fluid was observed to flow up the annulus and tubing simultaneously. In this case the flow rate is higher than the maximum flow rate of the pump and the ESP acts as a restriction. When this occurs, change in VSD operating frequency has little to no effect on performance.

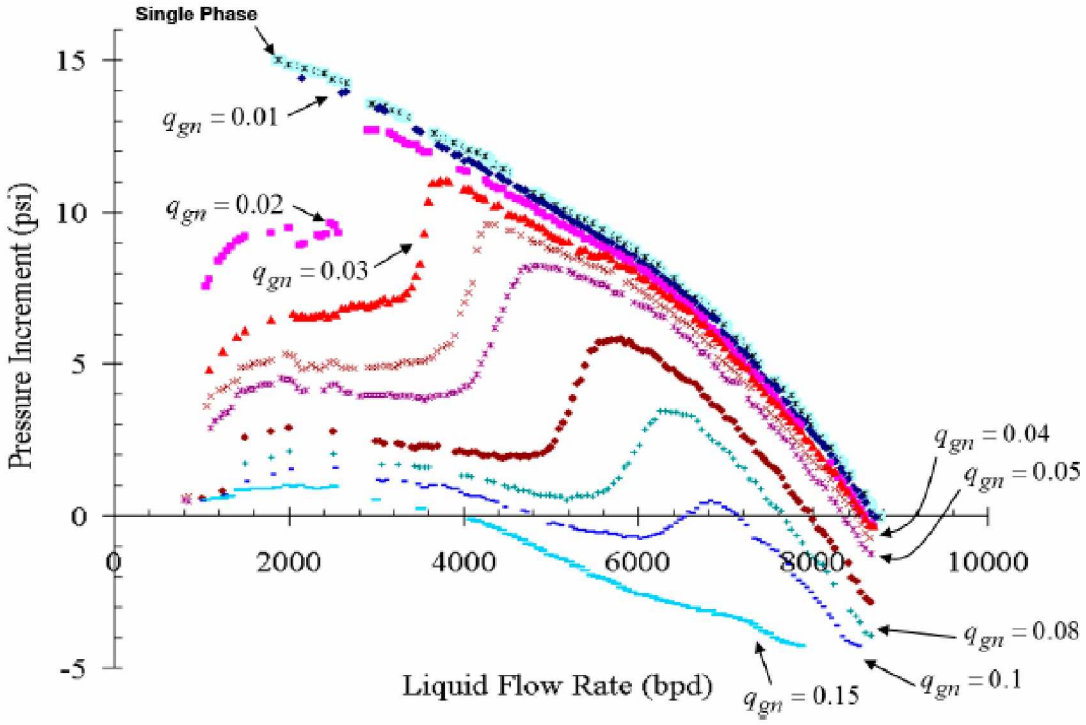

Figure 3.6 Pressure Increment Pump Curve with Increasing Gas Flow Rates Leading to Instabilities and Negative Pressure Increment (from Gamboa 2008).

Gas locking occurs in ESPs when the free gas fraction at a pump stage is greater than the stage can handle. Estevam et al. (2017) used an experimental setup that allowed visualization of gas-liquid flow inside a pump to determine the relationship between gas fraction and the onset of gas surging and gas locking. They determined that gas locking occurred when small dispersed bubbles coalesce into an elongated bubble in the impeller channel and diminish the flow area creating a stall condition. They used a two-fluid model to develop relationships to model the observed transition of flow pattern. The visualization of the elongated bubble is shown in Figure 3.7.

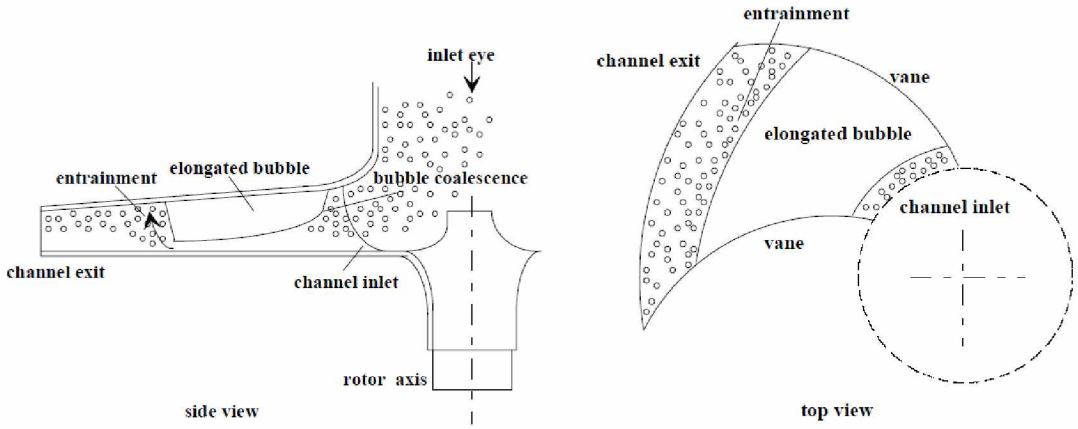

Figure 3.7 Gas Locking.

where the onset can be determined from correlations based on fluid properties and volume fractions. A dimensionless parameter was obtained to predict surging regions and gas locking based on the ratio of viscous drag and centrifugal forces on the gas bubbles. The calculation procedure is below

$$I_s = C_D F_{r\omega} \breve{r} \tag{3.19}$$

where the dimensionless parameters are I_s = Gas Surging Parameter, C_D = Drag coefficient, $F_{r\omega}$ = Froude number, $\breve{r}$ = Length parameter.

$$C_D = \frac{24}{R_e}(1 + R_e^{0.75}) \tag{3.20}$$

R_e = Reynolds number

$$\breve{r} = \frac{r_1 + r_2}{2d_{bm}} \tag{3.21}$$

where r_1 = Impeller inner radius, r_2 = Impeller outer radius, d_{bm} = Bubble diameter.

$$F_{r\omega} = \frac{V_{bs}|V_{bs}|}{(\omega\frac{1}{2}(r_1 + r_2))^2} \tag{3.22}$$

$$V_{bs} = V_{Ls} - V_{Gs} \tag{3.23}$$

where V_{bs} = Bubble relative velocity, V_{Ls} = Liquid superficial velocity, V_{Gs} = Gas superficial velocity.

With the surging parameter calculated, the onset of surging or gas locking can be determined by mapping against correlated parameters

$$I_{s,Surge} = -76(1 - \alpha) + 77 \tag{3.24}$$

$$I_{s,Gas-Lock} = -9(1 - \alpha) + 9 \tag{3.25}$$

where α = Gas fraction of fluid, $I_{s,Surge}$ = onset of surging parameter, $I_{s,Gas-Lock}$ = onset of gas locking parameter. If the calculated I_S is above the surging parameter, the regime in the impeller is dispersed bubble, if I_S is below the surging parameter and above the gas locking parameter the regime is surging unsteady flow, and finally if the calculated I_S is below the gas locking parameter gas locking is expected to occur. The correlation requires information about the fluid viscosity, density, flow rates for each phase, and pump impeller geometry. These numbers should all be known or can be calculated or estimated, but the correlation is sensitive to the bubble diameter.

The flow pattern in an ESP changes due to phase interactions similar to multiphase pipe flow. The performance degradation is linked to these flow patterns, so that predicting flow pattern is very important to determine performance degradation. Visualizing and measuring interactions in a multiphase pump is more difficult than in pipe flow, high resolution computer tomography (HireCT) is a non-intrusive way to measure the phase fraction in-situ. Because more than one phase is present in multiphase flow, the interface between the phases becomes important in modeling the fluid behavior. The fluid interfaces are not static and can be difficult to model which makes the prediction of ESP performance

difficult. Changes in the interface properties become important with multiphase flow when surface acting agents change the properties at the interface. Section 3.4 describes the effects of colloidal and interfacial effects on pump performance.

3.3 Solids

Solids production with oil and gas is generally problematic in regard to integrity of system components and erosion issues. Solids also produce problems with surface processing, since most sales contracts require a minimum basic sediment and water ($BS\&W$), the solids must be removed from the sales oil to a satisfactory degree. The literature in oil and gas is almost entirely related to solids effects on EsP reliability, but other industries have studied the effects of solid slurries on ESP hydraulic performance. The reason for the lack of literature in the oil industry seems to be due to the relative importance of the effects of solids. If the solids concentration is more than a couple percent by volume, ESP runlife is not expected to be very long. One scenario where high solids concentrations are pumped is during frac flowback procedures. The ESP is used to produce frac sand and fluid to clean up the well after hydraulic fracturing and hydraulic performance is not the most critical issue. It's worth looking at the literature to understand the relative impact solids have on performance.

The most cited experimental study on the effects of solids on centrifugal pump performance seems to be Walker and Goulas (1984). Their study tested centrifugal pumps with 2 different slurry mixtures, one with kaolin clay and one with coal fines, to determine the effects of the fluid properties on performance. Both mixtures had a water continuous phase with solids added in subsequent tests to measure the effect of increasing concentration while also measuring rheological properties at these concentrations. At increased concentrations, the fluid yield stress, plastic viscosity, and apparent viscosity increased for both slurries indicating non-Newtonian behavior and shear dependent properties. The effect on pump performance is shown in Figure 3.8, where concentration is quantified by the increasing fluid specific gravity. At a critical value of concentration, the

effect on performance at part load conditions drops dramatically yielding an unstable pump curve. The authors found that the decrease in performance near BEP matched the Hydraulic Institute corrections for Newtonian viscous fluids, where the slurry apparent viscosity was determined at a shear rate of 2*Ω (150 to 300 $\frac{1}{sec}$). The performance of two pumps, each at two different speeds and tested with two slurries of different particle size and specific gravity, was found to depend only on density and calculated viscosity.

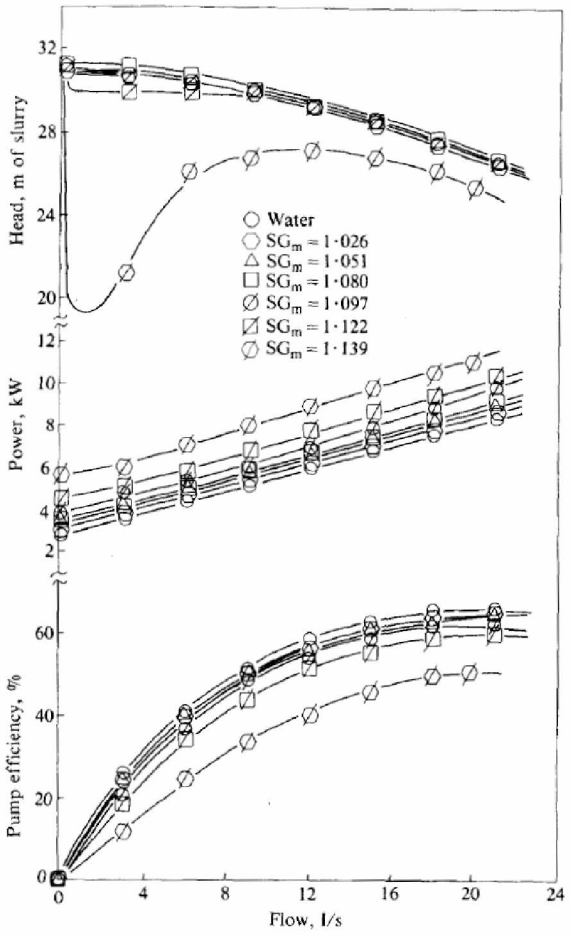

Figure 3.8 Effect of increasing Solids Concentration in a Slurry of Solids and Water on Pump Performance (Walker and Gouas 1984).

Liu et al (2014) used computational fluid dynamics to study the effect of liquid-solid flow in an ESP impeller. They used a particle model so that the solid particles are discrete and interact with the water only through viscous drag. The solid concentration was

constant at 20%. The study concluded that solids decrease the pressure rise in the pump slightly at 20% solids concentration. Solid particles tend to accumulate at the leading blade edge due to centrifugal forces and effect the velocity profile of the water disrupting streamlines. The study also concluded that erosion of the passageways greatly increased with the presence of solids. In applications with water and solids, erosion appears to be much more important than performance degradation. The effects on performance observed by Walker and Goulas may be due to interfacial interactions, such as adhesion, between the surfaces of the solids and the fluid. Disperions of particles in a fluid can exhibit behavior that is different from either of the constituent phases. The next section delves further into dispersions, or particles dispersed in a continuous phase, and the increased complexity they add to pump performance characteristics.

3.4 Dispersions

Dispersions are defined as collections of small particles of one phase dispersed in a second continuous phase. Dispersions can be categorized based on the phases of the medium and dispersed phases, as well as the approximate behavior of the dispersion. A solution is a homogeneous dispersion that if left for a prolonged period, will not settle. A suspension is a heterogeneous dispersion of large particles that if left for a prolonged period will settle. Finally, a colloidal dispersion is a heterogeneous dispersion of small particles that will not settle if left for a prolonged period. The definition of small and large particles and the time period considered will vary based on the system. In general, Figure 3.9 shows the naming convention for dispersions based on dispersed phase and continuous medium phase.

Since the medium most likely to occur in the case of centrifugal pumping of oil and gas is liquid, either oil or water, the dispersions of interest are foams, emulsions, and solid suspensions. The small size and large specific surface area, surface area per unit mass, of these particles makes their surface interactions important and lead to physical properties not experienced in the constituent molecules. In other words, the behavior of the fluid

Dispersed phase	Dispersion medium	Name
Liquid	Gas	Liquid aerosol
Solid	Gas	Solid aerosol
Gas	Liquid	Foam
Liquid	Liquid	Emulsion
Solid	Liquid	Sol, suspension
Gas	Solid	Solid foam
Liquid	Solid	Solid emulsion
Solid	Solid	Solid suspension

Figure 3.9 Dispersion Naming Convention (Schramm 2005).

system cannot be known just by knowing the properties of the elements that make up the system. Non-linear behavior and complexities may require breaking apart the system into more manageable pieces to make the system easier to understand, but this comes at the price of accurately describing the phenomena. Some assumptions may be made to find the bounds or limits on the values of some properties of complex dispersions to make approximations necessary for Engineering calculations. Monodisperse is used to describe a dispersion with particles of uniform size and polydisperse is used for a distribution of particle sizes.

The simplest case to start with the description of a dispersion is with a dilute dispersion, meaning dispersions with less than 10% dispersed particles by volume, with rigid spherical monodisperse particles. The basis of most studies on dilute dispersions is Einstein's (1911) work on spheres. Einstein's equation relates the dispersion viscosity μ to the continuous medium viscosity μ_s and dispersed fraction ϕ, where $[\mu]$ is the intrinsic viscosity. The value of intrinsic viscosity is 2.5 for an ideal dilute suspension of rigid spherical particles, but the value is shape dependent and must be determined experimentally for irregular shapes

$$\mu = \mu_s(1 + [\mu]\phi) \tag{3.26}$$

For dispersions of higher dispersed volume, called concentrated dispersions, the Brinkman (1952) model can be used

$$\mu = \mu_s(1-\phi)^{-[\mu]} \tag{3.27}$$

where the intrinsic viscosity $[\mu]$ has the value 2.5 again for an ideal dilute suspension of spherical particles. The above equation can be generalized to particles of any shape by introducing a maximum packing fraction (ϕ_m) from Krieger (1972).

$$\mu = \mu_s(1-\frac{\phi}{\phi_m})^{-[\mu]\phi_m} \tag{3.28}$$

The maximum packing fraction allows the modeling of multiple particle sizes but is highly dependent on particle size distribution. For a binary particle suspension, say large particles and small particles, as the fraction of large particles increases with constant total particle fraction, the viscosity decreases to a minimum in a phenomena known as the Farris effect (Farris 1968). The Farris effect is much greater at total dispersed fractions above 50% and the effect reduces as the dispersed fraction decreases. These equations have assumed spherical particles, however any asymmetry and deviation from spherical particles has a strong effect on the maximum packing fraction and thus viscosity. Figure 3.10 shows the rapid increase in fluid viscosity with increasing concentration of several maximum packing concentrations for a 125 cp continuous phase viscosity. The previous equations account for particles in a continuous flowing fluid but neglect the effects of particle interactions. These interactions can be included with higher order terms of the dispersed fraction. The value of the constant (n) varies from a value of n=6.2 for extensional flow (Batchelor, 1977), to n=14.1 for shear flow (Guth and Simba, 1936), but Barnes (1993) notes that values of n for shear flows have a wide range in the literature from n=5-15.

$$\mu = \mu_s(1+[\mu]\phi+n\phi^2) \tag{3.29}$$

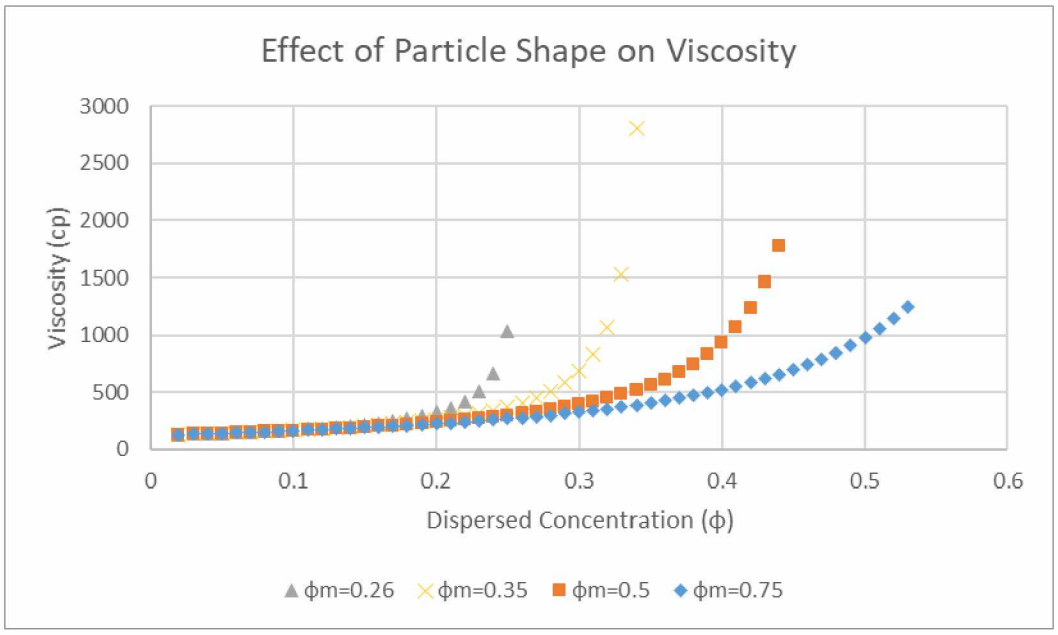

Figure 3.10 Dispersion Viscosity can be Several Times Larger than the Viscosity of the Dispersion Medium.

For the case of dispersions with deformable particles, such as emulsions and foams, the maximum packing fraction is usually much higher since the particles can deform and can be as high as 0.9 or more. Particle deformation allows the shear thinning tendency to approach a Newtonian plateau at a much lower viscosity than for solid suspension. Smaller droplet size and smaller size distribution increase the viscosity.

Foam is a dispersion of a gas phase in a continuous liquid phase, sometimes called a gas emulsion. The concentration of gas in foams is called quality Γ and defined as the ratio of gas volume to total volume of the fluid. Wet foam is a foam with quality up to 0.74, which is the maximum packing fraction possible for uniform spheres in a face centered cubic arrangement. Three-dimensional foam bubbles are assumed to be spherical up to this maximum and start to distort at higher fractions at which point they are called dry foams. In additional to quality, which is a measure of concentration, foams can be characterized by dispersity, a measure of foam surface area to fluid volume, and stability, a measure of the foam's lifetime. Gas emulsions in a low viscosity medium are short lived disperse systems

while highly viscous medium allows for stable, or long lived, systems. The presence of surfactants also increases the stability of gas bubbles. The viscosity of foam can be calculated with the dispersion viscosity equations for deformable particles. These calculations are used in models for foam drilling mud and related to Einstein's equation where the dispersed fraction ϕ=the foam quality Γ and the intrinsic viscosity is =3.6 (Lyons 2010).

$$\mu = \mu_s(1 + 3.6\Gamma) \tag{3.30}$$

Lyons (2010) states that foam is effectively Newtonian at qualities of 0.55-0.74 and behaves as a non-Newtonian shear thinning fluid at increasing foam quality. At these higher qualities the viscosity can be calculated using an adjusted Brinkman equation with the dispersed fraction again equal to foam quality and n=0.33-0.49.

$$\mu = \mu_s(1 - \Gamma)^{-n} \tag{3.31}$$

Alshmakhy amd Maini (2009) studied the viscosity of a foamy heavy oil with 3 different measuring devices including electromagnetic viscometer, capillary tubes and slim tubes with the purpose of understanding the phenomena of foamy oil flow through porous media. The authors found the viscosity to be similar to live oil viscosity for a large range of gas volume fractions and independent of shear rate, however the type of measuring device used had a significant effect on foamy oil viscosity measurement. The results of these experiments are counter to what would be expected by dispersion theory, but the authors admit that reported results appear to be oil specific and depends strongly on the rate of pressure drop. Marsden and Khan (1966) also studied the viscosity of a foamy heavy oil but with only high quality foam (0.70-0.96). The authors found that at high quality, foam viscosity exhibits shear thinning non-Newtonian behavior and that the apparent viscosity increases with increasing foam quality. Another important observation from this study was the increasing apparent viscosity with increasing surfactant concentration. Adil and Maini

(2007) found that the presence of asphaltenes can alter the behavior of foam by suppressing bubble coalescence. The asphaltenes act as a surfactant stabilizing the gas oil interface to allow stable bubbles and maintaining dispersed foam flow.

Surfactants, shortened from Surface Acting Agents, are substances that assemble at the interfaces between phases and change the property of the interfaces. They generally lower surface tension, or interfacial tension, and change the solubility of one fluid in another, where decreasing solubility can lead to the formation of more stable interfaces. Surfactants facilitate dispersion of particles and reduces the size of bubbles. They are usually amphiphillic, with both hydrophobic and hydrophillic surfaces, that adsorb at interfaces. Surfactants in oil and gas production can be asphaltenes, or solid fines that contain both oil-wet and water-wet surfaces. The presence of these surfactants are an important aspect for the formation of stable dispersions and the stability of the dispersion then plays an important role in the effect on the performance of an ESP. Since ESPs tend to consist of many stages, the fluid has to go through a complex path from pump inlet to pump discharge. If the dispersion is unstable and the dispersed phase coalesces easily, say in the first 5 stages of a 100 stage pump, then only 5% of the pump is operating with the more difficult fluid. As in the above foam studies, if the dispersion is stable due to the presence of surfactants, the performance is more difficult to predict. Studies of dispersion flow through ESP's should consider the surfactant content effects on phase interfaces.

Emulsions are dispersions of two immiscible liquids, such as oil and water. When oil is the continuous phase the emulsion is termed a water-in-oil emulsion and when water is the continuous phase it is termed an oil-in-water emulsion. A common scenario in oil wells is for the early life of the well to produce a higher oil cut with water cut increasing over time. As the water cut increases, emulsions can form and cause a significant increase in the fluid viscosity. At some watercut, usually around 50-60%, the emulsion will have an inversion from water-in-oil to oil-in-water and water will become the continuous phase. Beyond this inversion point the viscosity reduces rapidly to a normal viscosity levels. The

non-Newtonian behavior of some dispersions can make the estimation of viscosity within the ESP difficult. Viscosity is dependent on temperature, but also shear force and shear rate. Emulsions exhibit shear thinning behavior in studies of effective emulsion viscosity, where shear thinning with stress over time is described as Thixotropic, and shear thinning with increased force of stress is described as Pseudoplastic. The shear rate and shear force in an ESP is difficult to determine directly. The area of highest shear would be around the rotating impeller, while the flow through the diffuser would experience relatively low shear. One area of interest is if the fluid viscosity decreases at the high local shear of the impeller blade, does the relaxation time carry that low viscosity as it flows through the diffuser section or does the fluid "thicken" immediately after it leaves the impeller tip. Is effect of shear on the fluid instantaneous or does it take seconds, or mico or nano seconds. The distribution of particles and particles shapes play a role in the apparent viscosity of dispersions and as has been found in studies of flow though pumps the distribution and shape of particles can change through the pump due to the forces generated in the pump.

Khalil et al. (2006) studied emulsion effects on an ESP using three sets of mixtures: tap water and mineral oil, water-oil with fatty acid amine (FAA) added as a surfactant, and in the third set sodium dodecyl sulfate (SDS) added as an ionic surfactant.They determined that the addition of surfactants created a more stable emulsion which had a greater apparent viscosity a greater impact on pump performance degredation.

Morales et al (2013) studied emulsions through an ESP to determine the distribution of droplet formation at the pump discharge. They used a water and mineral oil mixture and measured the droplet size distribution at the pump outlet with varying water cut, flow rate, and rotational speed. They determined that the droplet distribution is strongly related only to pump rotational speed and as pump speed increases the droplet size decreases and the distribution of droplet sizes narrows. The authors varied water cut from 50-75% so that water was the continuous phase for the experiments. The authors determined that turbulent breakup is the mechanism for droplet formation with the caveat

that more testing is needed with higher viscosity oil as the continuous phase to determine if another mechanism may occur.

Dispersions complicate the flow of fluid which makes predicting fluid effects on pump performance difficult. ESP performance is very sensitive to viscosity, gas rate, and flow pattern in the pump impeller. Disperse particles can increase viscosity and decrease surface tension which changes the flow pattern through the pump. Models that do not account for these effects will not correctly model the performance or obtain a good match between well performance and ESP performance. The next chapter discusses a case study of an ESP installed in a well that has dispersed fluid and attempts to generate a match using the information in the previous sections.

CHAPTER 4

ESP WELL CASE STUDY

This case study uses data from an ESP well installed on the North Slope in Alaska. The goal of the study is to understand and model the ESP performance using the information from the previous sections. The method of investigating this field case was to build out calculations in a spreadsheet with the data obtained from the field and build a model of the well performance and ESP performance. This model was validated using the Halliburton Artificial Lift ESP sizing software to assure that the model generates a match with commercial software. The reason for not using the commercial software only is the limited tuning available in regards to tubing flow correlations, viscosity adjustment for the fluid streams, and a number of other necessary calculations that can be best investigated individually with a spreadsheet model. In other words, it is necessary to understand all of the intermediate calculations that happen in the background of commercial software which converts input data to an output. Once the model was validated, tuning parameters were used to generate a match of the field data to calculations.

Correlations are sometimes the only available resource for calculating fluid properties necessary to model well and ESP performance. When field data is available that is of good quality, that data can be used instead of correlations to better fit an individual field. This case study uses data from an oil well in Alaska where some fluid properties are available.

This well is a horizontal dual lateral producer with slotted liners run in both laterals. The lower completion is topped with a liner top packer at around 5,200' MD. The "upper" completion consists of the ESP assembly and production tubing. The upper completion is stung into the liner top packer with a seal bore assembly and above the stinger is a subsurface safety valve (SSSV). This allows reservoir isolation in the direction of flow when the SSSV is closed. Above the SSSV is a chemical injection mandrel with 3/8" control line

to surface and then a sliding sleeve to allow tubing to casing flow.

The ESP assembly is a "rigless" type with subsurface wet connect electrical system that allows the cable to be run independent of the motor, seals, and pump which can be installed later via wireline through the tubing string. The tubing deployed wet connect assembly has 3 sections each with an ID that is at least the ID of the tubing to allow tools to be run below the system. The 1st section includes the female wet connect that allows the ESP power cable to be "plugged in" and run to surface. The 2nd section is the intake section with drilled holes of sufficient area to prevent any flow restriction and allow production to flow from the annulus back into the tubing. The 3rd section includes a sliding sleeve that allows gas to exit the tubing annulus into the casing annulus. The thru-tubing deployed equipment lands inside the wet connect assembly with the male wet connect engaging with the female tubing deployed portion allowing a secure electrical connection. The motor and seals are run directly above this and extend into the 2nd section where incoming fluid flow is used to cool the motor. The ESP pump is landed on top of the motor and seal section with a set of coupling mating units that allow transfer of motor shaft torque to the pump.

On top of the pump discharge is a polished bore receptacle with a GS fishneck that allows wireline to engage the pump section. Wireline runs deploy top end jewelry with two more runs. The first run has a stinger to stab into the polished bore receptacle, a standing valve to prevent sand fallback into the pump, and a packoff element to isolate the discharge from the intake. The packoff must be set above the gas venting sliding sleeve to allow any gas that does not enter the pump to migrate back into the casing tubing annulus. The last wireline run is a tubing stop to prevent axial movement. The ESP motor has an integral gauge unit with sensors that measure motor temperature via a thermocouple in the motor oil, intake temperature of the production fluid, intake pressure of the fluid, and vibration of the motor.

Above the ESP assembly is a tubing deployed dual gauge with sensors reading pressure in the tubing and in the annulus. The tubing pressure reading is equivalent to the pump

discharge pressure. The measured distance from the pump discharge to the gauge is 80 ft and the difference in vertical distance is minimal. The downhole gauges are powered from surface via DC signal that operates even when the pump is not turning. This allows constant readings for pressure buildup when the well is not flowing and allows the determination of a static datum pressure. When the well is flowing, the motor gauge reads the flowing bottom hole pressure which allows us to generate an inflow performance curve when simultaneous well test data is also known. All gauge readings are captured in the surface Variable Speed Drive, or VSD, and communicated via SCADA to a central data gathering unit to be remotely monitored along with surface temperature and pressure readings. The VSD records the amperage draw at surface along with voltage and frequency of the motor. This motor is a permanent magnet motor with 4 poles, so an operating frequency of 120 Hz corresponds to 3600 RPM.

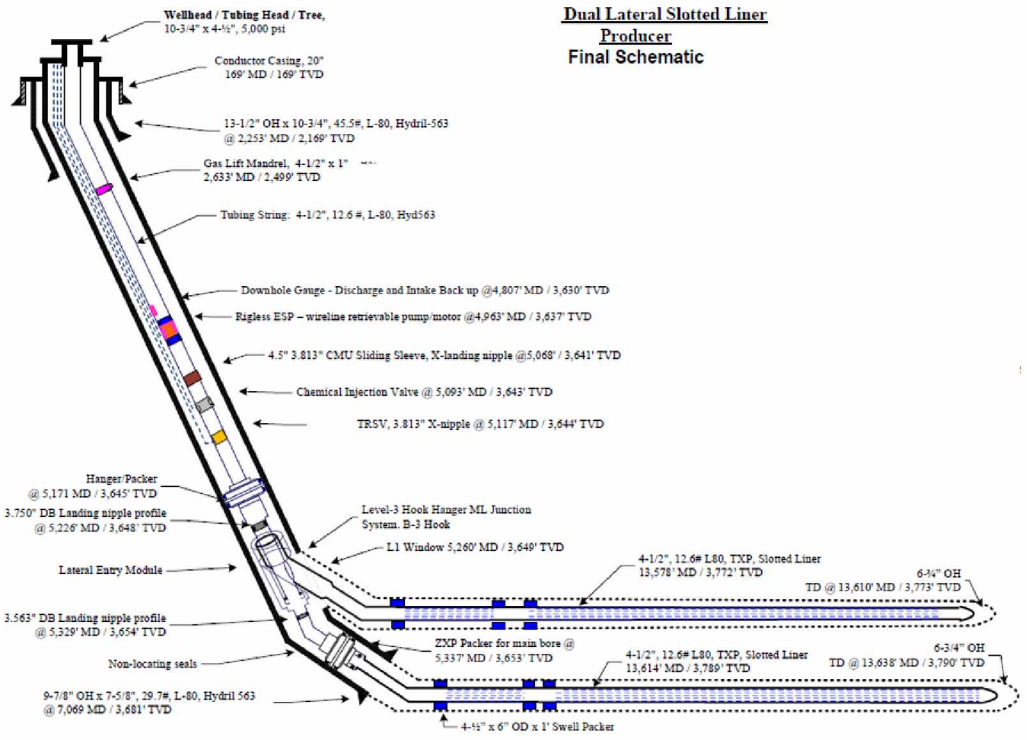

Figure 4.1 Completion Schematic.

The well completion schematic is shown in Figure 4.1. The pump set depth is 3550' TVD, 5,100' MD. The surface configuration is not shown, but it is important to note that the tubing and annulus flow comingle upstream of the production choke. This means the tubing and casing are jointly controlled with the production choke and the surface pressures remain nearly equal. The ESP assembly is just over 100' in length and set as deep as possible while landing in a section with minimal dogleg, below 2 deg/100' as shown in Figure 4.2.

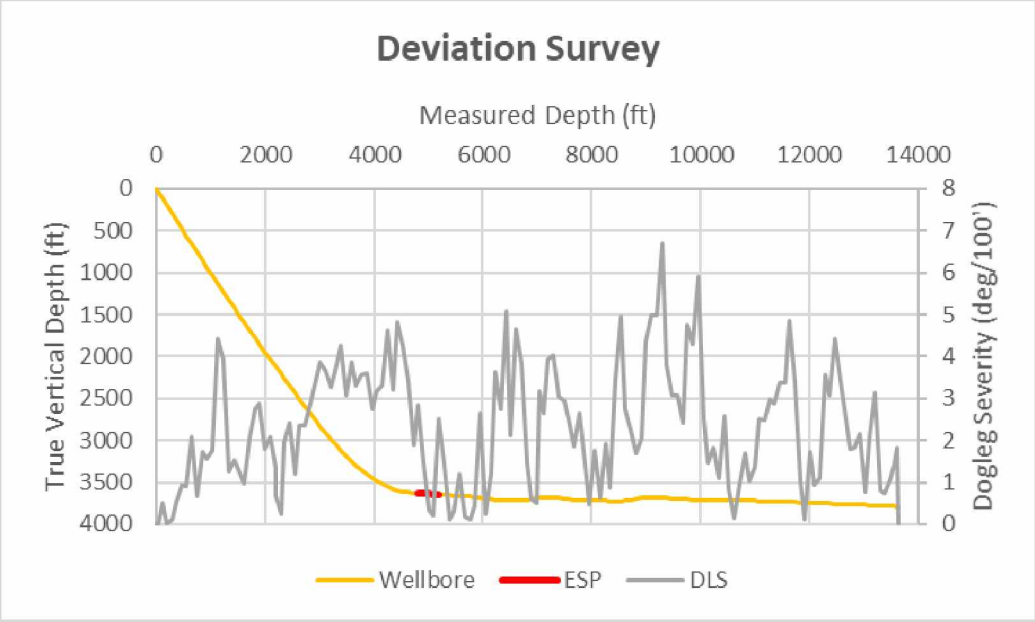

Figure 4.2 Deviation Survey.

Over the course of the first seven months of production, 20 well tests were performed to characterize the early time production. Figure 4.3 shows the information that is recorded for each test. There is a gap in the data from April to July, this gap corresponds to a shut-in period that was caused by external factors and is not related to any problems with this particular well. The average rate over this period is around 1,200 barrels per day at less than 2% water cut and gas liquid ratio of 300 scf/bbl. The rates over this period are in line with what was expected from the well at these drawdown pressures, indicating that the well productivity is in line with design, but the drawdown was expected to be greater with

an ESP. The well was brought online slowly to prevent sand production from an unconsolidated formation, but the ESP was unable to drawdown below 1,00 psi when the operating intake pressure was expected to be as low as 700 psi. The production choke was opened slowly to allow a controlled drawdown and then generally left fully open during production. After long shutin periods the well was choked back at startup again to control drawdown and then opened.

Test Start	Test Length	Choke Setting	Tubing Pressure (psi)	Flowing Tubing Temperature (F)	Oil Rate (STB/d)	Water Rate (STB/d)	% Water Cut	Density	Liquid Rate (STB/d)	Gas Rate (Mscf/d)	GOR	GLR	ESP Frequency (Hz)	Intake Pressure (psi)
10/1/2020 11:40	8:05	96	190	60	1102	23	2	0.918	1125	340	308	302	90	1110
9/25/2020 6:39	6:05	96	195	54	1051	27	2	0.922	1078	338	322	314	90	1159
9/10/2020 2:00	18:00	96	169	45	471	27	5	0.917	498	259	551	520	80	1178
8/24/2020 1:01	16:14	96	190	55	1122	7	1	0.918	1129	835	744	739	105	1075
8/9/2020 17:38	10:58	96	197	60	1351	12	1	0.921	1364	590	437	433	105	1115
8/7/2020 0:56	8:29	96	202	59	1409	2	0	0.889	1412	706	501	500	105	1110
8/4/2020 3:49	8:43	96	207	60	1550	1	0	0.865	1551	660	426	426	105	1117
7/26/2020 6:01	11:00	96	199	60	1554	1	0	0.913	1555	628	404	404	100	1186
7/25/2020 13:09	12:00	96	198	58	1325	1	0	0.916	1326	485	366	366	90	1206
7/25/2020 0:16	10:55	96	198	56	1182	25	2	0.927	1207	437	370	362	85	1215
7/16/2020 16:16	16:00	96	191	59	1257	20	2	0.926	1277	335	266	262	73.3	1261
7/10/2020 2:25	6:35	53	241	58	1471	1	0	0.913	1472	223	151	151	70	1388
4/16/2020 10:53	3:40	50	263	63	1404	9	1	0.917	1414	393	280	278	94	1151
4/12/2020 9:36	5:33	96	191	49	822	20	2	0.922	842	275	335	327	72	1213
4/11/2020 15:23	8:44	96	181	48	524	25	5	0.922	549	215	410	391	80	1221
4/8/2020 1:56	12:00	96	206	63	1566	2	0	0.916	1567	346	221	221	90	1150
3/28/2020 6:01	10:02	96	228	66	2649	1	0	0.903	2650	402	152	152	110	1212
3/24/2020 5:18	3:08	72	209	59	1570	2	0	0.917	1572	190	121	121	70.3	1413
3/22/2020 22:50	12:00	50	240	57	1305	20	2	0.924	1325	145	111	109	65	1456
3/22/2020 17:35	3:00	43	251	57	1250	50	4	0.928	1300	137	109	105	65	1476

Figure 4.3 Well test data.

Along with test rate data, viscosity data was recorded for a dead oil sample shown in Figure 4.4. At surface tubing temperature of around 60 °F, the dead oil viscosity is 600 cp and at bottomhole temperature of 80 °F the dead oil viscosity is 161 cp.

The well trend from some of the data gathered through SCADA is shown in Figure 4.5. The ESP frequency is read directly from the VSD output, while the output current value is taken from one of the three phases and divided by a transformer ratio of 7.2 to get downhole motor current. The output current of all 3 phases is monitored to assure all phases are balanced and within a small margin and only one reading is shown for clarity. The frequency and current drop to 0 when the VSD is shut down. The bottomhole

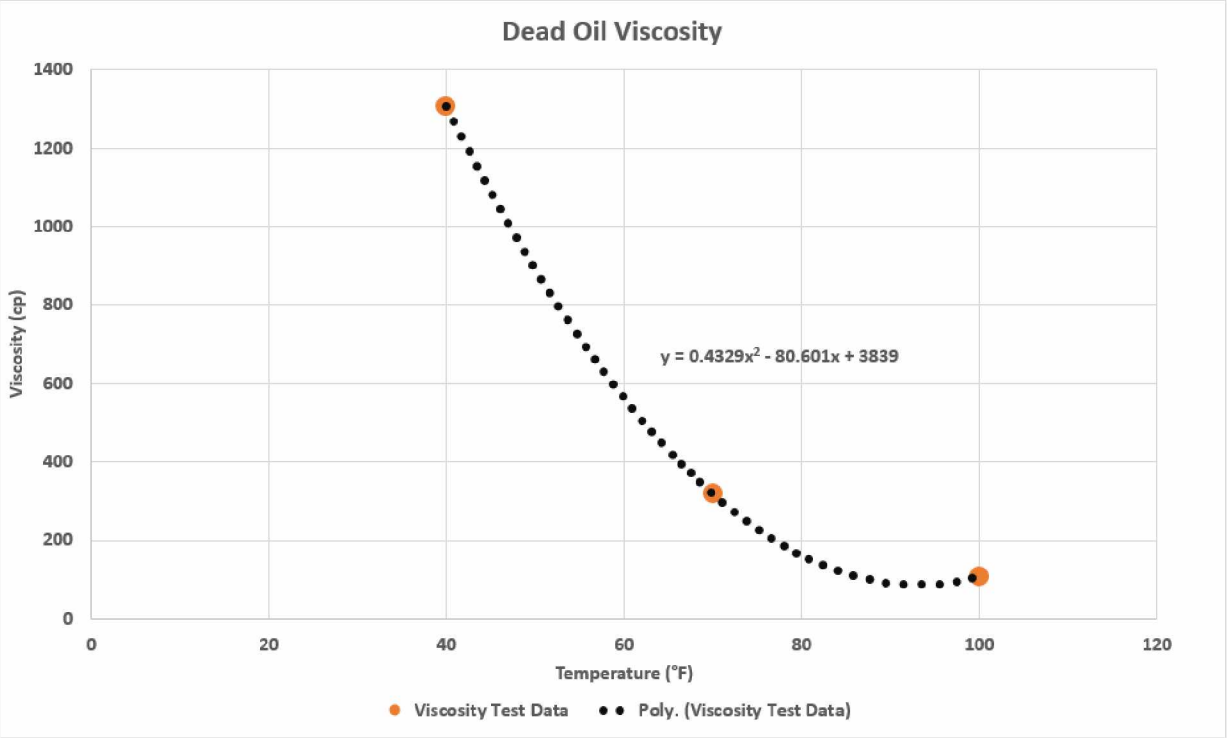

Figure 4.4 Dead oil viscosity data as a Function of Temperature.

pressure readings before startup indicate an initial static bottomhole pressure of 1690 psi. After a brief startup production period the well was shutin for approximately 3 months before production was resumed. The subsequent startup provided some data, but some troubleshooting was needed to assess the functionality of the subsurface safety valve. The last section of the trend provided a period of stable and steady production which was helpful in generating a match for the well and ESP performance.

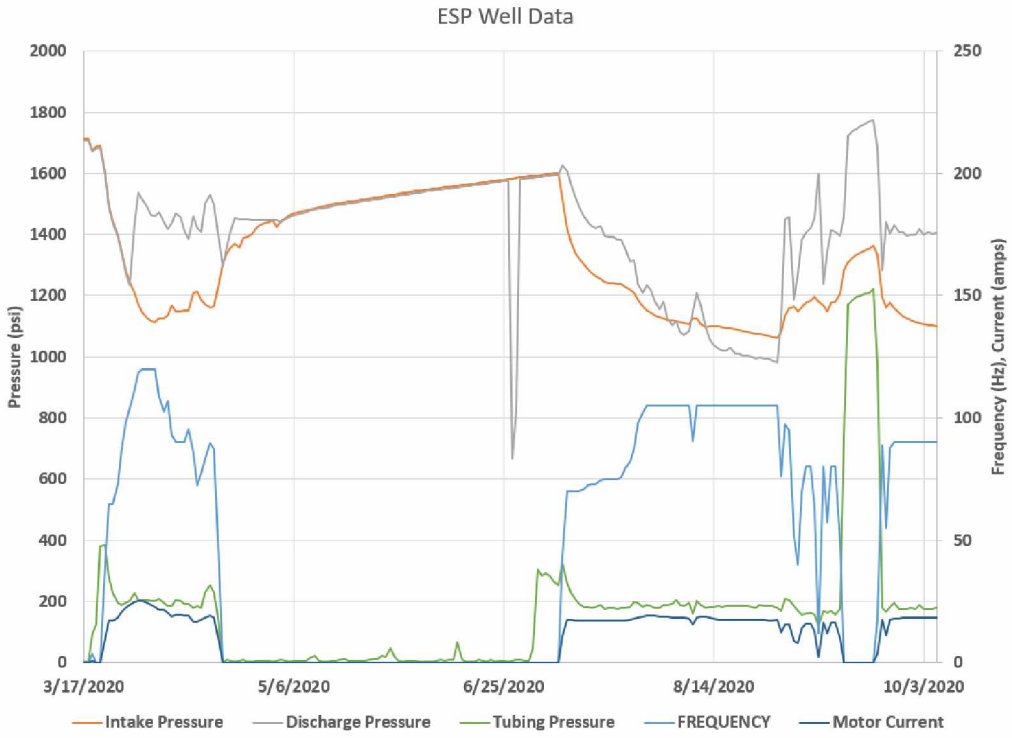

Figure 4.5 Well Trend Data over Case Study Period of 7 months.

The initial startup period data has erroneous readings for discharge pressure where it appears that the intake pressure and discharge pressure are equal, the early data is shown in Figure 4.6. This was due to SCADA assigning the discharge gauge annulus pressure rather than the tubing pressure. When the addressing was corrected in the system the trend appears normal with a pressure differential across the pump and relatively steady production up until the well was shut-in. The pressure differential across the pump was not very sensitive to pump operating frequency and the overall value of differential pressure was lower than expected with the ESP design. When the ESP was shut down and the well shut in temporarily, the bottomhole pressure rose slowly over 3 months to 1600 psi.

When the well was brought back online in early July, the drawdown again looked normal except that the discharge pressure dropped to below intake pressure for almost the entire month of August as shown in Figure 4.7. During this period the liquid and gas rates increased slightly from the previous trend and the gas-liquid ratio increased to a high of

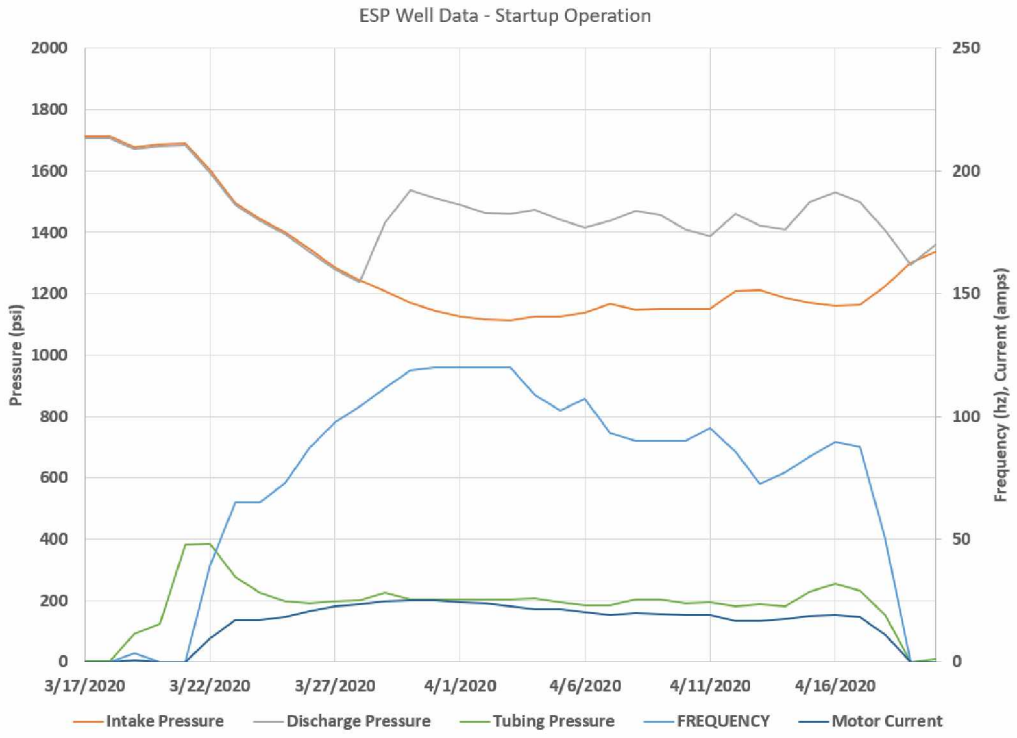

Figure 4.6 Well Trend Data during initial Startup Period.

730 scf/bbl. This may have been similar to the case study by Goridko et al (2020) with high gas rates that exceed the maximum rate of the ESP and occur with flow up the annulus. The intake pressure dropped to its lowest value and then the trend reversed suddenly. The ESP was cycled on and off several times and several function tests were performed on the downhole equipment to troubleshoot a problem, during which it was noted that the subsurface safety valve was not properly closing. The well was shut-in for about nine days while a plan forward was discussed. Asphaltene buildup was determined to be the likely cause. Xylene was pumped down through the chemical injection mandrel to try to break any buildup of asphaltene and then flushed with diesel.

When the well was restarted in September, the production and well trends stabilized with steady operation for several weeks. Figure 4.8 shows the steady trend with stabilized pressures at constant ESP operating frequency. During this period the pump is providing 300 psi differential pressure at a liquid rate of about 1100 bbl/day. This drawdown was still

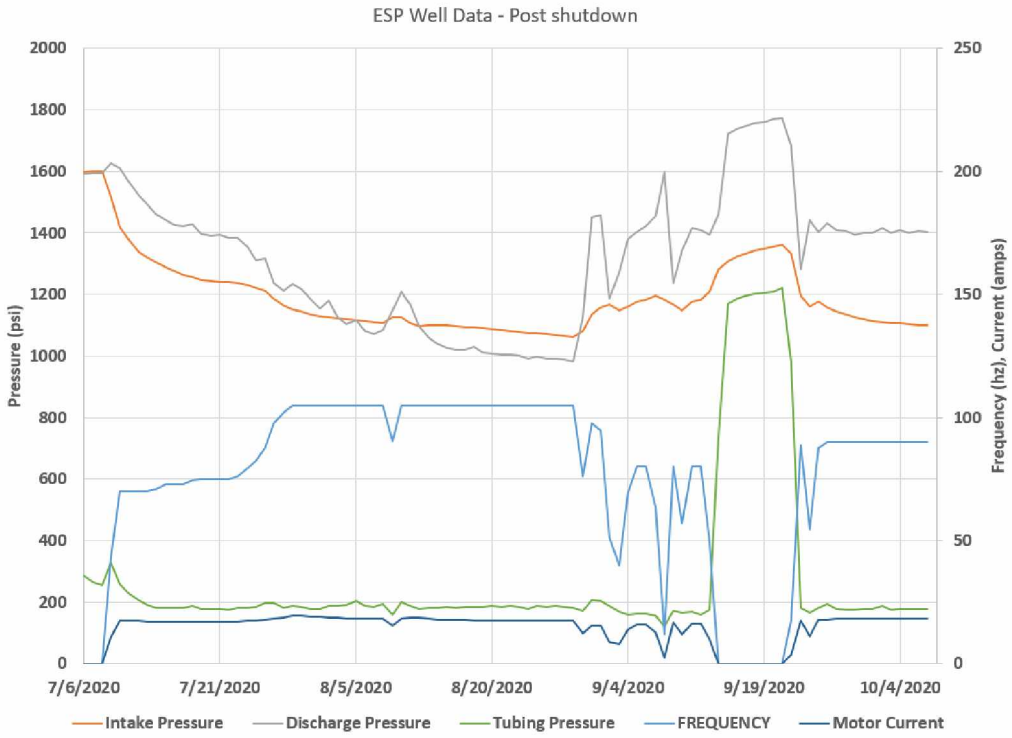

Figure 4.7 Well Trend Data Post Shut-in Period July-October.

lower than expected in the initial pump design for this operating frequency.

Several steps were taken to problem solve the well performance that may not be related to the pump. A pressure test verified that the downhole shear out valve was intact, the packoff above the pump is set and holding pressure, and the standing valve below the packoff is holding pressure. This test increased confidence that no hole in the tubing or leak is present that would allow recirulation from the pump discharge to the intake. The pump rotation was verfied by reversing rotation and monitoring operation. The correct rotation was verified and the pump was left running in the direction with the best performance. The surface facilities were walked down to verify the surface diverter valve that allows flow into the test separator was not leaking and allowing flow to bypass test. The surface facilities are in good condition because the well was recently installed and no problems were discovered in the test facilities. The welltest quality was checked to ensure the foamy oil was not affecting the welltest rates. A sample of oil was taken at surface and

examined qualitatively, the oil was very viscous and light. One field technician described the fluid as equivalent to soap bubbles from a bubble bath. No solids were visable in the oil but when rubbing it between your fingers it was described as gritty indicating fines production that is typical with this reservoir.

The next sections look at the well performance and ESP performance curves to try to match the well data with the observed ESP operation. The period of production from September-October was used since it is the only period of stable production.

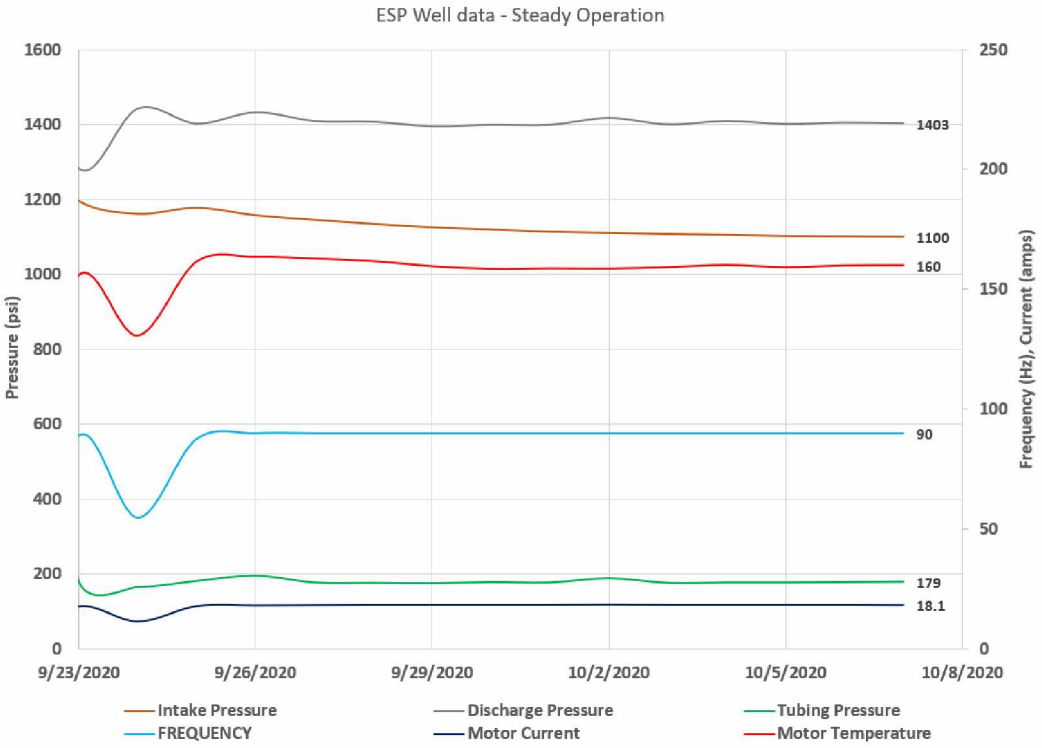

Figure 4.8 Well Trend Data With Steady Operation September-October.

4.1 Inflow and Outflow Well Performance Curves

The inflow and outflow performance curves for the well were modeled to match data collected for the well. The period of steady operation was used for the model since the early data was problematic. The first match I modeled is the pressure traverse. The pressures at surface, pump discharge, and pump intake are read from pressure gauges with readings of

around 179 psi, 1403 psi, and 1100 psi. To model the wellbore pressure from surface to the discharge gauge, a flow model can be used along with the welltest fluid rates. The Alhanati Simplified model was used to calculate the expected natural gas separation efficiency to determine the percentage of surface gas rate that flows through the pump vs through the annulus. The calculated efficiency is 6% so the majority of the free gas at the pump intake should be produced through the pump and up the tubing. The flow pattern calculation shows that flow through the 4 1/2" tubing is bubble flow at the pump depth and slug flow closer to surface. To calculate pressure drop I used the Hagedorn and Brown (1965) correlation modified with Griffith and Wallis (1961) for bubble flow. Using the separation efficiency to calculate the tubing gas rate, and then calculating the tubing gradient, the pressure traverse matches the discharge pressure reading as shown in Figure 4.9. The horizontal pressure jump from 1133.5 psi to 1400 psi signifies the pump boosting pressure.

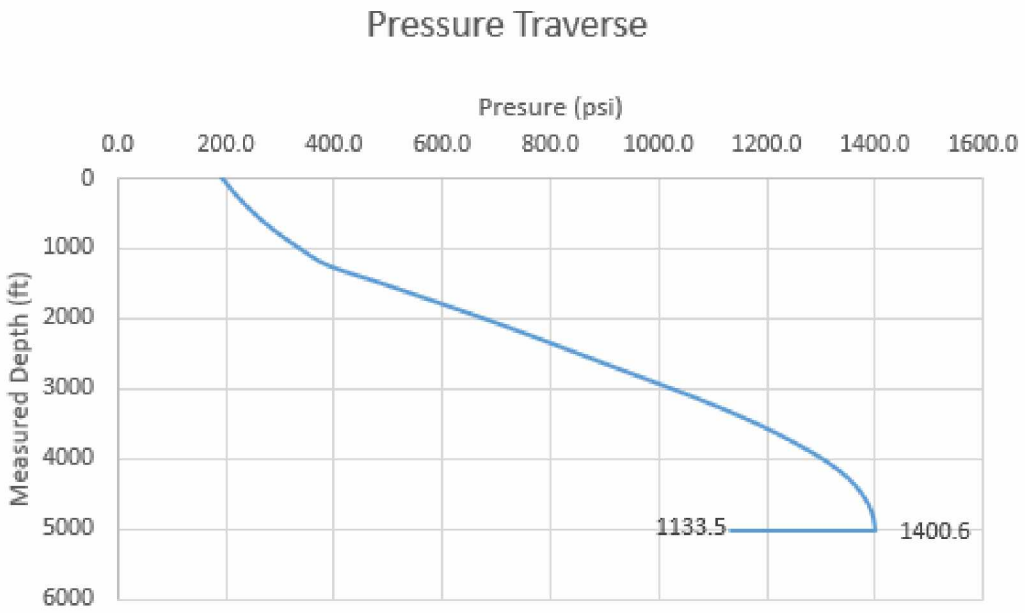

Figure 4.9 Pressure Traverse.

Using the tubing flow correlation, an Outflow Performance Relationship (OPR) can be drawn that relates different flowrates to the pressure required to move fluid to surface and overcome wellhead pressure, static pressure, and frictional pressure drop. The Inflow

Performance Relationship (IPR) is drawn using a Vogel relationship that passes through a welltest point at stabilized production. The IPR and OPR together make up the well performance relationship and are plotted with the welltest data in Figure 4.10. The welltest data for an adjacent well is shown in Figure 4.11 to compare the early time well productivity. The well is brought online with slowly increasing production to a peak rate, and then production falls at nearly constant pressure. The data for the well in this study is sparser due to the shutdown periods in the first 6 months of production and has generally lower rate and higher intake pressure but exhibits the same trend.

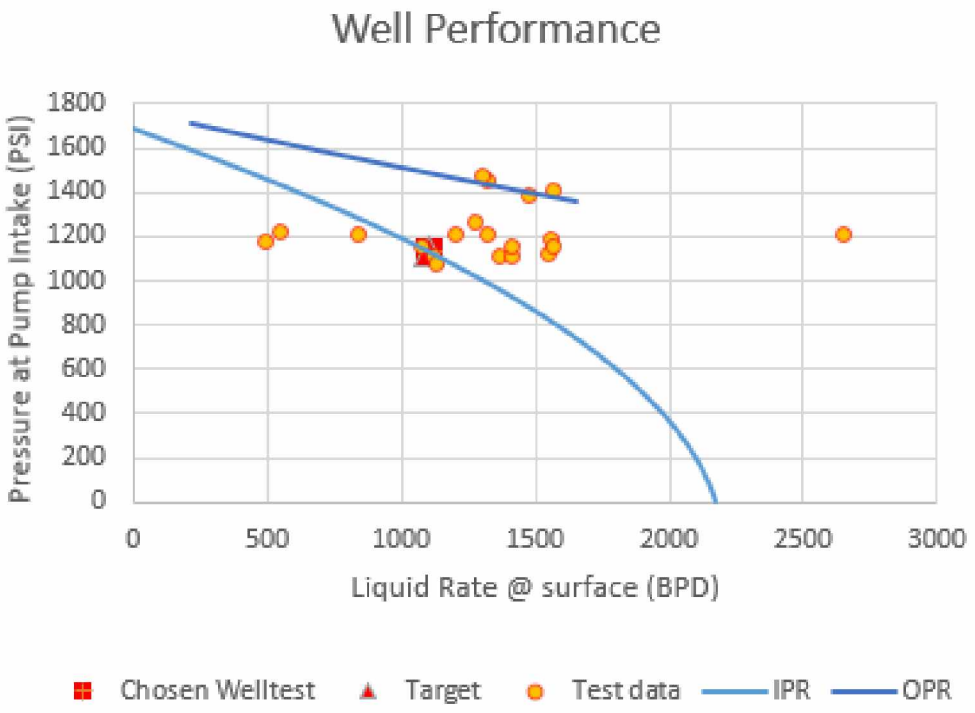

Figure 4.10 Well Inflow and Outflow Performance with Welltests plotted.

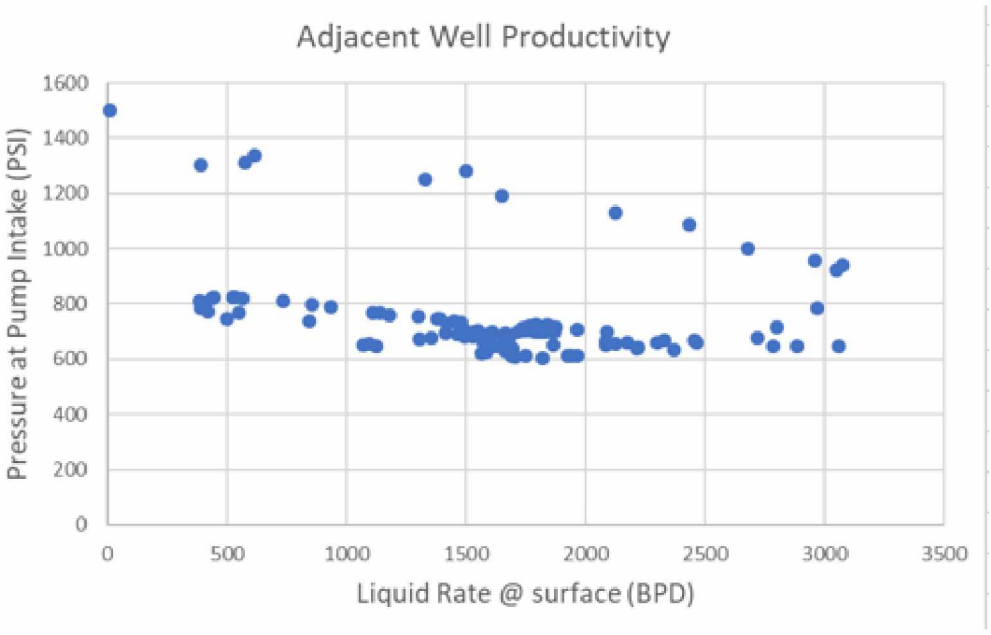

Figure 4.11 Adjacent Well Performance at Initial Startup.

This well does not have the ability to naturally flow to surface since the IPR and OPR curves do not intersect. The ESP must provide a pressure increase equal to the difference between the IPR and OPR curves, which equals about 300 psi differential pressure at 1100 bbl/day. The pressure differential curve in Figure 4.12 shows the difference between the IPR and OPR as a function of rate.

The pressure differential curve is converted to pump intake conditions in Figure 4.13. The total rate at pump intake is the sum of the water, oil, and gas rates at pump intake pressure and temperature. For a surface liquid rate of 1100 bbl/day with a GOR of 300 scf/bbl the total calculated fluid rate at pump intake is 1462 bbl/day. Since the pump performance is provided in feet of head, the pressure differential curve is converted to head so the two curves can be drawn together as in Figure 4.14. The new well performance curve is called the Total Dynamic Head (TDH). Where the two curves intersect should be the operating point of the well. When the performance curves do not match, either the pump curve or TDH curve should be adjusted to match the well conditions. Since the TDH curve has already been matched to the well conditions, the pump curve needs to be

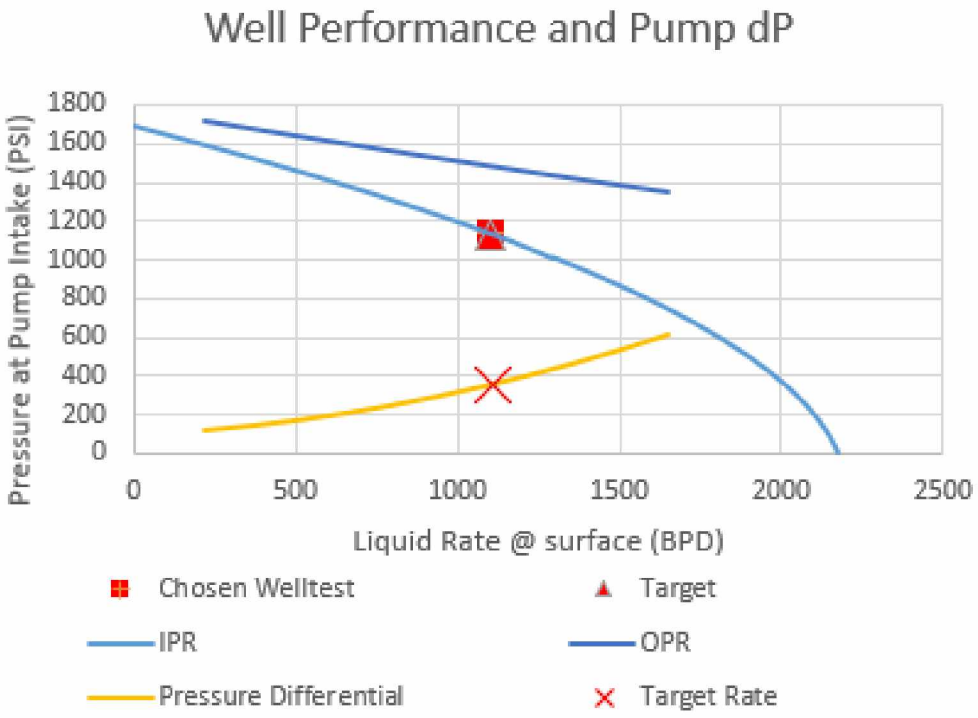

Figure 4.12 Well Inflow and Outflow Performance with Differential Pressure Required by Pump.

corrected for the well fluids.

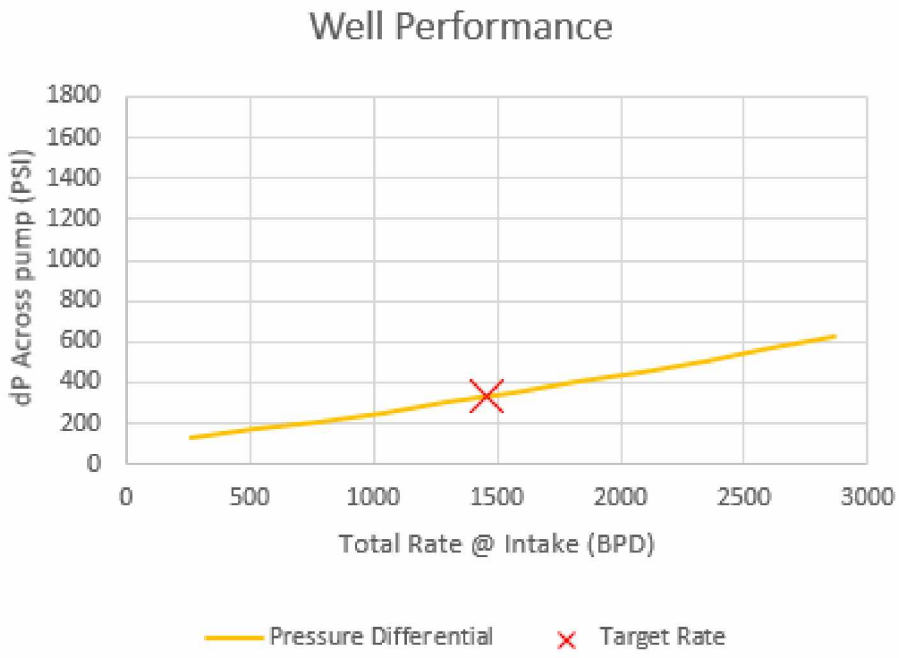

Figure 4.13 Differential Pressure Required by Pump plotted with Total Rate at Pump Intake Conditions.

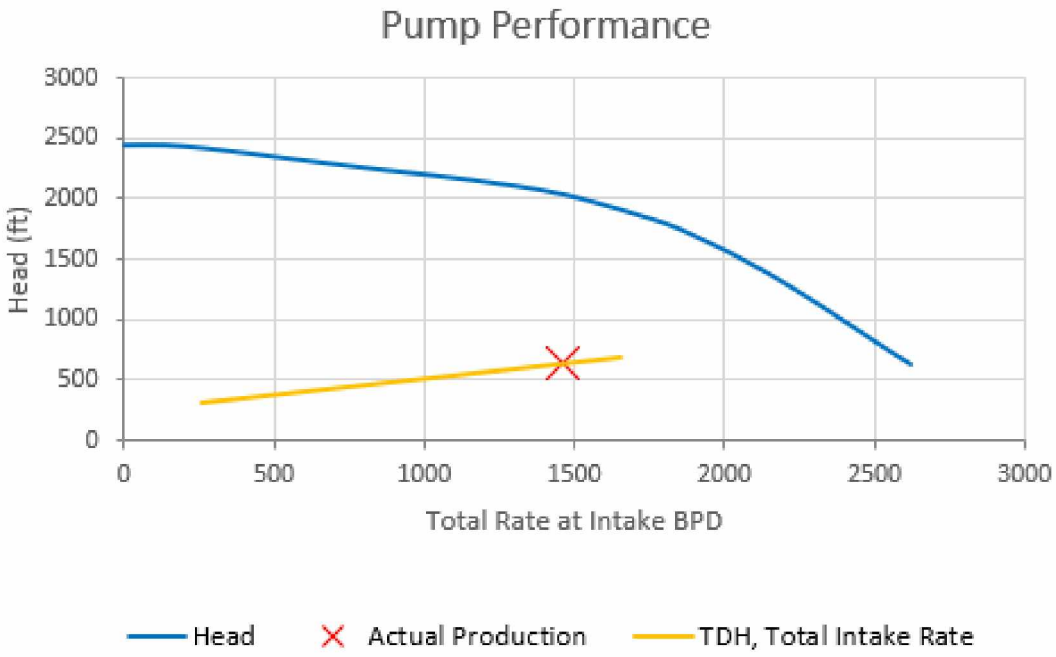

Figure 4.14 Differential Pressure Converted to Head, or TDH, and Plotted with the Pump Performance Curve Corrected for Operating Speed.

4.2 ESP Performance Characteristics

The ESP for this well is a tapered design to handle higher gas rates with a 48 stage SF3550 lower pump, 111 stage SF2700 upper pump, and standard bolt on intake. The "S" designation is for the manufacturer of the stage, Summit ESP a Halliburton Service. The "F" designation means the pumps are 400 series, or 4.00" OD, though both pumps have been reduced to 3.80" OD designed to be deployed thru-tubing via wireline or coiled tubing. The stage number is the pump rate in barrels per day at best efficiency point operating at 60 hz, or 120 hz with a 4 pole motor. The pump was sized to operate at 50 hz to provide room to increase the frequency if needed. The best efficiency point changes according to the affinity laws so the pump best efficiency rates are around 3,000 bbl/day for the SF3550, and 2,250 bbl/day for the SF2700 when operating at 50 hz. The pump performance curves are plotted using equation (4.1) and the parameters in Table 4.1 from the catalog pump curves. The head for each stage type is calculated and multiplied by the

number of stages. The pump curves are then combined by adding the head for each pump. This is the total pump head performance curve. The affinity laws are used to correct the pump curve for operating speed and the tornado plot is shown in Figure 4.15.

$$H(ft) = H_0 + H_1Q + H_2Q^2 + H_3Q^3 + H_4Q^4 + H_5Q^5 \tag{4.1}$$

Table 4.1 ESP Performance Curve Parameters with water at 3500 RPM.

Pump	H0	H1	H2	H3	H4	H5
2700	35.6	0.0012	$-9.820 * 10^{-6}$	$8.010 * 10^{-9}$	$-2.600 * 10^{-12}$	$2.67 * 10^{-16}$
3550	30.1	0.00154	$-1.620 * 10^{-6}$	$6.920 * 10^{-11}$	$4.780 * 10^{-14}$	$-8.460 * 10^{-18}$

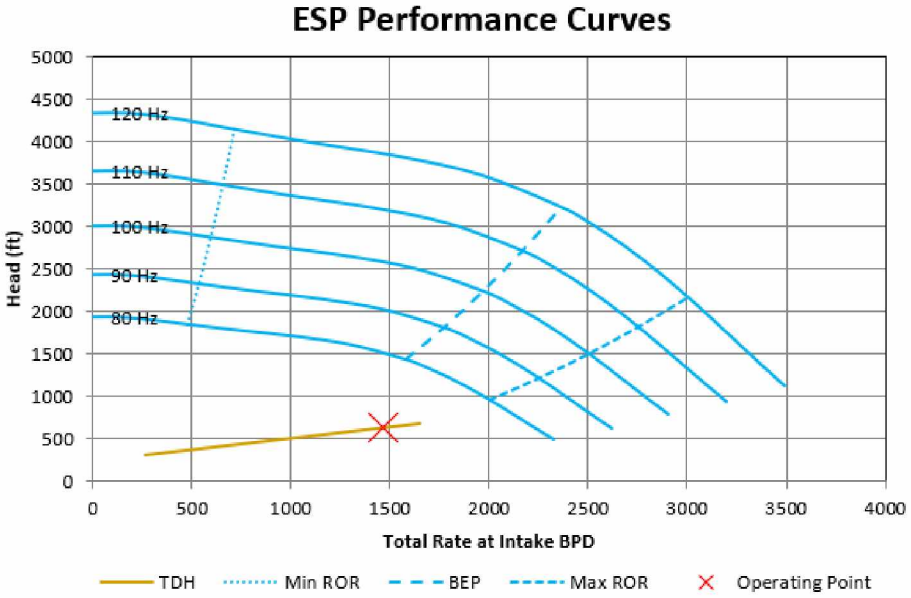

Figure 4.15 Pump Curves for Different Operating Frequencies and TDH curve with Operating Point.

The TDH curve does not intersect the pump curve at the correct operating frequency or rate. To de-rate the pump head, a viscosity correction was used based on the Hydraulic Institute method for de-rating due to Newtonian viscosity. With a dead oil viscosity of 192 cp, The calculated fluid mixture viscosity is 32 cp which has only a minor effect on pump

performance and does not fully explain the difference between the calculated and actual operating point as shown in Figure 4.16.

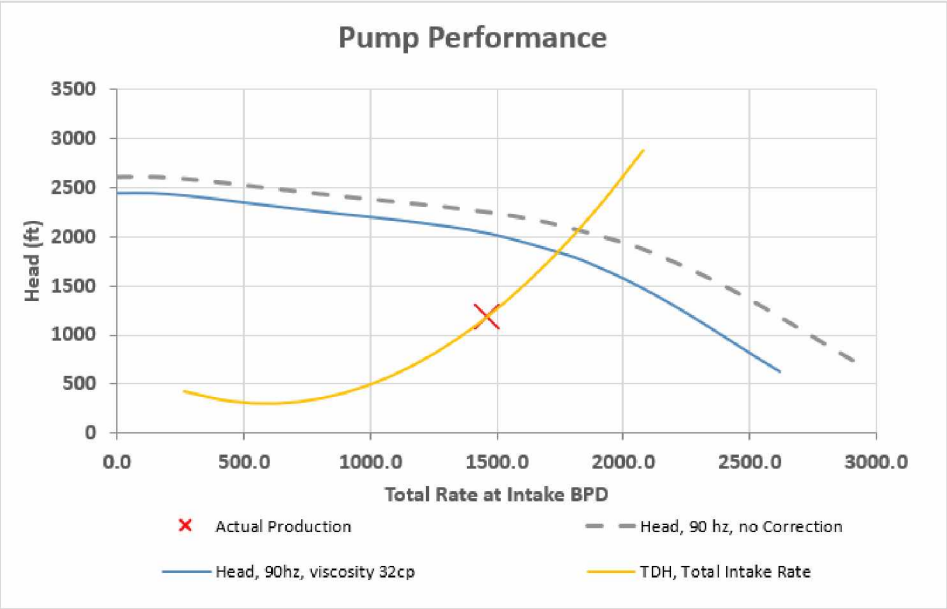

Figure 4.16 Pump Curves for Catalog Performance and de-rated for a fluid viscosity of 32cp.

4.3 Case Study Results

Using a calculated live oil viscosity of 82 cp at pump intake conditions, the calculated viscosity is 155 cp using calculations for foam dispersions discussed in Section 3.4. This value leads to a reduction in pump head generated of around 25% and a reduction in pump capacity of 40% but still overestimates the rate by about 100 bbl/day. The viscosity needed to get a good match for the pump using a viscosity de-rate is 192 cp as shown in Figure 4.17. While the results of the increased viscosity do not match the pump performance exactly, the predicted rate is much closer than when using just the mixture viscosity. The results indicate that a low watercut oil-gas mixture can reduce pump performance due to viscous effects similar to an oil-water emulsion. The low temperature and high viscosity crude, paired with asphaltenes and fines that act as surfactants, create a viscous foam that reduces the efficiency of an ESP. The operating efficiency in this case is

30%, well below the catalog of 60%. Since only one stabilized flow period occurred during the period of investigation the data for this study is limited. To verify that this de-rate accurately describes this well, more data would be needed using a similar approach over multiple well tests and operating conditions.

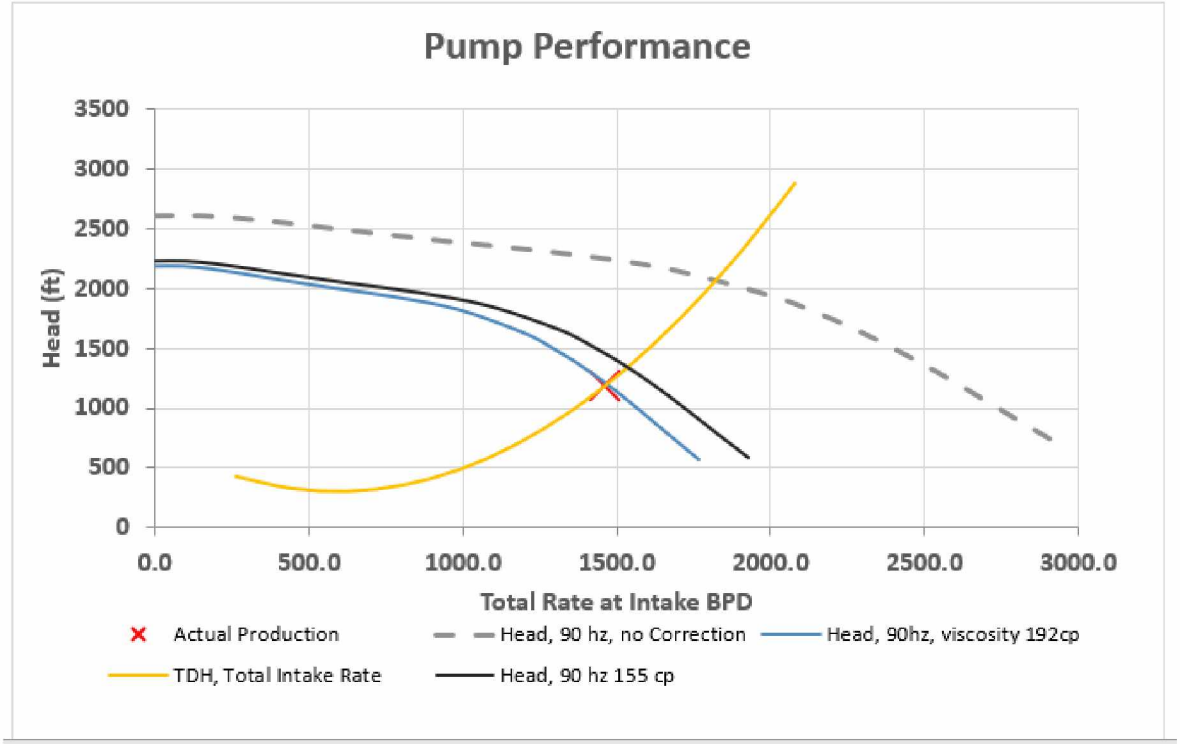

Figure 4.17 Pump Curves for Catalog Performance de-rated curves for a fluid viscosities of 155cp and 192 cp.

A lot of operations happened over the course of the 7 month period being investigated and only the most pertinent were discussed. The ESP performance did not match the well data when corrected for the expected viscosity and gas rate of the fluid. The ESP experienced periods of negative differential pressure, and changes in operating frequency seemed to have little effect on performance. A period of stable operation and production provided good data to correlate the ESP and well performance to get a good match. To account for the high de-rate required for the pump curve, the fluid properties required modeling as a disperse system. Rather than calculating fluid viscosity based on a

volumetric average of the individual fluid viscosities, a disperse model calculates a much higher viscosity which lines up better with the observed ESP performance. There is a complexity to the fluid that is difficult to capture in excel sheet calculations. In reality the local temperatures downhole will vary through the pump as areas of high friction create heat around the impeller. The ESP motor also generates heat that will provide additional heat to the fluid. The oils viscosity is highly dependent on temperature, where a 5 degree change in temperature can lead to a 70 cp change in viscosity. Centrifugal pumps tend to decrease the size of droplets due to high shear in the impeller, which could have an effect on the dispersion viscosity.

Despite these difficulties, an excel sheet was built that generates a reasonable match for well and pump performance curves that allows more flexibility in de-rating the pump for fluids that do not behave as simple mixtures. The next section includes some case studies to look at how Engineers have tackled difficult fluids operationally and through pump design.

4.4 Case Studies by Other Authors

ESPs are installed all around the world and case studies from other locations can be helpful in understanding how others have tackled tough problems with fluids. This section includes operations with difficult working fluids and some unique pumps that have been designed to handle extreme fluids.

Agrawal et al. (2019) present a case study in the Mangala field in India with the production of a polymer flooded field with ESP. Initial waterflood of the field yielded very good results with ESPs. The field later transitioned to polymer flood, and after polymer breakthrough occurred ESP performance declined. Motor temperatures increased, well productivity declined, and pump head and rate declined.

The reservoir produces between 20-28 API oil with an average 78% watercut at 149 °F reservoir temperature. Gas volume fractions at pump intake are typically less than 10%. The field has 30 running ESP wells and over 100 jet pumps with a trend towards an

increasing number of ESPs. The authors had good ESP data from several years of waterflood performance when polymer breakthrough occurred and performance declined. The authors performed deadhead tests by shutting in the well at surface and monitoring the head generated from pressure readings. This confirmed that the pumps were able to generate the expected head at zero rate, but under flowing conditions the pumps only produced 50% of expected rate. This indicated that the pump does not have mechanical wear which would lead to leakage and recirculation at no flow. The reduced head at higher flow was determined to be most likely due hydraulic and friction losses. A step rate test with the well choked back in 100 psi increments at constant speed provided operating points to determine the shape of the pump curve as shown in Figure 4.18. This test exhibited a sudden reduction in head at a critical rate, indicating a plugged pump as described by Divine (1993). This finding was verified with Dismantle, Inspection, and Failure Analysis (DIFA) of a failed pump that found thick polymer deposits in the pump stages. The polymer buildup likely led to increased torque and ultimately a shaft break. Injection of chemical solvents was attempted to remediate problems but early results indicate further optimization of chemical treatments is necessary.

Castro et al. (2015) present a case study in the Peregrino Field, Campos Basin offshore Brazil. The produced fluid is 13-15 API with viscosity of 129-364 cp and 73 scf/STB GOR. 30 ESPs are installed in the field with production rates from 2,000-20,000 bbl/day. 9 5/8" casing allowed 5.38", 5.62", and 6.75" OD pumps to be installed which are generally better suited to handle high viscosity than smaller OD pumps. Every completion was either installed with a packer above the ESP, or ESP installed in a capsule. Diverter valves installed above the ESPs direct falling sand to the annulus to prevent buildup of sand above pump when the ESP is shut down. Chemical injection was used to prevent emulsion problems. Early field development required large operating ranges for ESPs due to uncertainty in well productivity. The operator and ESP manufacturer aimed to standardize on 3 designs for the field to cover high, medium, and low rate wells with minimal inventory.

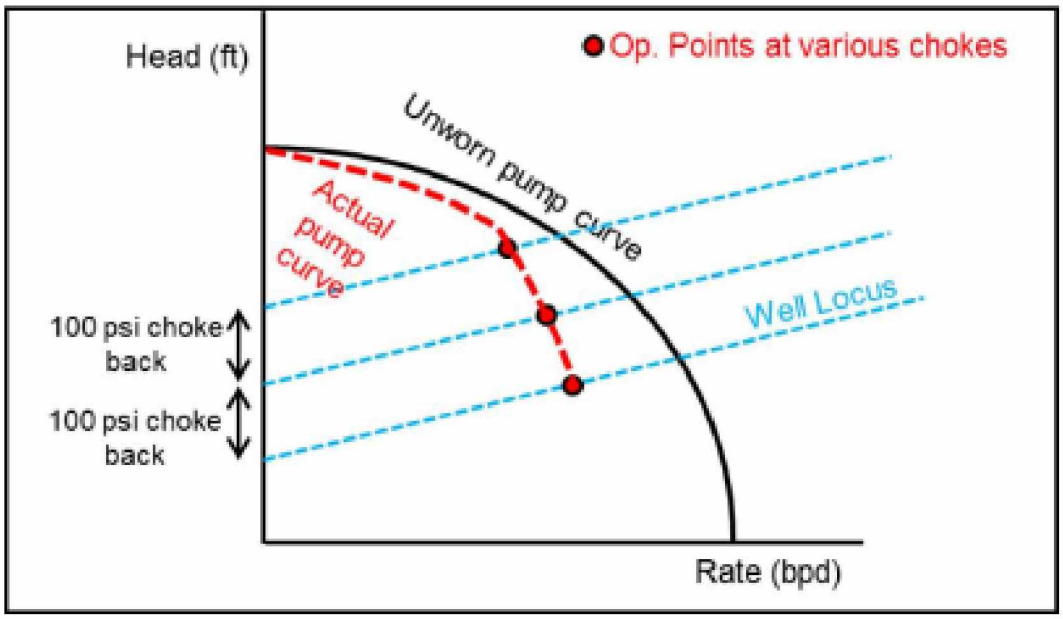

Figure 4.18 Pump Curve at Various Choke Points vs Catalog Curve used to Diagnose Severity of Plugging (Agrawal 2019).

Carpenter and McCrea (1995) studied Beta field offshore California with 55 ESP wells over 12 years for 560 total ESP installs. The field is a waterflood with average production of 400 bbl/day with 57% watercut. Although the wells have low GOR, all ESPs have gas separators. The crude was between 10 and 19 API. The reservoir temperature of 170 °F and operating intake temperatures around 200 °F lead to average insitu oil viscosity of 50 cp with a range of 30-500 cp. The lack of gas precluded gas lift as an artificial lift option. With wells producing lower than 400 bbl/day, ESPs become ineffective and hydraulic jet pumps were preferred.

ESP efficiency ranged from 35% at best to 10% at worst. The initial design method used viscous correction factors based on field viscosity data and manufacturers recommendation for derating head, rate, and BHP. In addition to de-rating, 12% free gas was assumed and 15% additional stages added and 20% additional horsepower. The pumps were sized to achieve drawdown to 200 psi intake from 1800 psi static bottomhole pressure. As information was gained from initial pumps, next pumps were installed with less safety

factor and fewer stages. Most wells reached steady state, but very heavy oil wells cycled as the pump and motor added heat which reduced fluid viscosity and the wells were pumped down. The pumps then gas locked due to low intake pressure and intake pressure rises again restarting the cycle.

Some wells were affected by emulsion formation, but emulsions were not deemed a significant problem. Attempts to treat with chemicals were not successful. A second producing platform called Eureka found 10 API crude unpumpable without dilution. A water injection system was devised to inject at the base of a shroud to increase water cut and reduce viscosity.

Lopez et al. (2014) studied an extra heavy oilfield in the Colombian Llanos Basin. With reservoir temperature of 180-185 °F the oil viscosity ranged from 62-1300 cp. 16 ESP runs in 5 representative wells were available for study. Average ESP efficiency for 4 inch OD pumps was 5.34%. For 5 inch pumps the average efficiency was 16.52% with maximum 32.45%. (60% higher efficiency compared to 400 series pumps). 100 samples from 60 wells were tested to develop a viscosity vs temperature correlation for the field.

Eremiokhale (2013) investigated ESP installations in offshore Nigeria's Y field. The produced oil was 11-14 API with viscosity of 100-200 cp at reservoir temperature. A pilot well with ESP yielded hopeful results and a total of 5 ESPs were later installed. Initial pumps were sized for 0% wc oil. As water cut increased, emulsions became problematic and pump efficiency decreased. The initial pumps were undersized for the emulsion and upgraded by about 10% BHP, 10% more stages, and increased pump capacity. Naturally occurring surfactants were confirmed to be present in the reservoir and foam was was noted as an issue, though no information was provided on the effect this had on viscosity. Gas lift backup allowed about 65% of ESP production to be recovered while an ESP was down waiting for a rig. Artificial lift redesigns include trickle feed demulsifying agent at pump intake and use of PCPs instead of ESPs.

Barrios et al (2017) studied high horsepower, high rate, multivane pumps for subsea boosting systems at BC-10 offshore Brazil. Testing and qualification of the system was performed at Shell's ESP test facility in Houston. Because of the cost and complexity of the system, full testing over the range of expected operating conditions was conducted in the lab. The authors tested for viscosity, flow rates, and gas volume fraction to develop curve corrections for the pumps. The pumps were of 10.25" and 8.75" OD and included multivane pumps as charge pumps. Charge pumps are usually designed to handle high gas fractions and process the fluid before entering the production pumps. The system was able to produce up to 1200 cp emulsions with 55% gas fraction in the field with behavior matching the experimental data. Demulsifier injection increased pump performance significantly by decreasing the apparent emulsion viscosity.

Best et al. (2017) applied PCP technology to ESPs for a Permian Basin study in an attempt to combat high gas volumes. The application used Geared Centrifugal Pumps (GCP) in a miscible CO2 flood where high gas liquid ratios created problems for traditional ESPs. The GCP is driven from surface through a rod string that utilizes a downhole 7:1 geared transmission to convert the low RPMs of the rod string to normal centrifugal pump operating speed. The system uses a drive head just like a surface driven PCP to allow centrifugal pump operation without downhole electrical equipment. This allows the system to operate at very high temperatures such as in SAGD applications for which it was initially designed.

This system was chosen in this study because it allowed a fiberglass dip tube to be run on the bottom of the pump through the perforations. This allowed maximum natural gas separation without concern of motor cooling. 2 units were tested in existing ESP wells with portable separators temporarily installed to compare production before and after installation of the GCPs. Total fluid volumes averaged 500 bbl/d. The measured gas separation efficiency for the systems were 92% and 77% with maximum GLRs of 1,330 and 424 scf/bbl respectively. The increased gas separation led to increased runtime due to

fewer gas lock shutdowns. Power meters installed on each well indicated an increase in efficiency when converted from ESP to GCP. Results indicate this system has potential to operate efficiently in high GLR applications, however one of the units failed after only 26 days due to rod part so the reliability of the system will need to be proven. The system also has a limiting value of 60 pump horsepower and is limited to a single pump section.

Difficult operations sometimes require ingenuity in the design of artificial lift systems. As heavy oil production becomes more common, the artificial lift industry will need to develop more reliable and efficient methods of operating in difficult fluids. Gas flow has already become achievable at higher rates with new impeller and diffuser designs. Viscous pumping is another challenge but there are some interesting options for better pump design.

One design that has been trialed in high gas and high viscosity applications is a helicoaxial design. This pump operates like a centrifugal with large axial stages as shown in Figure 4.19. The pump has been tested at greater than 50% gas volume fraction and viscosity upwards of 10,000 cp. The pump can also pump high sand concentrations without plugging. (Simpson 2017)

Figure 4.19 V-Pump Cohelical Axial Design Impeller and Diffuser (Simpson 2017).

This review is only a brief overview in regards to case studies involving ESPs, but covers a range of important concepts for solving artificial lift problems. Diagnosing a problem is an important step and the more data that is available the better. Table 4.2 provides an overview of additional case studies that are useful in that they present unique designs or operations.

Table 4.2 Selection of ESP Case Studies

Location/Field	Problem/Topic	Solution	Title	Year	Source Paper
Alaska Ugnu	High viscosity, sand	Heat trace, PCP	Alaskan Heavy Oil: First CHOPS at a Vast, Untapped Arctic Resource	2010	Young et. al. SPE-133592-MS
Brazil BC-10/ GoM Perdido	Subsea boosting	Caisson ESP application	The Development of Subsea Boosting Capabilities for Deepwater Perdido and BC-10 Assets	2010	Gilyard and Brookbank SPE-134393-MS
Brazil Peregrino Offshore	Reliability in Heavy Oil	DIFA, ESP component redesign	ESP Technology Improvements in Peregrino Field	2019	Castro et. al. SPE-194401-MS
California Offshore DST	Heavy oil, drill stem testing	Continuous monitoring	Experience with Electric Submersible Pumps for Testing Heavy Oil Reservoirs from Floating Drilling Vessels	1986	Crossley OTC-5318-MS
California McKittrick	Gas, sand	Cohelical Axial Multiphase Pump	Piloting a Cohelical-Axial Multiphase ESP Design in a Sandstone Reservoir Where Rod Pumping Failed	2019	Dunn and Harris SPE-194410-MS
China Bohai Bay	Heavy oil	Continuous monitoring, encapsulated ESP	Successful Application of ESPs in Bohai Bay Development	2012	Sheridan et al. SPE-156176-MS
Columbia Maranta Block	Heavy oil	Transition from ESP to Long Stoke Pumping Unit	Replacement of ESP with Long Stroke Pumping Units in Heavy and High Viscous Oil in Maranta Block Wells	2015	Sarmiento et al. SPE-177272-MS

Table 4.2 Continued.

Location/Field	Problem/Topic	Solution	Title	Year	Source Paper
Columbia Rubiales field	Heavy oil, reliability	Real time monitoring, completion design	Lessons Learned from Extending Run Life for Hundreds of ESPs in a Heavy Oil Environment	2018	Mogollon et al. SPE-189736-MS
Congo Likalala and Kombi fields	Gas	Poseidon Pump	Poseidon Gas Handling Technology: A Case Study of Three ESP Wells in the Congo	2011	Camilleri et. al. SPE-141668-MS
Italy Vega and Gela Fields	Heavy oil, high cost RWO	Jet pump backup with ESP completion	Jet Pump Testing in Italian Heavy Oils	1994	De Ghetto and Giunta SPE-27595-MS
Mexico Samaria Luna Field	Reliability, gas, high temp	Root Cause Analysis, operating procedures	Design, Operation, Diagnosis, Failure Analysis and Optimization of ESP Systems in Wells with Great Depths, High Temperature, high GOR and High Concentrations of CO2, N2, H2S in Samaria Luna Field	2017	Ramirez and Martinez SPE-185275-MS
Nigeria Y Field Offshore	Emulsion viscosity	Chemical injection, convert to PCP	Development of Heavy Oil Reservoirs: A Case Study of a Low API Reservoir Offshore Nigeria	2013	Eremiokhale et. al. SPE-167573-MS
Romania Sinoe offshore	Scale, gas	Chemical injection, gas separator	First Installation of 5 ESPs Offshore Romania- A Case Study and Lessons Learned	2010	Camilleri et al. SPE-127593-MS

Table 4.2 Continued.

Location/Field	Problem/Topic	Solution	Title	Year	Source Paper
Saudi Arabia Three reservoir study	Emulsion viscosity	Fluid characterization, solids management, chemical treatment	An Investigative Study of Potential Emulsion Problems Before Field Development	2007	Kokal et al. SPE-102856-PA
Suriname Tambarejo	Low rate, heavy oil	Converted PCP to ESP for greater drawdown	Increased Rates, Reserves, and Revenues from Heavy Oil Reservoir Using ESP Technology: A Suriname Case Study	2009	Grauwde SPE-122006-MS
Thailand Nong Yao Field	Sand production	Sand screens	The First Application of Specialty Sand Screens in Combination with Fully Integrated ESP Technology in the Nong Yao Field, Gulf of Thailand	2017	Chigbo et al. SPE-185377-MS
Tunisia Sidi El Itayem Field	Gas	Multiphase Poseidon Pump, recirculation	Field Tests of the Poseidon Pump	1992	Gie SPE-23624-MS
UK Bentley Field North Sea	Heavy oil, drill stem test	Encapsulated POD ESP	Methodologies, Solutions, and Lessons Learned from Heavy Oil Well Testing with an ESP, Offshore UK in the Bentley Field, Block 9/3b	2011	Brennan et al. SPE-148833-MS

Table 4.2 Continued.

Location/Field	Problem/Topic	Solution	Title	Year	Source Paper
Venezuela Jobo and Cerro Negro	Heavy oil	Sidetrack of vertical wells, convert from PCP to ESP with dilution	Production Optimization of Re-entries by Means of Electrical Submersible Pump	1996	Joubert et al. SPE-37137-MS
Venezuela South Monagas Unit	CO2 and SRB corrosion, gas	Design, monitoring, metallurgy, chemical injection	Case Study: Successful Implementation of ESPs in a High-GOR, Poorly Consolidated, Corrosive Field	2005	Guevara et al. SPE-96991-MS
Venezuela Orinoco Belt	Heavy oil	Conversion from Rod Pump to ESP	Producing Extra Heavy Oil from the Orinoco Belt by Electrical Submersible Pumping System – a Pilot Test	1994	Gonzalez and Reina SPE-26987-MS
Venezuela Urdaneta West	Power consumption in heavy oil	Extrapolate from existing well performance	Proposed Methodology to Predict Electric Power Requirements for ESP Wells in a Heavy Oil Field- A Case Study	2008	Brito and Montero SPE-118073-MS

CHAPTER 5

CONCLUSIONS

This project reviewed the fundamentals of centrifugal pumps and how fluid properties affect their performance. The factors that effect pump boosting pressure most adversely are viscosity, gas fraction, and flow regime through the pump. Viscosity can reduce the head and rate capacity of the pump significantly. High gas volume reduces the head capacity of the pump and can lead to surging. If the gas bubbles transition from dispersed flow to elongated bubble flow the pump can gas-lock and overheat the motor. The flow path through an ESP is complex and mechanistic models are not yet developed enough to be generally applicable, so simplifying assumptions are often made. Empirical methods used to develop correlations can accurately be applied to model pump performance with viscous crude and gas, but studies with stable dispersions are limited. With multiple components, interfacial properties become important and can dominate the bulk fluid properties. An apparent viscosity can be used to bridge the gap and account for disperse fluids.

The methods reviewed for calculating dispersion viscosity and pump de-rate were applied to a field case study and with reasonable accuracy described the performance of the pump with a viscous foamy crude. Prior knowledge of the produced reservoir fluids indicated solids production and emulsions are common is this field. Even though this well has a low water rate, it seems the production of natural surfactants such as fines and asphaltene lower the surface tension of the oil and gas mixture and create a stable foam that has properties similar to an oil-water emulsion. The viscosity of the fluid appears to be higher than an oil-gas mixture due to colloidal and interface effects. Pump sizing may need to increase the number of stages and horsepower accordingly.

The formation of small stable bubbles allows for high gas fraction to flow through the pump without gas-locking. The natural gas separation efficiency is low so that almost all of

the gas produced at surface flows through the pump. Gas corrections must take into account the high gas rate from reduced separation. The effect is reduced pump head and rate capacity with higher fluid volume through the pump.

The completion of an ESP in wells with emulsion or foaming tendency may consider chemical injection to reduce the effect of these fluids on the ESP with the use of emulsion breaker or anti-foam. Retention time is an issue that would need to be investigated to determine if the chemicals would work quickly enough during production to affect pump performance. Dilution of the produced fluid may also effectively reduce the viscosity. When solids and fines are produced with well fluids they can act as surfactants so limiting the production of solids may improve ESP performance. Experimental testing of the produced fluid with an ESP in a test loop is not practical in all scenarios due to high costs and test loop limitations. A possible path forward for better performance prediction would be to test ESP pump stages in a flow loop with a viscous mineral oil over a range of viscosities and develop catalog performance curves for higher viscosity fluid. To utilize viscous pump curves, accurate produced fluid viscosity information is necessary. The viscosity measurements of produced fluids could be used with the manufacturer's viscosity curves to better predict pump performance. Viscosity variation with temperature, pressure, and shear may be important in determining the fluid viscosity at pump intake and through the pump. With the significant volumes of heavy oil worldwide yet to be produced, understanding the effects this oil will have on pumps is likely to become more important.

References

Adil, I., & Maini, B. (2007, April). Role of Asphaltenes in Foamy Oil Flow. JCPT, 46(4), 18-23.

Agrawal, N., Chapman, T., Baid, R., Singh, R. K., Shrivastava, S., Kushwaha, M. K., ... Aggarwal, S. (2019, April 8). ESP Performance Monitoring and Diagnostics for Production Optimization in Polymer Flooding: A Case Study of Mangala Field. Society of Petroleum Engineers. doi:10.2118/194656-MS

Alhanati, F.J.S. Bottomhole Gas Separation Efficiency in Electrical Submersible Pump Installations. Ph.D. Thesis, The University of Tulsa, Tulsa, OK, USA, 1993.

Alshmakhy, A., & Maini, B. B. (2010, January 1). Viscosity of Foamy Oil. Society of Petroleum Engineers. doi:10.2118/136665-MS

ANSI/HI 9.1-9.5. (2000). Pumps – General Guidelines. New Jersey.

ANSI/HI 9.6.7. (2010). Rotodynamic Pumps - Guideline for Effects of Liquid Viscosity on Performance. New Jersey.

Aoghs.org. (2020, June 10). Inventing the Electric Submersible Pump. Retrieved October 12, 2020, from American Oil & Gas Historical Society: https://aoghs.org/technology/electric-submersible-pump-inventor

API RP 11S2. (1997). Recommended Practice for Electric Submersible Pump Testing. Washington, D.C.

Barnes, H., Hutton, J., & Walters F.R.S., K. (1993). An Introduction to Rheology. Amsterdam, The Netherlands: Elsevier.

Barrios, L., Rojas, M., Monteiro, G., & Sleight, N. (2017, April 24). Brazil Field Experience of ESP Performance with Viscous Emulsions and High Gas Using Multi-Vane Pump MVP and High Power ESPs. Society of Petroleum Engineers. doi:10.2118/185141-MS

Batchelor, G. (1977). The Effect of Brownian Motion on the Bulk Stress in a Suspension of Spherical Particles. J. Fluid Mech, 97-117.

Best, G., Delaloye, R. J., Nicholson, B. L., & Morrow, W. B. (2017, April 24). Geared Centrifugal Pump Performance in an Enhanced Oil Recovery Field. Society of Petroleum Engineers. doi:10.2118/185131-MS

Brennan, B., Lucas-Clements, C., Kew, S., Shumakov, Y. A., Camilleri, L. A. P., Akuanyionwu, O. C., ... Simpson, J. (2011, January 1). Methodologies, Solutions, and Lessons Learned from Heavy Oil Well Testing with an ESP, Offshore UK in the Bentley Field, Block 9/3b. Society of Petroleum Engineers. doi:10.2118/148833-MS

Brinkman, H.C., 1952. The viscosity of concentrated suspensions and solutions. The Journal of Chemical Physics, 20(4), 571.

Brito, R., & Montero, J. (2008, January 1). Proposed Methodology to Predict Electric Power Requirements for ESP Wells in a Heavy Oil Field - A Case Study. Society of Petroleum Engineers. doi:10.2118/118073-MS

Camilleri, L. A. P., Banciu, T., & Ditoiu, G. (2010, January 1). First Installation of Five ESPs Offshore Romania - A Case Study and Lessons Learned. Society of Petroleum Engineers. doi:10.2118/127593-MS

Camilleri, L. A. P., Brunet, L., & Segui, E. (2011, January 1). Poseidon Gas Handling Technology: A Case Study of Three ESP Wells in the Congo. Society of Petroleum Engineers. doi:10.2118/141668-MS

Carpenter, D. E., & McCrea, A. A. (1995, January 1). Beta Field History: Submersible Pumps in Heavy Crude. Society of Petroleum Engineers. doi:10.2118/29508-MS

Castro, V., Leite, D., Lemos, D., Marins, J., Pessoa, R., & Magalhães, J. (2015, May 27). ESP Application on Heavy Oil in Peregrino Field. Society of Petroleum Engineers. doi:10.2118/173948-MS

Castro, V., Pastre, L., & Marins, J. (2019, May 6). ESP Technology Improvements in Peregrino Field. Society of Petroleum Engineers. doi:10.2118/194401-MS

Chigbo, I. T., Opdal, S. T., Tarasombut, P., Gordon, G., Rekijtisirikul, N., Duangprasert, T., ... Wells, D. G. (2017, April 4). The First Application of Specialty Sand Screens in Combination with Fully Integrated ESP Technology in the Nong Yao Field, Gulf of Thailand. Society of Petroleum Engineers. doi:10.2118/185377-MS

Crossley, E. G. (1986, January 1). Experience With Electric Submersible Pumps For Testing Heavy Oil Reservoirs From Floating Drilling Vessels. Offshore Technology Conference. doi:10.4043/5318-MS

Daugherty, R.L. "A Further Investigation of the Performance of Centrifugal Pumps when Pumping Oils." Bull. 130, Goulds Pumps, Inc., 1926.

De Ghetto, G., & Giunta, P. (1994, January 1). Jet Pump Testing in Italian Heavy Oils. Society of Petroleum Engineers. doi:10.2118/27595-MS

De Leonardis, D., Shumakov, Y., Morton, K. L., & Sarac, S. (2017, April 5). ESP-DST Well Testing in a Complex Reservoir in the Barents Sea: Establishing New Methodologies and Lessons Learned. Society of Petroleum Engineers. doi:10.2118/185892-MS

Divine, D. L., Lannom, R. W., & Johnson, R. A. (1993, August 1). Determining Pump Wear and Remaining Life From Electric Submersible Pump Test Curves. Society of Petroleum Engineers. doi:10.2118/22399-PA

Dunn, P., & Harris, D. (2019, May 6). Piloting a Cohelical-Axial Multiphase ESP Design in a Sandstone Reservoir Where Rod Pumping Failed. Society of Petroleum Engineers. doi:10.2118/194410-MS

Einstein, A., 1911. Elementary consideration of the thermal conductivity of dielectric solids. Ann. Phys., German, 34,pp.591.

Eremiokhale, O., Zeito, G., & Orioha, H. (2013, August 5). Development of Heavy Oil Reservoirs: A Case Study of a Low API Reservoir Offshore, Nigeria. Society of Petroleum Engineers. doi:10.2118/167573-MS

Estevam, V., Franca, F. A., & Alhanati, F. J. S. (2005, May 25). Two-Fluid Model Based Relationships for Gas-Liquid Centrifugal Pumping Analysis. BHR Group.

Farris, R.J., 1968. Prediction of the Viscosity of Multimodal Suspensions from Unimodal Viscosity Data. Transactions of the Society of Rheology 12, 281. doi:10.1122/1.549109

Gamboa, J. Prediction of the Transition in Two-Phase Performance of an Electrical Submersible Pump. Ph.D. Thesis, The University of Tulsa, Tulsa, OK, USA, 2008.

Gie, P. (1992, January 1). Field Tests of the Poseidon Pump. Society of Petroleum Engineers. doi:10.2118/23624-MS

Gilyard, D. T., & Brookbank, E. B. (2010, January 1). The Development of Subsea Boosting Capabilities for Deepwater Perdido and BC 10 Assets. Society of Petroleum Engineers. doi:10.2118/134393-MS

Gonzalez, R., & Reina, M. (1994, January 1). Producing Extra Heavy Oil from the Orinoco Belt by Electrical Submersible Pumping System - A Pilot Test. Society of Petroleum Engineers. doi:10.2118/26987-MS

Goridko, K. A., Kobzar, O. S., Khabibullin, R. A., Verbitsky, V. S., Litvinenko, K. V., & Grishaev, M. S. (2020, October 26). Analysis of Self Flowing through Annulus of wells operated with Electric Submersible Pumps, Western and Eastern Siberia Fields Cases. Society of Petroleum Engineers. doi:10.2118/201878-MS

Gorla, R., & Khan, R. (2003). Turbomachinery Design and Theory. New York, USA: Marcel Dekker.

Grauwde, G. (2009, January 1). Increased Rates, Reserves, and Revenues From Heavy Oil Reservoir Using ESP Technology: A Suriname Case Study. Society of Petroleum Engineers. doi:10.2118/122006-MS

Griffith, P., and Wallis, G. B. (August 1, 1961). "Two-Phase Slug Flow." ASME. J. Heat Transfer. August 1961; 83(3): 307–318. doi.org/10.1115/1.3682268

Guang, L.W. (2000). The Sudden Rising Head Effect in Centrifugal Pumps. World Pumps, 2000(409), 34-36. doi:10.1016/S0262-1762(00)90229-3

Guevara, L. A., McKee, J. P., Marin, H., Sanmiguel, M., Rincon, G., & Vera, L. (2005, January 1). Case Study: Successful implementation of ESPs in a High-GOR, Poorly Consolidated, Corrosive Field. Society of Petroleum Engineers. doi:10.2118/96991-MS

Guo et al. (2009). Molecular Diffusion Coefficients of the Multicomponent Gas−Crude Oil Systems under High Temperature and Pressure. Industrial and Engineering Chemistry Research, 48(19), 9023-9027. doi:10.1021/ie801671u

Guth, E., & Simba, R. (1936). Investigations of the Viscosity of Suspsensions and Solutions: Part 3. The Viscosity of Spherical Suspensions. Colloid & Particle Science, 74(3), 266-275.

Hagedorn, A.R. and Brown, K.E. (April 1965). Experimental Study of Pressure Gradients Occurring During Continuous Two-Phase Flow in Small-Diameter Vertical Conduits. JPT 475; Trans., AIME, 234

Halliburton.comA,https://www.halliburton.com/content/dam/ps/public/artificial˙lift/contents/Brochures/web/summit-tiger-shark-pump.pdf?node-id=1582039188019&nav=en-US˙artificial-lift˙public)

Halliburton.comB,https://www.halliburton.com/content/dam/ps/public/artificial˙lift/contents/Data˙Sheets/web/tiger-shark-gas-handler-pump.pdf?node-id=1582039188019&nav=en-US˙artificial-lift˙public

Hydraulic Institute. 1969. Determination of Pump Performance When Handling Viscous Liquid, HI Standards, 20th Edition.

IFCpump.com. (2020). Borets Horizontal Pumping Systems. Retrieved October 18, 2020, from Industrial Fluid Consultants: http://ifcpump.com/category/borets

Joubert, G., Brito, H., & Yibirin, J. (1996, January 1). Production Optimization Of Re-Entries By Means Of Electrical Submersible Pump. Society of Petroleum Engineers. doi:10.2118/37137-MS

Khalil, Mohamed & Kassab, Sadek & Ismail, Ashraf & Elazab, Ibrahim. (2008). CENTRIFUGAL PUMP PERFORMANCE UNDER STABLE AND UNSTABLE OIL-WATER EMULSIONS FLOW.

Kokal, S. L., Ghamdi, A., & Meeranpillai, N. S. (2006, January 1). An Investigative Study of Potential Emulsion Problems Before Field Development. Society of Petroleum Engineers. doi:10.2118/102856-MS

Korpela, S.A., 2011. Principles of Turbomachinery. John Wiley & Sons, Inc., New Jersey, USA.

Krieger, I.M., 1972. Rheology of monodisperse latices. Advances in Colloid and Interface science, 3(2), pp.111–136.

Lea, J. F. and Bearden, J. L.: "Effect of Gaseous Fluids on Submersible Pump Performance", JPT, December 1982 and SPE 9218.

Lopez, J. E., & Jimenez Morales, G. esperanza. (2014, June 10). ESP Optimization in an Extra Heavy Oil Field: Case Study in Colombian Llanos Basin. Society of Petroleum Engineers. doi:10.2118/170039-MS

Liu, G., Cao, W., Li, Y., Wang, D., & Liu, B. (2014). Study on solid-liquid two-phase unsteady flow in multistage pump. Stevenage: The Institution of Engineering & Technology. doi: 10.1049/cp.2014.1244

Lyons, W.C., 2010. Working Guide to Drilling Equipment and Operations. Elsevier, Oxford, UK.

Marsden, S. S., & Khan, S. A. (1966, March 1). The Flow of Foam Through Short Porous Media And Apparent Viscosity Measurements. Society of Petroleum Engineers. doi:10.2118/1319-PA

Marquez, R. Modeling Downhole Natural Separation. Ph.D. Thesis, The University of Tulsa, Tulsa, OK, USA, 2004.

Mogollon, M., Arguelles, A., Rodriguez, A., Anaya, O., Miranda, S., Velasquez, E., & Villalobos, J. (2018, March 13). Lessons Learned from Extending Run Life for Hundreds of ESPs in a Heavy Oil Environment. Society of Petroleum Engineers. doi:10.2118/189736-MS

Morales, R., Pereyra, E., Wang, S., & Shoham, O. (2012, December 14). Droplet Formation Through Centrifugal Pumps for Oil-in-Water Dispersions. Society of Petroleum Engineers. doi:10.2118/163055-PA

Murakami, M. and Minemura, K., 1974, "Effects of Entrained Air on the Performance of a Centrifugal Pump, First Report - Performance and Flow Conditions," Bulletin of JSME, Vol. 17, N°. 110, pp 1047-1055

oedigital.com. (2016). Rethinking Subsea Pumping. Retrieved October 18, 2020, from oedigital.com: https://www.oedigital.com/news/448219-rethinking-subsea-pumping

Pressurepumping.com. (2020). Frac Pumps. Retrieved October 18, 2020, from Pressurepumping.com: https://www.pressurepumping.com/equipment/frac-pumps

Production-technology.org. (2017). Pump Performance CUrve - Part 01. Retrieved October 25, 2020, from Production Technology: https://production-technology.org/pump-performance-curves/

Ramirez, M., & Martinez, J. F. (2017, April 24). Design, Operation, Diagnosis, Failure Analysis and Optimization of ESP Systems in Wells with Great Depths, High Temperature, High GOR and High Concentrations of CO2, N2, H2S in Samaria Luna Field. Society of Petroleum Engineers. doi:10.2118/185275-MS

Reamer, H., & Sage, B. (1958). Diffusion Coefficients in Hydrocarbon Systems. Methane in the Liquid Phase of the Methane-Propane System. Industrial and Engineering Chemistry, 3(1), 54-59. doi:10.1021/i460003a013

Riling, G. Sizing Submersible Pumps for Viscosity Effects. PE July 1976: 64-72

Sarmiento, D. B., Prada, J. W., Quiros, H. M., Mora, J., & Sun, D. (2015, November 18). Replacement of ESP with Long Stroke Pumping Units in Heavy and High Viscous Oil in Maranta Block Wells. Society of Petroleum Engineers. doi:10.2118/177272-MS

Schramm, L.L., 2005. Emulsions, Foams, and Suspensions: Fundamentals and Applications. Wiley-VHA, Weinheim, Germany

Sheridan, E., Janjua, Z., McRae, J., Paranji, S. S., & Long, M. P. (2012, January 1). Successful Application Of ESPs In Bohai Bay Development. Society of Petroleum Engineers. doi:10.2118/156176-MS

Sheth, K., Crossley, A., Viscosity Correction Factors. Paper presented at SPE Gulf Coast Section Electric Submersible Pump Workshop, Woodlands, TX. April 29-May 1, 2009.

Simpson, A., Rhys-Davies, J., Husman, M., & Youri, E. (2017, April 24). A Tough, Truly Multiphase Downhole Pump for Unconventional Wells. Society of Petroleum Engineers. doi:10.2118/185152-MS

SPE.org. (2018, January 15). Electrical˙submersible˙pumps. Retrieved October 18, 2020, from Petrowiki.spe.org: https://petrowiki.spe.org/Electrical˙submersible˙pumps

Stepanoff, A.J. 1940. Pumping viscous oils which centrifugal pumps. Oil Gas J. (4).

Stepanoff, A J. 1949. How Centrifugals Perform When Pumping Viscous Oils. Power (June): 85-87.

Stepanoff, A.J., 1967. Centrifugal and Axial Flow Pumps: Theory, Design and Application, 5th Ed. John Wiley & Sons, New York.

Sulzer.com. (2020). Subsea. Retrieved October 18, 2020, from Sulzer.com: https://www.sulzer.com/en/applications/oil-gas-chemicals/upstream/subsea

Takacs, G. 2018. Electrical Submersible Pumps Manual: Design, Operations, and Maintenance Second Edition. Burlington, Vermont, USA: Gulf Professional Publishing

Turpin, J.L., Lea, J.F., Bearden, J.L. Gas-liquid through centrifugal pumps-correlation of Data. In Proceedings of the Third International Pump Symposium, Houston, TX, USA, 20–22 May 1986.

Turzo , Z., Takacs, G., Zsuga, J. Equations correct centrifugal pump curves for viscosity. OGJ May 29, 2000:57-61.

Walker, C.I. & Goulas, A. 1984. Performance characteristics of centrifugal pumps when handling non-Newtonian homogeneous slurries, Proc. Instn. Mech. Engrs. Vol. 198A, No. 1, pp. 41-49.

White, F. M. (2011). Fluid Mechanics, Seventh Edition. New York, USA: McGraw Hill.

Wiesner, F. J. 1967. A Review of Slip Factors for Centrifugal Impellers. ASME J Eng Power 89 (4): 558-566. doi:10.1115/1.3616734.

Wilson, K. C., Addie, G. R., Sellgren, A., and Clift R. (2006). Slurry Transport Using Centrifugal Pump, 3rd edition. Blackie Academic and Professional, London.

Young, J. P., Mathews, W. L., & Hulm, E. (2010, January 1). Alaskan Heavy Oil: First CHOPS at a vast, untapped arctic resource. Society of Petroleum Engineers. doi:10.2118/133592-MS

Zhou, D., & Sachdeva, R. (2008, January 1). Design Tapered Electric Submersible Pumps For Gassy Wells. Society of Petroleum Engineers. doi:10.2118/113661-MS

Zhu J., Zhang, H.Q. 2018. A Review of Experiments and Modeling of Gas-Liquid Flow in Electrical Submersible Pumps, Energies J. 180 (11): 1-41. doi.org/10.3390/en11010180.

Zhu, J., Zhu, H., Cao, G. et al. 2019a. A New Mechanistic Model for Oil-Water Emulsion Rheology and Boosting Pressure Prediction in Electrical Submersible Pumps. SPE-196155-MS.

Zhu, J., Zhu, H., Cao, G. et al. 2019b. A New Mechanistic Model to Predict Boosting Pressure of Electrical Submersible Pumps Under High Viscosity Fluid Flow with Validations by Experimental Data. Paper presented at the SPE Gulf Coast Section Electric Submersible Pumps Symposium, The Woodlands, Texas, USA, 13-17 May. SPE-194384-PA.